Enhanced Core Cooling for a Transformer

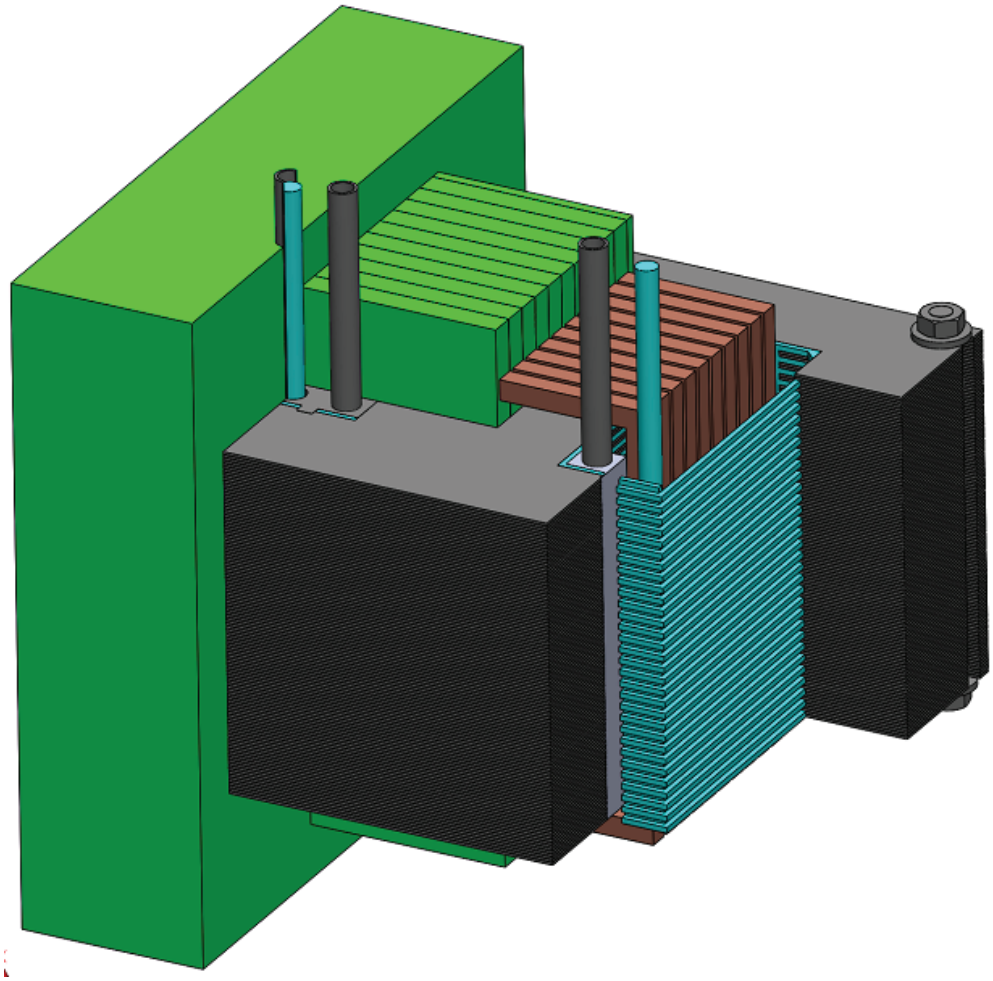

MASTER'S THESIS BY ROLF NYBORG BROGE
DEPARTMENT OF MECHANICAL AND MANUFACTURING ENGINEERING
AALBORG UNIVERSITY
1ST OF SEPTEMBER 2015

Study Board of Industry and
Global Business Development
Fibergerstraede 16
DK - 9220 Aalborg East
Phone +45 99 40 93 09
lft@m-tech.aau.dk
www.ses.aau.dk

Title:
Enhanced Core Cooling for a Transformer

Semester:
EMSD4, Spring 2015

Semester theme:
Master thesis

Project period:
2/2-2015 - 1/9-2015

ECTS:
30

Supervisor:
Ass. Prof. Peter Omand Rasmussen

Project group:
112b

Participants:
Rolf Nyborg Broge

Number printed: 3
Number of pages: 81
Number of appendix: 2
Appended CD: 5 folders
Submission date: 1st of September 2015

Synopsis:

This thesis concerns design, manufacturing, modelling and test of a water cooling system for a transformer. The cooling system is invented by Johnson Controls, and is intended to be implemented in a permanent magnet synchronous motor (PMSM), used to drive an axial compressor for a water vapour chiller. The cooling system is named "Enhanced Core Cooling". The cooling system appears to be highly effective, thereby permitting higher power densities in electrical machines.
A well-functioning waterproof prototype of the transformer is build, and several DC and AC test are performed to clarify the cooling systems ability to handle copper and iron losses.
The temperature distribution in the transformer is modelled by four different models: an analytic model, a lumped parameter model, a FEM analysis and a CFD analysis. The analytic model show the right tendencies but are too simplified to be accurate compared to the temperature measurement. The lumped parameter model and the FEM analysis are generally consistent with the temperature measurement, and may be used as simple and effective design tools the further development of the Enhanced Core cooling system in electrical machines. The CFD model behaves non conservative as the heat transfer for forced water convection is overestimated.
It is finally discussed how the Enhanced Core Cooling can be implemented in a PMSM. It is estimated that the Enhanced Core Cooling can sink up to 6 kW from the PMSM. With an estimated loss of 1 kW, the Enhanced Core Cooling is concluded to be an effective solution to cool the PMSM.

Preface

This thesis is written in the spring and summer of 2015, at the 4th semester of the M.Sc Programme *Electro-Mechanical Systems Design*, Aalborg University.
The thesis concerns manufacturing, testing and modelling of a liquid cooling system for a transformer. The thesis builds on top of the result found in "Manufacturing, Modelling and Control of a High Speed Permanent Magnet Synchronous Machine including a Thermal Analysis" [Mathiasen and Olesen, 2014].

The thesis is made in cooperation with Sabroe a part of Johnson Controls Inc. A special thanks go to Lars Skovlund Andersen from Johnson Controls for sparring and supplying of CAD drawings and materials for manufacturing.

Dansk Skalform A/S, Dantrafo A/S, Tommy Frandsen (AAU), Nordjysk Elitesport and Jens Christian M. Rauhe (AAU) are also thanked for their support to the thesis.

During the thesis the following computer programs are applied: Solidworks, Matlab, Simulink, PLECS, Mathcad, LabVIEW and Latex.
Relevant material and models concerning the thesis is found at the appended CD.

Reading guide
Harward reference system is used througout the thesis, thus references are stated by last name or company name and year of publication. A complete bibliography is found in the back the thesis.

SI-units are used unless otherwise stated. The units of the used variables is found in the nomenclature list in the beginning of the thesis.

Rolf Nyborg Broge

Resume

Dette kandidatspeciale omhandler udvikling, fremstilling og test af en ny type vandkølet transformer. Transformeren er et statisk forstudie der belyser muligheder og udfordringerne ved kølesystemet, før det implementeres i en permanent magnet synkron motor (PMSM). Specialet er lavet i samarbejde med Johnson Controls som ønsker at bygge PMSM'en ind i en aksial vanddampskompressor, der skal drive et rumkølesystem. Pga. vakuum i vanddampskompressor er det nødvendigt at udvikle et separat vandkølesystem til at aflede effekttab fra PMSM'en, da almindelig konvektion ikke er en mulighed i vakuum.
Dette specialet bygger videre på erfaringer fra kandidatspecialet "Manufacturing, Modelling and Control of a High Speed Permanent Magnet Synchronous Machine including a Thermal Analysis" [Mathiasen and Olesen, 2014], som forsøgte at udvikle vandkølesystem med køling imellem statortænderne og endviklingerne i PMSM'en.

Kølesystemet der testes i dette speciale består af kølekanaler direkte i transformerens kerne, hvorved der opnås ideel termisk overførsel mellem blik og kølesystemet. Kølesystemet kaldes derfor "Forbedret kerne køling" ("Enhanced Core Cooling").

Blikkene til transformerens kerne er specialfremstillet, og samlet således at der er fremkommer kølekanaler. For at gøre transformeren vandtæt og for at adskille det elektriske kredsløb fra kølesystemet, er transformeren støbt ind i epoxy. Forud for epoxyindstøbningen er kølesystemet fyldt med voks, således epoxyen ikke trænger ind i kølesystemet. Efter epoxyen er hærdet, smeltes voksen ud.
14 termokoblere er støbt ind i transformeren, således temperaturfordelingen kan overvåges og sammenlignes med termiske modeller igennem forsøg.

Fire forskellige termiske modeller af transformeren er udviklet. En analytisk, en lumped parameter model, en FEM model og en CFD analyse. De analytiske beregninger viser de rigtige tendenser, men er upræcises pga. forsimplinger. Lumped parameter og FEM modellerne stemmer i tilfredsstillende grad overens med de målte temperature i forsøgene.
Temperaturene beregnet i CFD analysen er generelt for lave, hvilket vurderes at skyldes at CDF analysen overestimerer varmeoverførselskonstanten mellem blik og vand.
Både jævnstrøms- og vekselstrømsforsøg er udført på transformeren, således kølesystemets evne til aflede hhv. kobber- og jerntab er undersøgt.

Transformeren er testet med effekttab på over 2 kW, uden at den blev varmere end tilladeligt. En projektion af kølesystemet til PMSM'en viser at kølesystemet har potentiale, til at aflede over 6 kW varme fra PMSM'en. Det er estimeret at tabene i PMSM vil være i omegnen af 1 kW, hvorfor det vurderes at kølesystemet er anvendeligt til at køle PMSM'en, når den bygges ind en vanddampskompressor som tiltænkt.

Contents

1 Introduction **1**
1.1 Problem Analysis . . . 2

2 Problem Statement **5**

3 Design and Manufacturing of Transformer **7**
3.1 Core . . . 7
3.2 Core Thermocouples . . . 9
3.3 Wax Moulding . . . 10
3.4 Winding . . . 12
3.5 Resin Moulding . . . 13
3.6 Experimental Set-up . . . 15
3.7 Summary and Discussion . . . 15

4 Power Losses of the Transformer **17**
4.1 Core Loss . . . 17
4.2 Copper Loss . . . 23
4.3 Measured Losses . . . 26

5 Thermal Models **29**
5.1 Analytic Model . . . 29
5.2 GD Novel Lumped Parameter . . . 37
5.3 Thermal FEM Analysis . . . 50
5.4 Fluid Flow/Thermal CFD analysis . . . 51

6 Thermal parameter determination **53**
6.1 Ambient Air heat Transfer Coefficient and Epoxy Emissivity . . . 53
6.2 Forced Cooling Water Heat Transfer Coefficient . . . 54

7 Test and Verification **59**
7.1 Results and Comparison of Models . . . 59
7.2 Discussion and Uncertainties . . . 68

8 Projection to PMSM **75**
8.1 Johnson Controls Solution . . . 75
8.2 Alternative Solution . . . 76

9 Conclusion **79**
9.1 Design and Manufacturing of Prototype Transformer . . . 79
9.2 Thermal Modelling and Verification . . . 79
9.3 Future work . . . 81

Bibliography **83**

A Appendix **85**

B Appendix **105**

Nomenclature

Name	Description	Unit
δ	Skin depth	m
$\dot{m}$	Mass flow	$\frac{m^3}{s}$
$\dot{q_{co}}$	Volumetric heat generation copper	$\frac{W}{m^3}$
$\dot{q_{ir}}$	Volumetric heat generation iron	$\frac{W}{m^3}$
$\dot{q}$	Volumetric heat generation	$\frac{W}{m^3}$
$\dot{V}$	Volume flow	$\frac{m^3}{s}$
ε	Emissivity	-
μ	Permeability	$\frac{H}{m}$
ν	Kinematic viscosity	$\frac{m^2}{s}$
Ω	Angular frequency	$\frac{rad}{s}$
Φ	Magnetic flux	Wb
ρ	Resistivity	$\frac{\Omega}{m}$
σ	Conductivity	$\frac{1}{\Omega m}$
σ_{SB}	Stefan-Boltzmann constant	$\frac{W}{m^2K^4}$
φ	Power factor	-
A	Cross sectional area	m^2, mm^2
A	Surface area	m^2, mm^2
A_{co}	Cross sectional area copper	m^2, mm^2
A_{window}	Cross sectional area winding window	m^2, mm^2
A_{path}	Magnetic path cross sectional area	m^2
B	Flux density	T
B_r	Residual magnetic flux density	T
c_{H_2O}	Specific heat capacity water	$\frac{J}{kg \cdot K}$
C_1	Integration constant	-
C_2	Integration constant	-
c_p	Specific heat at constant pressure	$\frac{J}{molK}$
D_h	Hydraulic diameter	m
e	Electromotive force	V
E_{rms}	rms electromotive force	V
f	Frequency	Hz
F_R	Resistance factor	-
h	Height	m, mm
H	Magnetic field intensity	$\frac{A}{m}$
h_{air}	Heat transfer coefficient air	$\frac{W}{m^2K}$
h_c	Heat transfer coefficient water	$\frac{W}{m^2K}$

h_{rad}	Heat transfer coefficient radiation	$\frac{\mathrm{W}}{\mathrm{m^2K}}$
i	Current	A
I_{rms}	rms current	A
k	Thermal conductivity	$\frac{\mathrm{W}}{\mathrm{mK}}$
k_{co}	Thermal conductivity copper	$\frac{\mathrm{W}}{\mathrm{mK}}$
k_{re}	Thermal conductivity resin	$\frac{\mathrm{W}}{\mathrm{mK}}$
K_e	Eddy current loss constant	-
K_h	Hysteresis loss constant	-
K_u	Copper fill factor	-
l	Length	m, mm
l_{path}	Magnetic path length	m
L_l	Leakage inductance	H
L_m	Magnetizing inductance	H
N	No. of turns	-
n	Hysteresis loss exponent	-
P	Active power	W
P_{co}	Copper loss	W
P_{cond}	Heat transferred by conduction	W
$P_{conv.air}$	Ambient air convection	W
P_{core}	Core loss	W
P_e	Eddy current loss	W
P_h	Hysteresis loss	W
P_{loss}	Power loss	W
P_{rad}	Radiation power	W
q''	Heat flux	$\frac{\mathrm{W}}{\mathrm{m^2}}$
R	Electrical resistance	Ω
R_{AC}	AC resistance	Ω
R_{co}	Copper resistance	Ω
R_{cont}	Thermal contact resistance	$\frac{\mathrm{m^2K}}{\mathrm{W}}$
R_{conv}	Thermal convection resistance	$\frac{\mathrm{m^2K}}{\mathrm{W}}$
R_{core}	Equivalent core loss resistance	Ω
R_{DC}	DC resistance	Ω
R_{ec}	Eddy current resistance	Ω
R_{rad}	Thermal radiation resistance	$\frac{\mathrm{m^2K}}{\mathrm{W}}$
Re	Reynolds number	-
S	Apparent power	VA
t	Time	s

t	Thickness	m, mm
T	Temperature	K, C
$T_{\infty A}$	Ambient air temperature	K, C
$T_{\infty C}$	Cooling water temperature	K, C
T_{ref}	Reference temperature	K, C
T_{amb}	Ambient temperature air	K, C
T_{comp}	Compensation temperature	K
T_{in}	Cooling water inlet temperature	K, C
T_{out}	Cooling water outlet temperature	K, C
u	Voltage	V
u	Flow velocity	$\frac{\mathrm{m}}{\mathrm{s}}$
U_{rms}	rms voltage	V
V_{core}	Core volume	m^2
w	Width	m, mm
W	Work	J
W_h	Hysteresis loop area	m^2
x	Variable length	m, mm

Subscripts

Name	Decription	Unit
x	1. cartesian coordinate	-
y	2. cartesian coordinate	-
z	3. cartesian coordinate	-
11	Thermal element, plan 1 No. 1	-
12	Thermal element, plan 1 No. 2	-
13	Thermal element, plan 1 No. 3	-
14	Thermal element, plan 1 No. 4	-
15	Thermal element, plan 1 No. 5	-
16	Thermal element, plan 1 No. 6	-
17	Thermal element, plan 1 No. 7	-
21	Thermal element, plan 2 No. 1	-
22	Thermal element, plan 2 No. 2	-
23	Thermal element, plan 2 No. 3	-
24	Thermal element, plan 2 No. 4	-
25	Thermal element, plan 2 No. 5	-
31	Thermal element, plan 3 No. 1	-
max	Peak value of alternating parameter	-

Introduction 1

Controlling the temperature by cooling and heating is an enormous industry. It is used all over the world to ensure e.g. personal comfort, control processes and in the food industry. A common way to control the temperature is to use a heat pump, which moves thermal energy from one place to another. The thermal energy is transported in a fluid medium, in general called the refrigerant. In order to take advantage of the phase change energy, the refrigerant needs to have its gas to liquid phase change temperature below the desired cooling temperature, why refrigerants as freon (fluorocarbons PFCs), HFC (hydrofluorocarbon) and ammonia traditionally are used.

All the traditionally refrigerants has downsides in relation to toxicity, flammable hazardous and ozone depletion. Environmental friendly refrigerants has been a huge research topic the past decades, but finding an environmental neutral refrigerant has not been successful, until water was supposed.

Regarding to environment, water is the ideal refrigerant as it is non toxic, non flammable and do not deplete the ozone. The downside of water as a refrigerant, is that it has to be operated at vacuum levels about 1 KPa to 6 KPa, in order to lowering the boiling point to approximately 7° C and 35° C respectively [Johnson, 2003]. The specific volume of vapour at this vacuum level is very large, why a large amount of vapour needs to be handled compared to traditional refrigerants. An axial compressor type can be used to handle the large amount of water vapour.

A prototype, developed by Johnson Controls, of a water vapour chiller driven by a axial compressor is seen in figure 1.1. The axial compressor consist of seven steps. Each step contains a rotational impeller that accelerate the vapour, and a stationary impeller that aligns the flow in the axial direction, so the flow is ready for the following rotational impeller. The seven stages in the axial compressor are all rotated by a common axle, which is driven by an external induction motor.

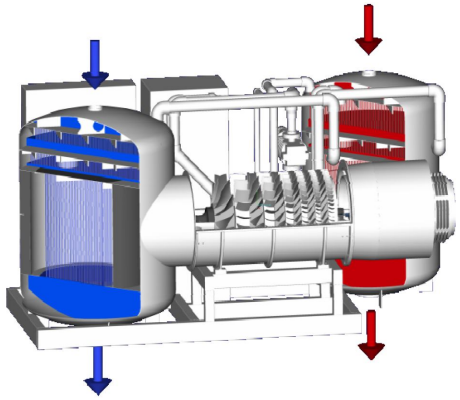

Figure 1.1. Water vapour chiller prototype invented by Johnson Controls [Andersen and Omand, 2015].

To increase the efficiency of the chiller it is proposed to make some changes of the axial compressor. Changes involves eliminating of the stationary impellers. Instead, each compressor stage is suggested to drive in opposite direction, thereby eliminating the losses at the stationary impellers and further increase the efficiency as the angle of attack between rotor/vapour is improved. Furthermore it is proposed that the velocity of each compressor stage should be controlled individually, as this permit operating at the most efficient velocity for each stage. The modifications makes it possible to reduce the number of compressor stages from seven to four.

The requirement of the compressor stages to be operated in opposite directions and individual velocities, raises the need of a new drive, as the stages can not be driven by one common axle and motor.
The proposed solution is to build a permanent magnet synchronous motor (PMSM), with outer rotor, into each compressor stage.

The vacuum in the axial compressor makes it impossible to cool the PMSM's by traditional air convection. This raises the need of forced water cooling of the PMSM's. The PMSM water cooling is complicated by very limited space and the low compressor environment pressure.

1.1 Problem Analysis

The master's thesis "Manufacturing, Modelling and Control of a High Speed Permanent Magnet Synchronous Machine including a Thermal Analysis" [Mathiasen and Olesen, 2014] concerns the development, modelling and manufacturing of a water cooled PMSM, used to drive a compressor stage in the axial compressor. The developed PMSM is an outer rotor type, and the stator is mounted on a stationary axle. The thesis test an "end plate" cooling system, where cooling water is flowing from the central axle into channels in plastic plates, mounted on each end of the stator, see figure 1.2. The end plates is located in between the stator laminations and the end winding.

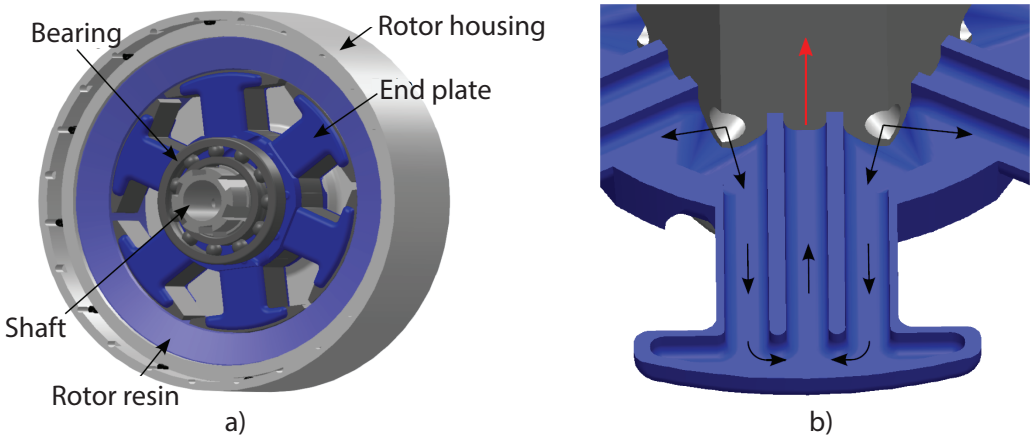

Figure 1.2. End plate cooling system for a PMSM. Figure a) shows the unwound stator with the cooling plate at the end of the stator. Figure b) shows the cooling channels in the end plate [Mathiasen and Olesen, 2014].

The stator of the PMSM is cast into resin to make it waterproof. Unfortunately it did not succeed

to make the cooling system waterproof, as it leaked between the stator laminations and from the assembly between the end plates and the axle. It was therefore not possible to test the water cooling system during operation of the PMSM. In addition to the leakage issues, problems regarding electrical shorts and unexpected bearing losses complicated the tests of the PMSM.

In order to develop and test a cooling system for the PMSM used to drive the axial compressor, it is decided to make a static study, by applying the cooling system to a transformer instead of a PMSM. By testing the cooling system on a transformer, it is expected that issues that precluded test on the PMSM can be avoid, as the transformer is a simple electrical machine without any rotational parts. Simplifying the PMSM to a transformer, further ease the bookkeeping of the losses, as only core and resistive losses are present.

A completely new invented cooling system concept is intended to be tested on the transformer. The new cooling concept is invented by Johnson Controls, but is not tested yet. The concept is called "Enhanced Core Cooling", and implies that cooling channels are integrated directly in the core. This gives an optimal heat transfer between the heat source and the cooling water, why it is predicted to give an effective cooling of the machine. Another benefit of the Enhanced Core Cooling system is that the machine may be made more compact, as the cooling system occupy minimal space. Altogether this reveals the possibility of producing a machine with unprecedented power density, which is necessary to drive the axial compressor by build-in PMSM's.

1.1.1 Requirements to the Enhanced Core Cooling

The thesis [Mathiasen and Olesen, 2014] estimates that a PMSM used to drive a stage in the axial compressor, will have a copper loss of 250 W and an iron loss of 750 W, because of the high operational speed (15000 rpm). This means that the Enhanced Core Cooling system in the transformer has to be able to sink at least 1000 W of heat, when it is sized in proportion to the PMSM. The maximum allowable temperature of the transformer is set to 155° C, in order to protect the enamel on the winding.

The cooling system has to be waterproof to the ambient and to the electrical system, so that electrical short circuits are avoided.

Problem Statement 2

On basis of the issues revealed in [Mathiasen and Olesen, 2014], it is decided to test the liquid cooling system called "Enhanced Core Cooling" on a transformer in contrary to a PMSM.

The object of this thesis is to develop, manufacture and test the Enhanced Core Cooling system for a transformer, thereby clarifying potential pitfalls and challenges that has to be treated before implementation in the PMSM.

This leads to the main problem statement of the thesis:

"How to manufacture, test and thermally model the Enhanced Core Cooling system for a transformer?"

The problem is treated with special emphasis on the following topics:

- Designing and manufacturing of a prototype transformer containing waterproof cooling channels in the core.
- Modelling of the thermal circuits and analysing the effects of the core cooling channels.
- Model and measure the losses and heat distribution in the prototype, and compare it to the models.
- Project the results gained from the transformer to a PMSM.

The overall design of the Enhanced Core Cooling system for a transformer is made by Johnson Controls. This leaves only minor details to be designed which are conducted in cooperation with Johnson Controls.
The manufacturing process builds on the experiences gained from the PMSM in [Mathiasen and Olesen, 2014], as an equivalent procedure is used to manufacture the transformer.

Four different types of thermal models are developed and tested towards temperature measurements made on the prototype transformer. The thermal models includes an analytic model, a lumped parameter model, a finite element model (FEM) and a computational fluid dynamics (CFD) model.
The approach used to set up the lumped parameter model and the applied heat source compensation method, are the same as successfully was used in [Mathiasen and Olesen, 2014], why alternative approaches are not investigated.

Design and Manufacturing of Transformer 3

This chapter describe the design and the manufacturing process of the Enhanced Core Cooling transformer. The transformer contains a closed EI-shaped core, a primary winding and a search coil. It do not contain a secondary winding, why the actual function of the transformer resembles an inductor. The "transformer" name originates from the project proposal, and will be used during this thesis.

The cooling channels are designed to run inside the winding window of the core, thereby achieving an effective cooling of both the core and the winding. The transformer is build in the following steps:

- Special core stacking sequence and installation of thermocouples in core
- Confine the core and the inlet/outlet manifolds in the wax mould.
- Inject wax into the manifolds and cooling channels.
- Eject the core and secure the wax by electrical tape.
- Wind of the transformer and install winding thermocouples.
- Cast the transformer assembly into resin.
- Melt the wax out of the transformer assembly.

The described steps should leave a waterproof enhanced core cooling transformer, with the coolant and winding separated by resin.

3.1 Core

The outer dimensions of the transformer core is 115 mm x 96 mm x 63 mm (lxwxh), see figure 3.2, and is made from 0.5 mm non oriented electric steel laminations, see data sheet on appendix CD. Five laminates are weighted to 168.1 grams, yielding an individual weight of 33.6 grams each. The total weight of the core is calculated in equation 3.1.

$$M_{core} = 124pc. \cdot 0.0336 \frac{kg}{pc.} = 4.17kg \tag{3.1}$$

The winding windows are, opposed to normal, placed non-symmetric in the laminate. They are shifted 1 mm towards the lower left corner, see figure 3.1. The purpose of shifting the winding windows, are to obtain cooling channels around the windows by flipping the laminates opposite each other when stacking the core.

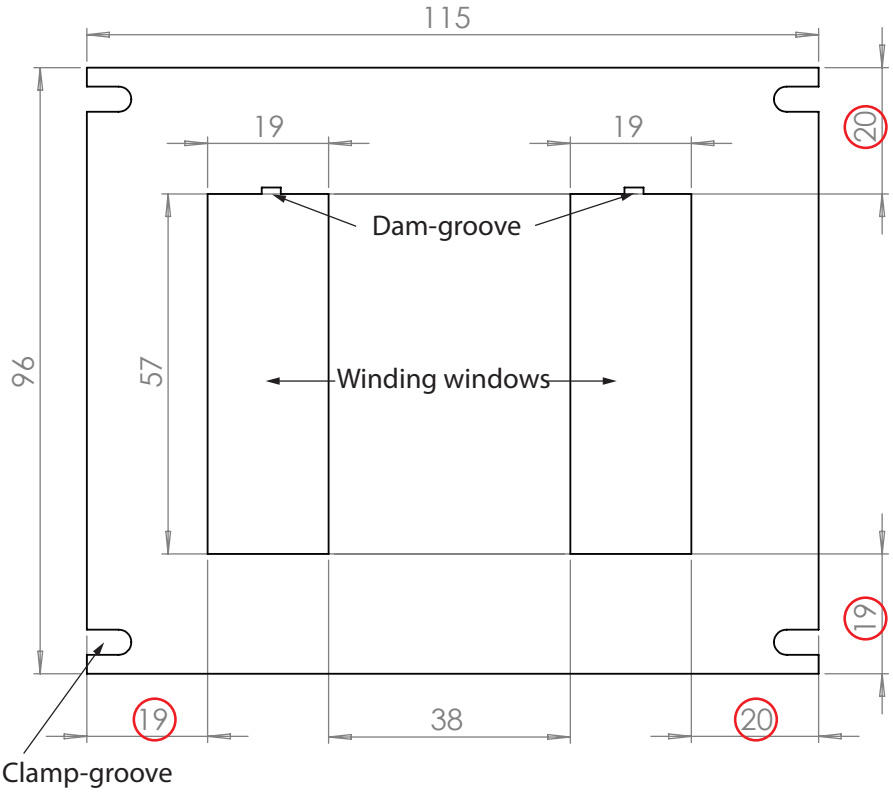

Figure 3.1. Transformer laminate, notice the red circles that underlines that the winding windows are shifted toward the lower left corner. Dimensions are in mm.

A stacking factor of 0.98 is achieved, giving 124 laminates. The laminates are flipped for every two laminations, resulting in 31 1x1 mm cooling channels around the winding windows, see figure 3.2. In the upper zoom window of figure 3.2 it should be noted that the water running in the cooling channels has to shift layers at the corners. The layer shifting is made possible by the wax chamfer seen in figure 3.6b, which entails that resin cast around the winding will have a chamfer.

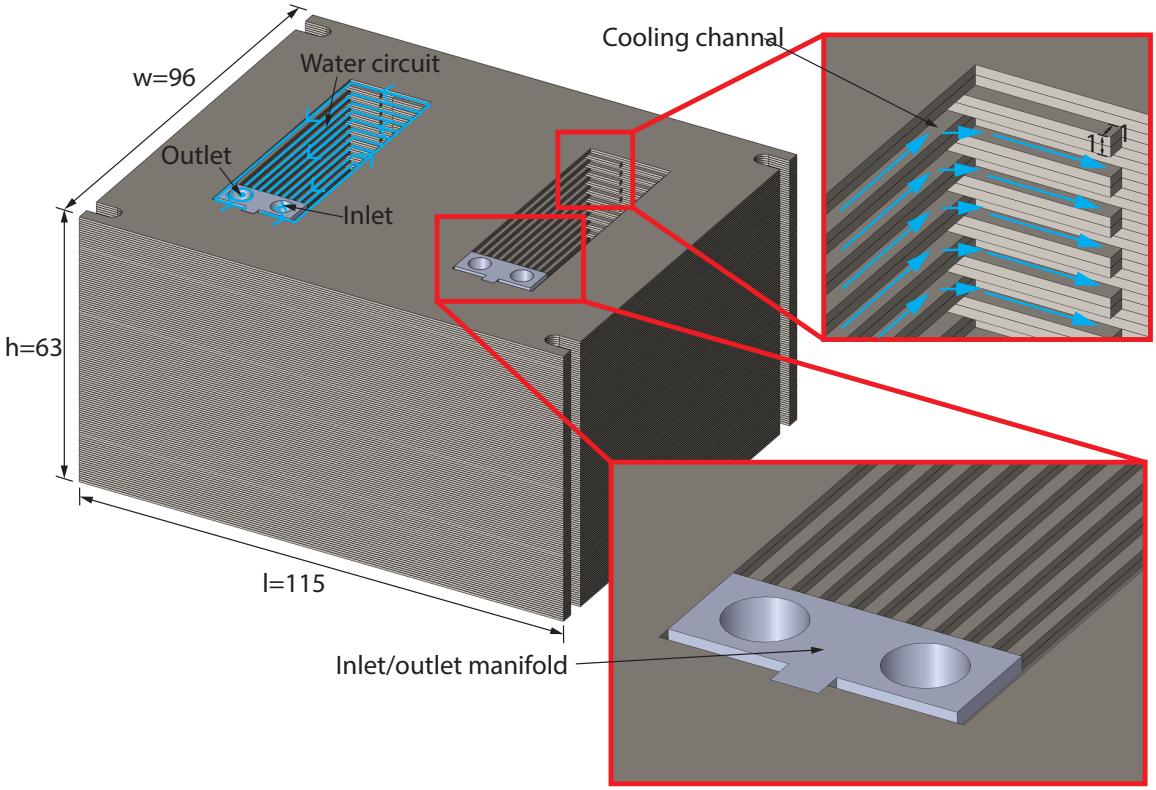

Figure 3.2. Transformer core showing the enhanced core cooling. Dimensions are in mm.

The cooling water is feed through two inlet/outlet plastic manifolds. Each manifold has an inlet side and an outlet side, separated by a dam, see 3.3. The dam ensures that the incoming water has to run through the core cooling channels, before it leaves at the outlet.

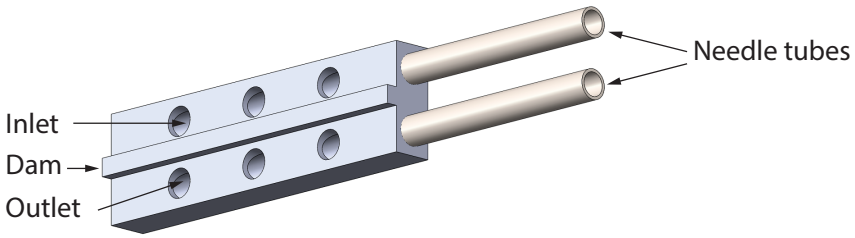

Figure 3.3. The inlet/outlet manifold and needle tubes.

The cooling water is directed to and from the manifolds by needle tubes. The 4 mm bore of the needle tubes limits the flow through the cooling system, as these have the minimum cross sectional areal of the cooling system.

3.2 Core Thermocouples

To monitor the temperature of the transformer during experiments, 14 thermocouples are installed in the core, winding and resin shell. Five core thermocouples are installed during the core laminate stacking, as they are located in the mid plane of the core, see figure 3.4b. The thermocouples are

located at strategic locations, in relations to the thermal models of the transformer. The red numbers in figure 3.4b correspond to the element numbers in the lumped parameter model given in figure 5.8. The centre lamination is different from the remaining laminations, as this entails some slits for the core thermocouples, see figure 3.4a.

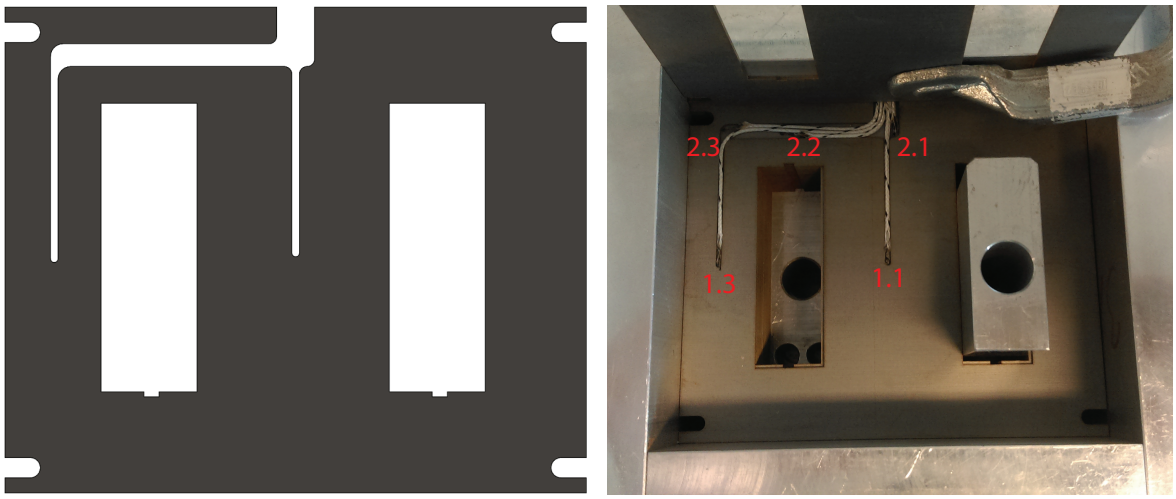

Figure 3.4. Installation of the five core thermocouples. Figure a) shows the thermocouples slits in the centre laminations. Figure b) shows the installed thermocouples and the numbers relates to the thermal model elements given in figure 5.8.

The installed thermocouples are of type J (iron - constantan), which has a temperature measurement range from -40° C to 750° C. The measurement range is by far sufficient, as the degeneration of the insulation of the copper winding starts to accelerate at temperatures above 155° C. After installation of the five core thermocouples, the remaining half core lamination stack is installed in top.

3.3 Wax Moulding

The Enhanced Core Cooling is sealed by casting the transformer into epoxy. To avoid epoxy blocking the cooling system, the lost wax moulding method is used. Before the epoxy moulding, wax is injected into the manifolds and core cooling channels. Once the epoxy has set hard, the wax is melted out of the cooling system, leaving an assumed clean cooling system.

The wax is injection moulded into the cooling system, hence the core needs to be confined in a mould, see figure 3.5. The wax mould consists of an inlet plate, a distributor plate, four side plates, a lid plate and two winding window spacers. The lid is bolted on top of the mould before wax is injected into the core cooling system. The winding window spacers has chamfered corners in the opposite end as the manifolds. The chamfers lets the cooling water run around the corners while it is shifting cooling channel layers.

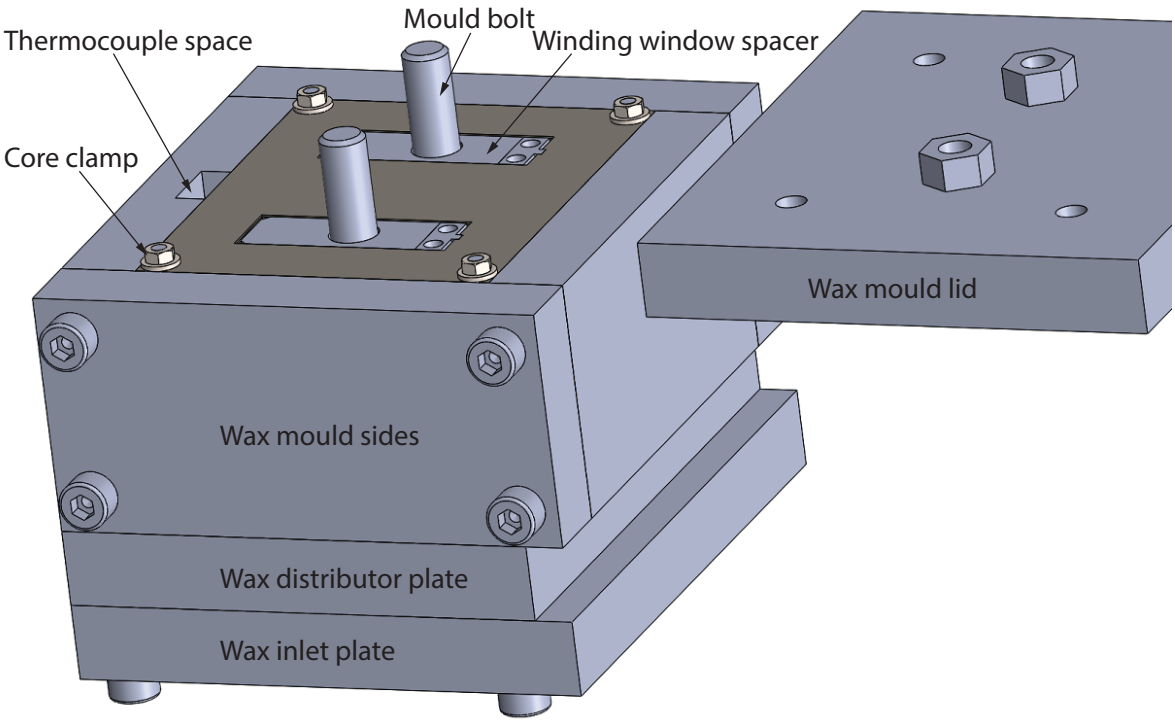

Figure 3.5. The wax mould. The lid is clamped on top of the mould before wax is injected into the core cooling system.

During the wax injection process it appears to be a problem to get the wax all the way around in the cooling system, before the wax harden in the small channels and blocks the further flow, see figure 3.6a. To avoid this problem the mould and transformer is preheated to 50° C, which is below the wax melting temperature. The preheating did not had the desired effect, as the harden front did not moved further into the cooling channels. Instead of doing further experiments with wax injection and preheating, it was decided to fill up the cooling system manually, by disassemble the mould and inject the wax directly by a disposable syringe. After some manually wax fitting, the cooling system was successful filled with wax, see figure 3.6b.

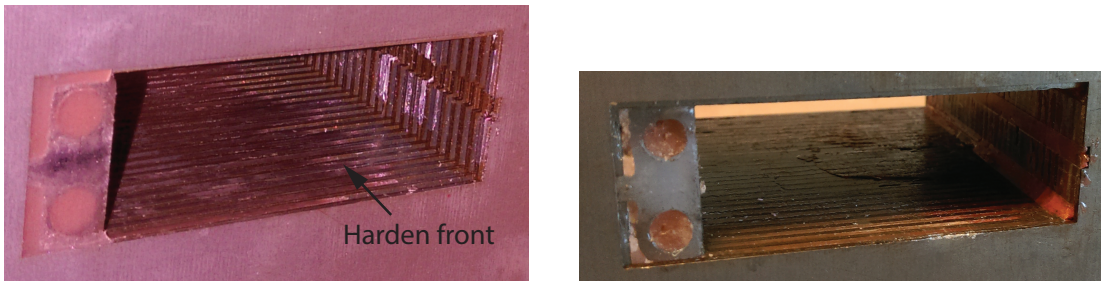

Figure 3.6. Picture a) shows the wax harden front after injection moulding. Picture b) shows the final wax filling after manually fitting.

3.4 Winding

Before the transformer is wound, the winding windows are sealed by electrical tape. This is done to protect the wax and the enamelled copper wire during the winding process, and to secure electrical insulation between the winding and core. Two layers of 3M polyester electrical tape type 57 are applied to the transformer as seen on figure 3.7.

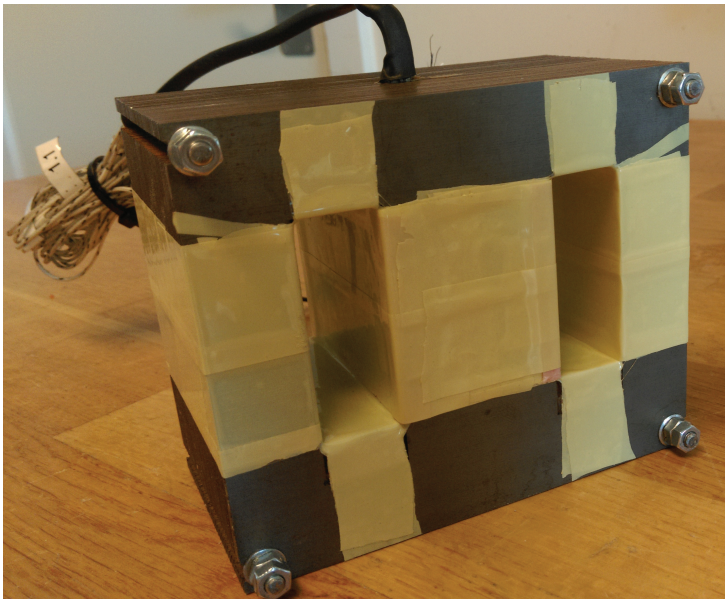

Figure 3.7. Two layers of 3M electrical tape protects the wax and the winding.

The transformer emf equation [Sen, 2013] is used to determine the number of turns in the transformer winding, see equation 3.2. It is decided that the maximum root mean square (rms) voltage to bring the core to magnetic saturation ($B_{max} = 2T$) is 200 V. This enables to supply the transformer by the 230 V utility grid, which may vary up to $\pm 10\%$, resulting in a minimum voltage of 207 V.

$$N = \frac{E_{rms}}{4{,}44 B_{max} f A} = \frac{200V}{4{,}44 \cdot 2T \cdot 1000Hz \cdot 0.002394m^2} = 9.4\text{turns} \tag{3.2}$$

Where A is the magnetic cross sectional area of the transformer and f is the maximum frequency. On basis of equation 3.2 10 turns is decided. It is decided to make each turn consist of 20 parallel 1 mm enamelled copper wires. This results in a copper fill factor of 0.156, see equation 3.3.

$$K_u = \frac{A_{co}}{A_{window}} = \frac{(0.5mm)^2 \cdot \pi \cdot 20 \cdot 10}{18mm \cdot 56mm} = 0.156 \tag{3.3}$$

Normally it is of interest to maximize the copper fill factor, as this minimizes the copper loss. However, this thesis concerns cooling, why it is acceptable to have increased losses.

The wound transformer, including a 10 turns search coil used to measure the flux density in the core, and additional winding thermocouples are seen in figure 3.8a.

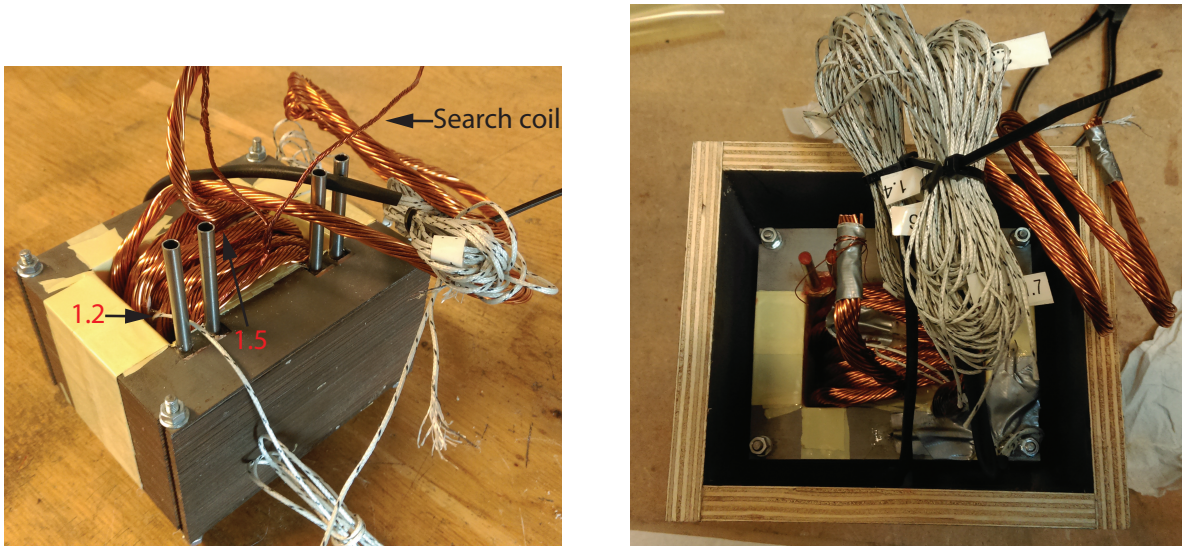

a) b)

Figure 3.8. The wound transformer including a search coil and additional winding thermocouples. The red numbers and the numbers on the labels relates to the thermal model elements given in figure 5.8.

In addition to the five core thermocouples, two winding thermocouples and seven surface and resin thermocouples are mounted in the transformer, see figure 3.8b showing the transformer in the resin mould.

3.5 Resin Moulding

The transformer is moulded into Huntsman Araldite/Aradur (resin/hardener) epoxy. A volume of 1.27 L is used to cover the transformer, and creating a 10 mm thick shell around the transformer. The mould is build in water resistance plywood and screwed together. The final outer dimensions of the epoxy cast transformer is 135 mm x 116 mm x 119 mm (lxwxh).

The epoxy casting process is done in the following sequence:

1. Spray mould release in the inside of the mould.
2. Preheat unmixed resin, hardener, mould and transformer to 55° C.
3. Mix resin and hardener according to data sheet.
4. Degassing the epoxy at 1.5 mbar in a half hour.
5. Pour the epoxy into the mould containing the transformer.
6. Reheat the complete transformer and epoxy assembly to 55° C.
7. Degas the transformer and epoxy assembly at 1.5 mbar in 2 hours.
8. Cure the resin at 55° C in 20 hours.
9. Cure the resin/melt off wax at 100° C in 20 hours.

The reason for preheating the resin and transformer is to lower the viscosity of the epoxy, and thereby assist the penetration of epoxy in the winding. The temperature of 55° C is decided on basis of the wax melting temperature (60° C), which is not allowed to melt before the resin is cured to a firm state. The relative long degassing time of two hours is due to persistent gas bobbles, properly from the winding and between the core laminates. After the final 20 hours of curing at 100° C, the last wax remains in the cooling system is attempted to be cleaned out by blowing compressed air through the cooling system. Further, the wax is cleaned out by flushing boiling water through the system. Finally the cooling system is filled with water, and the transformer is heated to 150° C in a furnace, after which the cooling system again is blown through by compressed air. A picture of the finished transformer after resin moulding is seen in figure 3.9. A cut view of the if the CAD modelled transformer is seen at the frontage.

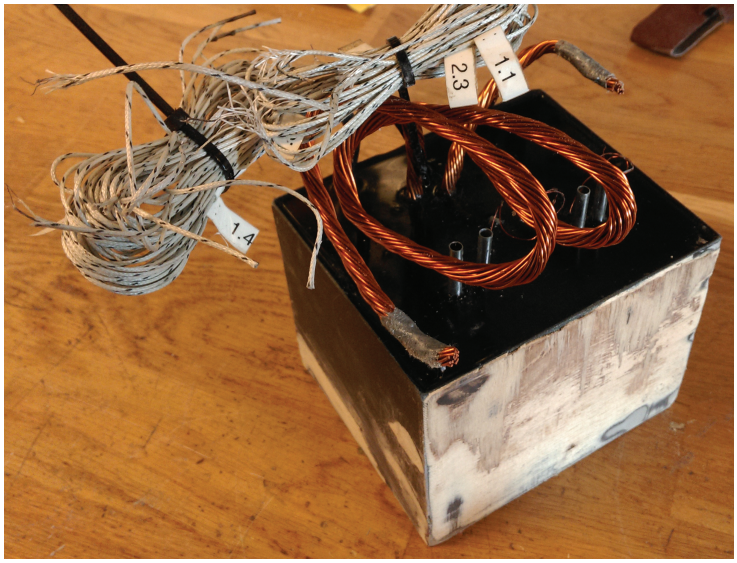

Figure 3.9. The epoxy moulded transformer. Traces of the plywood mould is seen on the sides.

The fluid volume of the cooling system, see figure 5.15, according to the CAD model is 18.6 ml. It is measured that the cooling system holds 12 ml of water, which means that more than 6 g is missing compared to the CAD model. It is hard to say where the remaining wax is located - if it is a thin layer all over the cooling system, or if it completely blocks some of the cooling channels. However, the water flow is easy going when flushing water trough the cooling system.

A study of how to dissolve the wax is conducted, in hope that the wax could be cleaned out this way. Literature suggest an organic non polar solvent to dissolve wax, e.g. cleaner's naphta. An experiment is conducted by soaking wax, electrical tape and cured resin in cleaner's naphta. The electrical tape and the resin did not take damage, which is desirable to avoid damaging the transformer. At first the wax did not take remarkable damage, but after two days in cleaner's naphta, the wax was getting porous and greasy. The experiments indicates that setting up a closed system recirculation cleaner's naphta through the cooling system for several days, might be a way to clean out the remaining wax. To increase the speed of the process it might be suggested to elevate the temperature.

3.6 Experimental Set-up

The transformer is placed in an experimental set-up consisting of an electrical-, a measurement and a cooling set-up.

The electrical set-up entails a California Instruments MX30-3Pi AC/DC power supply with a build in power analyser. The power supply is connected to the transformer with two 3 m long high power cables, with a rated maximum current of 300 A.
The measurement set-up entails an oscilloscope and a CompactRIO. The oscilloscope measures the current in the transformer supply cables, the voltage drop over the transformer supply terminals and the induced voltage in the search coil. The CompactRIO is logging the temperature data from the 14 thermocouples, the inlet and outlet temperatures and the flow rate of the cooling water.
The cooling set-up entails a radiator, a fan, a reservoir, a flow limiting valve and a cooling water pump. The cooling set-up is connected to the transformer via two 2 m long silicone hoses. The experimental set-up is seen in figure 3.10.

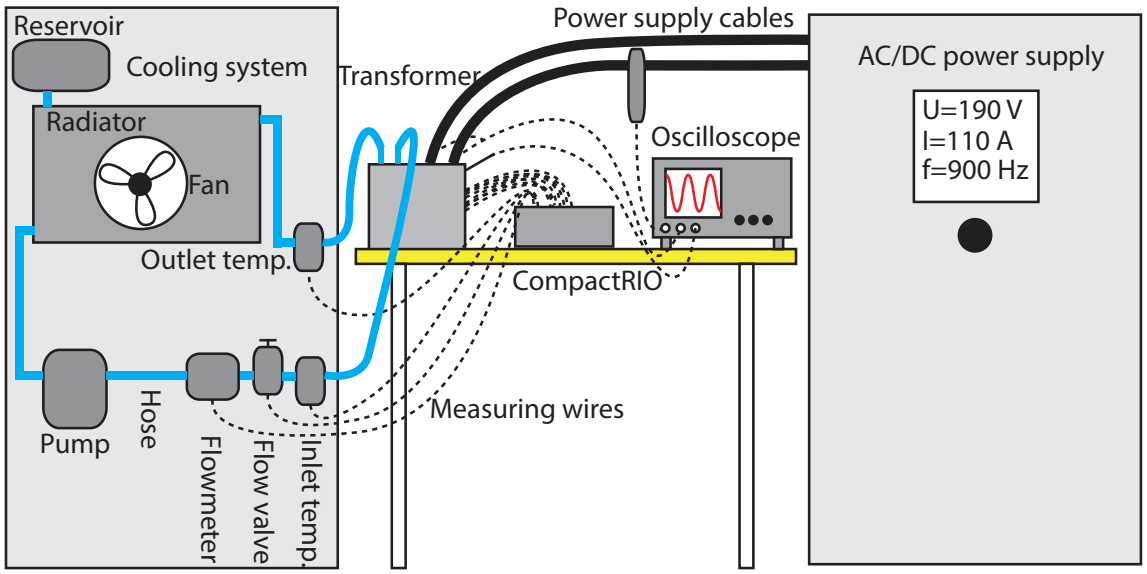

Figure 3.10. The experimental set-up. Blue lines are cooling water hoses, dotted lines are measuring wires and the bold black lines are power supply cables.

3.7 Summary and Discussion

The main challenges in producing a transformer containing the enhanced core cooling system, is regarding the lost wax moulding and removal. It was problematic to inject the wax into the cooling system, as the wax did harden too quickly in the cooling channels, and thereby obstructed the wax flow to the furthermost cooling channels. It was attempted to solve the problem by preheating the mould and transformer, but the attempt failed. It is highly probable that the wax filling problem can be solved by preheating the mould and transformer, to a temperature just below the wax melting point. A number of experiments has to be conducted to obtain the correct temperature, injection pressure, pressure hold time and cooling time.

Another problem regarding the wax, is to remove it from the cooling system, as experiments shows that approximately one third is remaining after flushing the system with hot water.
Ideally the wax should be soluble in water, thereby the cooling system would be self cleaning when cooling water flows through the system.
Alternatively should a wax cleaning system be set up, circulating cleaners naphtha for several days through the cooling system, thereby dissolving the remaining wax and ensure maximum efficiency of the cooling system.

Power Losses of the Transformer 4

This chapter concerns the power losses in the transformer.
The electrical circuit of the transformer is seen in figure 4.1.

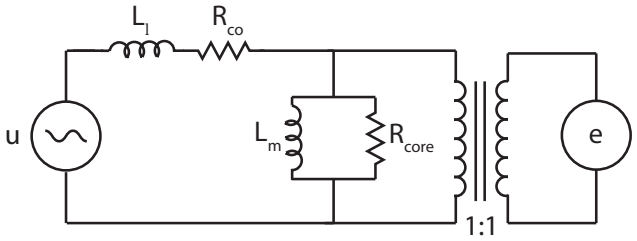

Figure 4.1. The electrical circuit of the transformer, with inspiration from [Sen, 2013].

The circuit consist of a voltage source (u), a leakage inductance (L_l), a copper resistance (R_{co}), a mutual magnetizing inductance (L_m), an equivalent core loss resistance (R_{core}), and a one to one transformer measuring the electromotive force (e). No leakage inductance and resistance is present in the secondary transformer winding, as no current is flowing in the search coil. The copper resistance and the equivalent core loss resistance will produce losses when an AC current is flowing in the circuit

The losses are divided into core losses (P_{core}) in the transformer steel laminates and copper losses (P_{co}) in the winding. The total power loss in the transformer is the sum of core and copper losses, equation 4.1.

$$P = P_{core} + P_{co} \tag{4.1}$$

4.1 Core Loss

Core loss originate from two different phenomenons: Hysteresis and eddy currents. The total core loss is given by the sum of the hysteresis and eddy current losses, see equation 4.2.

$$P_{core} = P_h + P_e \tag{4.2}$$

Hysteresis and eddy current losses are examined further in the following sections.

4.1.1 Hysteresis Loss

The magnetic core in the transformer is made of silicon steel laminations. When an AC current is flowing in the transformers supply winding, an alternating magnetic field intensity (H) is induced in the silicon steel laminates. Initially, the laminates consists of small random oriented magnetic particles. When the magnetic particles are exposed to the magnetic field intensity, they will arrange themselves in parallel to the magnetic field intensity, and thereby produce a magnetic flux density (B).

Figure 4.2a shows the B-H characteristic of initially unmagnetized iron, when it is exposed to an alternating magnetic field.

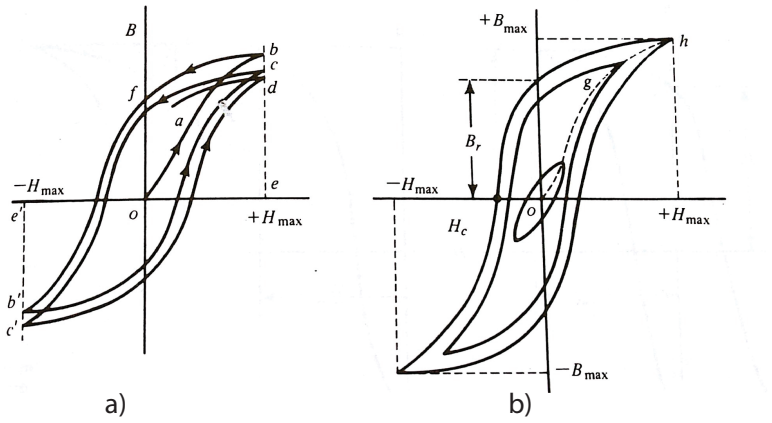

Figure 4.2. a) B-H characteristic of initially unmagnetized iron. b) Hysteresis loops [Matsch and Morgan, 1987].

The magnetization curve starts at (o) where both the field intensity and flux density are zero, by increasing the current, the field intensity is increased to its maximum value of $+H_{max}$ at the point (b).

Changing the direction of the magnetic field intensity means that the magnetic particles has to change direction as well. The magnetic particles offers resistance in changing direction, why flux density will lag compared to the magnetic field intensity. This means that when the magnetic field intensity reaches zero again, a residual magnetic flux density (B_r) is remaining in the core material. Decreasing the field intensity further in its negative range makes the flux density zero at some point, the field intensity at B=0 is called the coercive force. Decreasing the field intensity to its maximum negative value $-H_{max}$ makes the flux density negative too, point (b'). The field intensity is now increased again till point (c) is reached, and the hysteresis loop is almost complete. Every time the hysteresis loop passed through, it will be closer to the previous loop, finally forming the hysteresis loop. Figure 4.2b shows three hysteresis loops for different magnetic field intensities.

During a hysteresis loop energy is lost in turning the direction of the magnetic particles. This loss is called hysteresis loss, and heats up the core. The hysteresis loss can be evaluated by examination of the energy transfer during the interval of time t_1 to t_2, see equation 4.3, [Sen, 2013].

$$W = \int_{t_1}^{t_2} p\,dt = \int_{t_1}^{t_2} ei\,dt \tag{4.3}$$

Substituting Faraday's law ($e = N\frac{d\Phi}{dt}$) into equation 4.3 gives equation 4.4.

$$W = \int N\frac{d\Phi}{dt} i\,dt = \int_{\Phi_1}^{\Phi_2} Ni\,d\Phi \tag{4.4}$$

Using the definition of flux density ($\Phi = \int B\,dA$) and Ampere's circuit law ($Ni = \oint H\,dl$) results in equation 4.5.

$$W = lA\int_{B_1}^{B_2} H\,dB \tag{4.5}$$

In equation 4.5 lA is equal the volume of the core (V_{core}), and $\int_{B_1}^{B_2} H\,dB$ is equal a small area of the hysteresis loop between B_1 and B_2. Integration over the complete hysteresis loop, gives the total power loss per loop.

$$W|_{cycle} = V_{core}\oint H\,dB = V_{core}\cdot W_h \tag{4.6}$$

Where W_h is the area of the hysteresis loop. It is difficult to evaluate the area of the hysteresis loop, but it can be estimated by equation 4.7, when the hysteresis loop originates from a sinusoidal excitation.

$$W_h = KB_{max}^n \tag{4.7}$$

Where B_{max} is the maximum flux density, the exponent n is between 1.5 and 2.5, and K is a constant depending on the lamination shape, thickness and permeability [livares Galvan et al.].

The volume of the transformer, and K is combined to one constant called K_h. Further, equation 4.6 is multiplied by the frequency (f) of the current supplying the transformer, to obtain the total hysteresis loss, see equation 4.8.

$$P_h = K_h B_{max}^n f \tag{4.8}$$

4.1.2 Eddy Current Loss

The alternating magnetic field in the core laminates induces a voltage, which will produce a circulating current in the laminates. This current is called eddy current. The silicon steel laminates has an electrical resistance, why the eddy current will result in an eddy current loss. Eddy current loss can be minimized in two ways: either by increasing the resistivity of the core material, or by laminating the core. The core laminates are electrical insulated from each other by a thin insulating coating, thus the eddy currents are limited inside each laminate [Sen, 2013].

An analytic expression for the eddy current loss is deduced by examine the lamination seen in figure 4.3.

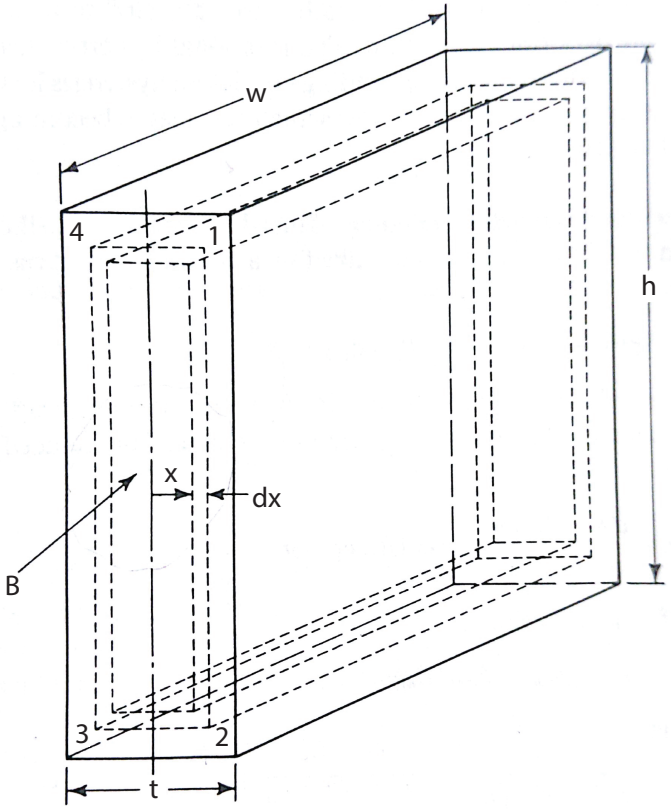

Figure 4.3. Lamination. The flux density (B) is in the direction of the width (w), normal to the eddy current part 1-2-3-4... [Matsch and Morgan, 1987].

The thickness of the laminate is (t), the width is (w) and the hight is (h). The eddy current path is 1-2-3-4..., normal to the direction of the flux density (B). [Matsch and Morgan, 1987].

The assumed sinusoidal alternating flux (Φ) in the laminate is defined by equation 4.9

$$\Phi = \Phi_{max} sin(\omega t) = AB_{max} sin(\omega t) \tag{4.9}$$

Where A is the cross sectional area of the laminate, normal to the flux.

The induced voltage (e) in the 1-2-3-4 path of the laminate is given by equation 4.10

$$e = \frac{d\Phi}{dt} = \omega AB_{max} cos(\omega t) \tag{4.10}$$

The peak value (E) of the induced voltage is given by equation 4.11

$$E_{max} = \omega AB_{max} \tag{4.11}$$

The rms value of the induced voltage is given by equation 4.12. Furthermore the angular frequency is transformed to frequency ($\omega = 2\pi f$).

$$E_{rms} = \frac{E_{max}}{\sqrt{2}} = \frac{2\pi AB_{max}}{\sqrt{2}} = 4.44 fAB_{max} \tag{4.12}$$

Equation 4.12 is seen to be the transformer equation, with only one turn (N=1), used to determine the number of turns in the transformer, in section 3.4.

The cross sectional area encircled by the dotted box, in figure 4.3 is approximated to $2xh$. The induced voltage in the path, between the stippled lines, is therefore given by equation 4.13, for any x.

$$E_{rms} = 4.44 fB_{max} 2hx \tag{4.13}$$

With the induced voltage known, only the resistance of the eddy current path needs to be determined, in order to calculate the eddy current loss by Ohm's law. The differential resistance of the eddy current path, with the thickness dx, in figure 4.3 is given by equation 4.14. The thickness of the laminate is omitted in the eddy current path length, as $t << h$.

$$dR = \frac{\rho l_{path}}{A_{path}} = \frac{2h\rho}{w\,dx} \tag{4.14}$$

The differential eddy current loss in the laminate is determined using Omh's law, see equation 4.15.

$$dP_e = \frac{E_{rms}^2}{dR} = \frac{(4.44 fB_{max} 2hx)^2}{\frac{2h\rho}{w\,dx}} = \frac{(4.44 fB_{max})^2 2hwx^2 dx}{\rho} \tag{4.15}$$

Integrating equation 4.15 over the maximum thickness of the eddy current path ($x = \frac{t}{2}$) gives the total eddy current loss in one lamination.

$$P_e = \int_0^{t/2} dP_e = \int_0^{t/2} \frac{(4.44 f B_{max})^2 2hw \left(\frac{t}{2}\right)^2 dt}{\rho} = \frac{(4.44 f B_{max})^2 wht^3}{12\rho} \tag{4.16}$$

The quantity 4.44 was introduced instead of $\frac{2\pi}{\sqrt{2}}$ and *wht* equals the volume of the lamination, using this in equation 4.16 gives the final expression for the eddy current loss in one lamination. If the volume of the core is used instead of the volume of one lamination, the total eddy current loss is calculated, see equation 4.17.

$$P_e = \frac{V_{core} \pi^2 f^2 t^2 B_{max}^2}{6\rho} \tag{4.17}$$

Equation 4.17 can be simplified to equation 4.18. Where the constant K_e depends on the volume of the core, the thickness of the lamination and the resistivity of the laminations.

$$P_e = K_e B_{max}^2 f^2 \tag{4.18}$$

Experiments on laminated silicon steel cores shows that the eddy current loss typically is 50 % larger than calculated by equation 4.17. This is caused by the large grain size in silicon steel [Matsch and Morgan, 1987].

It is possible to determine the constants K_h and K_e experimentally for a specific transformer, e.g. by the two-temperature method or the two-frequency method [livares Galvan et al.]. However K_h and K_e are not determined for the Enhanced Core Cooled Transformer, as there is no need of hysteresis and eddy current loss separation in this thesis.

The total core loss is estimated on basis of the lamination data sheet, [Cogent, 2009]. The data sheet for the 0.5 mm electrical silicon steel (Sura M400-50A), used in the transformer core, listing the core losses at different frequencies from 50 Hz to 2500 Hz, and at different flux densities from 0.1 T to 1.8 T.
Selected values are seen in table 4.1

	Power loss $\left[\frac{W}{kg}\right]$				
B [T]	**50 [Hz]**	**100 [Hz]**	**200 [Hz]**	**400 [Hz]**	**1000 [Hz]**
0.2	0.09	0.26	0.64	1.80	7.49
0.5	0.46	1.27	3.33	9.37	39.0
0.8	1.01	2.80	7.68	22.7	103.1
1.0	1.49	4.15	11.7	35.9	173.3
1.3	2.46	6.88	20.2	64.9	334.6
1.5	3.57	9.82	28.3	91.7	488.4
1.8	5.47	-	-	-	-

Table 4.1. Selected typical loss values for the 0.5 mm electrical silicon steel (Sura M400-50A), used in the transformer [Cogent, 2009].

The listed values are for one kilo of lamination. According to equation 3.1, the total weight of the core is 4.17 kg, why the listed should be multiplied by this when calculation the iron losses.

4.2 Copper Loss

Copper loss is in general given by the voltage drop over the winding times the current, or using Ohm's law, the current squared times the winding resistance, equation 4.19.

$$P_{co} = R_{co} I_{rms}^2 \tag{4.19}$$

4.2.1 DC Resistance in Winding

The resistance in the winding is determined theoretically and experimentally.

Theoretical

The theoretical resistance in the winding at 20° C is calculated by equation 4.20. The winding is measured to be approximately 3 m long, and consists of 20 parallel 1 mm wires. The resistivity of copper at 20° C is set to $1.75 \cdot 10^{-8} \Omega m$.

$$R_{co20} = \rho_{co20} \cdot \frac{l}{A} = 1.75 \cdot 10^{-8} \Omega m \frac{3m}{(0.0005m)^2 \cdot \pi \cdot 20} = 3.3 m\Omega \tag{4.20}$$

Experimental

The DC resistance in the transformer winding is determined experimentally by applying a DC voltage to the winding, and simultaneously measure the current and voltage in the winding. The voltage drop over the winding is measured at the winding terminals at the transformer, thereby excluding the voltage drop in the supply cables. Five measurements is made at different current levels, and the current is plotted as function of voltage drop. The slope of the linear trendline (3mΩ) is equal to the

resistance of the winding, according to Ohm's law, see figure 4.4. The temperature of the winding is 20.4° C during the experiment.

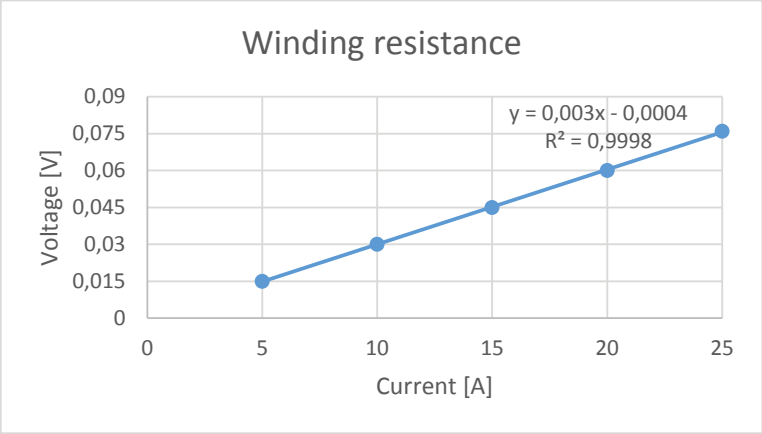

Figure 4.4. The DC resistance is determined to 3 mΩ in the transformer winding, by applying Ohm's law.

The measured resistance is fairly in agreement with the theoretical determined. The minor difference might be caused by measurement uncertainties and the actual winding length.

The resistance in the winding increases with elevated temperatures, the temperature corrected resistance can be calculated by equation 4.21. The temperature coefficient $\alpha = 0.004C^{-1}$ is a materiel constant. The winding resistance at a operation temperature of 100° C is calculated in equation 4.21.

$$R_{co100} = R_{co20}(1 + \alpha(T - T_{ref})) = 3m\Omega(1 + 0.004C^{-1}(100°C - 20°C)) = 4m\Omega \tag{4.21}$$

It is seen that the resistance is raised by one third, by raising the temperature 80° C.

4.2.2 AC Copper Loss

When AC current is flowing in the winding of the transformer, skin and proximity effects may increase the copper loss.

Skin Effect

The AC current $i(t)$ flowing in the supply winding of the transformer produces a magnetic field $H(t)$ around it. A piece of the winding conductor is seen in figure 4.5a. Just as described for the core material, the magnetic field will produce eddy currents in the copper wire itself, see figure 4.5b. The eddy currents will flow in the same direction as the applied current in the exterior part of the wire, and in the opposite direction as the applied current in the interior part of the wire. This means that the current density $J(t)$ will be major at the perimeter of the wire, and exponentially decay towards the middle of the wire, see figure 4.5c.

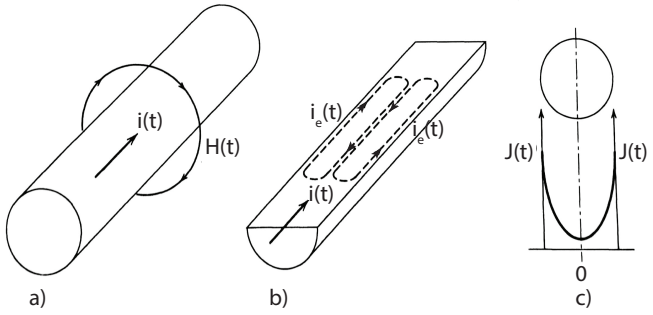

Figure 4.5. a) A copper wire carrying an AC current. b) Induced eddy current. c) Current density distribution in conductor caused by skin effects [Mohan et al., 2003].

The copper loss increases when skin effects is pronounced, as the "effective" current carrying cross sectional area reduces. It is generally said that skin effects can be neglected if the diameter of a conductor is less that two times the skin depth ($d \leq 2\delta$) [Mohan et al., 2003]. The skin depth is the distance from the surface of the conductor to the point where the current density has fallen to $\frac{1}{e} = 0.37$.

The skin depth (δ) can be calculated from equation 4.22.

$$\delta = \sqrt{\frac{2}{\omega \mu \sigma}} \tag{4.22}$$

Where ω is the applied angular frequency, μ is the permeability and σ is the conductivity.

Calculating the skin depth for the maximum frequency of 1000 Hz, and using a permeability of $1.256 \cdot 10^{-6} \frac{H}{m}$ and a conductivity of $5.96 \cdot 10^{7} \frac{1}{\Omega m}$ for copper, gives a skin depth of 2 mm. The diameter of the conductor is 1 mm, why skin effect can be neglected.

Proximity Effect

Proximity effect is like skin effect caused by induced eddy currents in the winding. Every conductor in the winding produces a magnetic field, which induces eddy currents in the adjacent conductors, see figure 4.6.

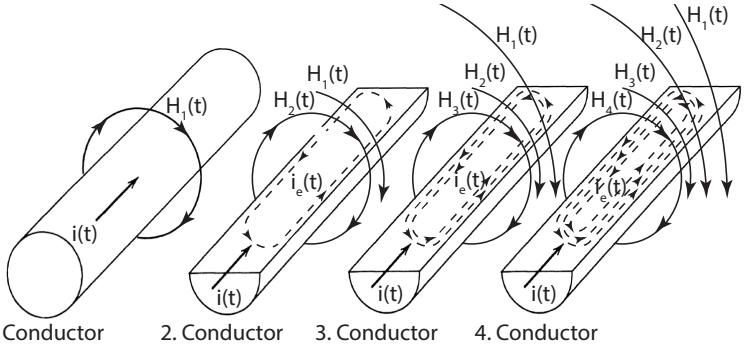

Figure 4.6. The proximity effect illustrated by four parallel conductors. The figure is made with inspiration from [Mohan et al., 2003].

The eddy currents will accumulate in pace with the magnetic field the conductor is exposed to. This means that the eddy current loss increases dramatically when conductors are placed in multiple layers in a electrical machine. The effective AC resistance (R_{AC}) of the winding is given by equation 4.23 [Mohan et al., 2003].

$$R_{AC} = F_R R_{DC} = \left(1 + \frac{R_{ec}}{R_{DC}}\right) R_{DC} \tag{4.23}$$

Where F_R is the resistance factor and R_{ec} is the effective eddy current resistance. When the diameter of the conductors is less than the skin depth, the resistance factor will be something greater than one. On the other hand, if the diameter of the conductors is greater that the skin depth, the resistance factor can be one or two decades [Mohan et al., 2003].

By equation 4.22 the skin depth was calculated to 2 mm at maximum operation frequency. In view of the conductor diameter of 1 mm, it is assumed that the resistance factor will be somewhere between 1 and up to 1.5.
Because of the large skin depth compared to the conductor diameter, the resistance factor is neglected. The copper loss is therefore calculated on basis of the measured DC resistance alone.

4.3 Measured Losses

To investigate accuracy of the power analyser, build into the AC power supply, an experiment is conducted by exposing the primary winding to an AC quasi sinusoidal voltage. The alternating current produce copper and core losses in the transformer. The measurements from the power analyser is seen in table 4.2 .

Description	**Name**	**Measurement**	**Unit**
Frequency	f	500	Hz
rms voltage	U_{rms}	89.94	V
rms current	I_{rms}	30.5	A
Peak current	I_{peak}	68.2	A
Active power	P	485	W
Apparent power	S	2740	VA
Power factor	φ	0.17	-

Table 4.2. Measurements from AC power supply/analyser for sinusoidal waveform.

The current and the voltage in the winding are measured by an oscilloscope during the experiment, see figure 4.7. The blue curve shows the current (i), the red curve shows the voltage (u) in the primary winding and the green curve shows the induced emf (e) in the search coil.

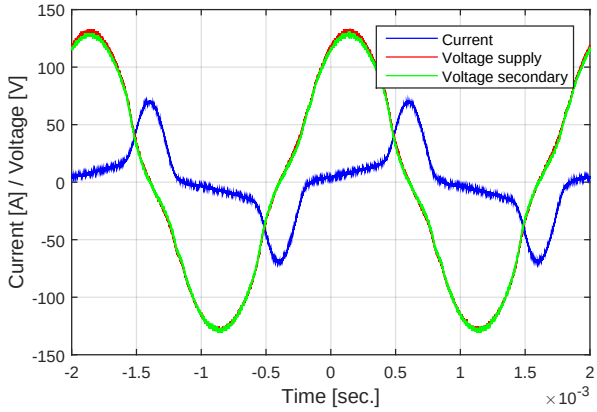

Figure 4.7. Measurements from the oscilloscope. The blue curve shows the current, the red curve shows the voltage in the primary winding and the green curve shows the induced EMF in the search coil.

The data from the oscilloscope is analysed in Matlab, and the results are seen in table 4.3.

Description	**Name**	**Measurement**	**Unit**
rms supply voltage	U_{rms}	88.71	V
rms current	I_{rms}	31.04	A
Active power	P	559	W
Apparent power	S	2753	VA
rms search coil voltage	U_{rms}	87.6	V

Table 4.3. Results from the oscilloscope measurements.

It is seen that the rms voltage and rms current measured by the oscilloscope deviates by -1.2 V and 0.5 A, respectively. This minor deviation may be explained by the voltage drop in the supply cables, and the 8 bit resolution of the oscilloscope, which results in a measurement resolution of approximately 1.2 V and 1.2 A, for the present experiment.

The active power, calculated from the oscilloscope measurement, gives 559 W. Compared to the power analyser measurement of 485 W, the calculated power deviates by 74 W corresponding to 15 %. The reason for the deviation may mainly be caused by the phase angle, as the voltage and current measurements is found to be of acceptable accuracy.
Several experiments shows that the power, calculated from the oscilloscope measurement, is higher than the power measured at the power analyser. It would reasonable if the power analyser measured more power than the oscilloscope, as this could be explained by power loss in the supply cables. However no physical explanation of the measured power divination between the oscilloscope and power analyser can be found. Inconsistent measurements from the power analyser indicates that this is unreliable, why the oscilloscope measurements is found to be most trustworthy.

4.3.1 Iron Losses from Lamination Data Sheet

The iron loss for the present experiment may be estimated from data sheet values, see 4.1 [Cogent, 2009], to back up the measurements from the power analyser and the oscilloscope.

The flux density of the transformer is calculated from the emf measured in the search coil, see equation 4.24

$$B_{max} = \frac{E_{rms}}{4.44NfA} = \frac{87.6V}{4.44 \cdot 10 \cdot 500 \cdot 0.002394} = 1.65T \tag{4.24}$$

The iron loss for the flux density of 1.65 T and a frequency of 500 Hz is not found in the data sheet for the lamination steel. The power loss for the specific values is estimated by fitting a plane to the data in the data sheet, see figure 4.8

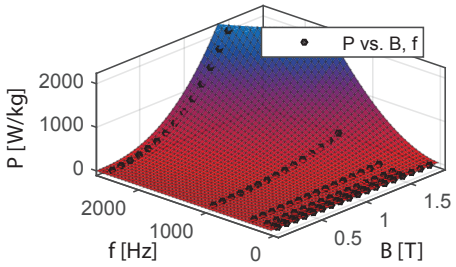

Figure 4.8. The iron loss in watts per kilo, fitted from the values in the data sheet for steel laminations [Cogent, 2009].

The plane is fitted to equation 4.25, which is theoretically based on the eddy current and hysteresis core loss, equations 4.18 and 4.8.

$$P_{core} = KB_{max}^{\beta} f^{\alpha} = 0.000664 \cdot B^{2.533} \cdot f^{1.806} \tag{4.25}$$

Where K, β and α are constants determined from the fit.
The total iron loss for the 4.16 kg core is thereby estimated to 735 W. This is 52 % and 32 % more than the measured loss by the power analyser and the oscilloscope, respectively. The huge divination is hard to explain by other than the data sheet do not fit to the lamination steel.

4.3.2 Separation of Copper and Iron Losses

The copper loss and iron loss are separated by calculating the copper loss from the measured rms current, and the DC resistance in the primary winding. The DC resistance in the primary winding is determined on basis of measurements ($R = 3m\Omega$), and is modified by the measured temperature of the winding ($T_{wind} = 42^{\circ}$ C), to $R = 3.3m\Omega$. The copper loss is calculated in equation 4.26.

$$P_{co} = RI_{rms}^2 = 3.3m\Omega \cdot (31.04A)^2 = 3.2W \tag{4.26}$$

The remaining 555.8 W is assumed to be core loss, according to equation 4.2. The copper loss is seen to be a very little part of the total loss in this experiment. The actual copper loss may be greater because of skin and proximity effects, which has been neglected.

Thermal Models 5

This chapter describes the thermal models of the transformer. The goal of the thermal models is to predict the temperature distribution in the transformer as a function of losses and cooling, and thereby determine the ability of the Enhanced Core Cooling system.

It is important to control the temperature in electrical machines to obey tight tolerances and to avoid too fast degeneration of the enamel on the winding. In the transformer assembly it is the enamelled winding that limits the maximum temperature. The winding is of insulation class F, which has a maximum allowed temperature of 155°.

Four levels of models are used, starting with an analytic model to a complex fluid flow/thermal CFD analysis.

The four models are:

- Analytic model.
- Novel GD lumped parameter.
- Simplified thermal FEM analysis using Solidworks.
- Fluid flow/thermal CFD analysis using Solidworks.

5.1 Analytic Model

The analytic calculations serves as a feasibility study, used to estimate if the Enhanced Core Cooling system is practicable, regarding to mass flow rate, flow velocity and Reynolds number of the cooling water, and if it is capable of sinking the required heat from the transformer, without exceeding the maximum allowable temperature.

A number of assumptions is made in order to set up the analytic calculations. The assumptions are listed below.

- 750 W iron loss corresponding to a volumetric heat generation rate of $1.32 \cdot 10^6 \frac{W}{m^3}$.
- 250 W copper loss corresponding to a volumetric heat generation rate of $0.90 \cdot 10^6 \frac{W}{m^3}$.
- Ambient air temperature is 21° C.
- The cooling water temperature is allowed to increases by 10° C through the cooling system.
- The inlet temperature of the cooling water is 45° C.
- The outlet temperature of the cooling water is 55° C.
- The transformer surface temperature is 75° C.

The analytic calculations takes base in a total power loss of 1000 W, with 750 W of iron loss and 250 W of copper loss. The losses are chosen on basis of [Mathiasen and Olesen, 2014], as these are the estimated losses in a PMSM used to drive one stage of the axial compressor, when it operates at maximum continuously load.
The temperature increase of the cooling water, when it passed the transformer, depends on the flow rate of the cooling water. 10° C is seen as an reasonable temperature increase, but it may be increased if the required flow is too extensive.
The inlet temperature of the cooling water depends on the radiator capability and the ambient air temperature. Assuming an ambient air temperature of 21° C, an inlet temperature of 45° C is considered as a conservative guess.
The surface temperature of the transformer depends on the thermal properties of the cooling system, the transformer and the ambient, why it is difficult to give an educated guess. However, a surface temperature of 75° C is chosen, as this is 25 ° C above the average cooling water temperature, which seams reasonable.

5.1.1 Heat Transfer Mechanism

The heat generated in the transformer is shunted by three heat paths: convection through the cooling water, convection through the ambient air, and radiation from the outer surface. The strength of the three cooling paths are investigated, to get an overview of there individual capabilities.

Radiation

Radiation is energy transferred by electromagnetic waves. The radiation from the epoxy shell enclosing the transformer, to the ambient air, is given by equation 5.1, which describes the heat emitted (P_{rad}) from a small object to an infinite space [Incropera et al., 2006].

$$P_{rad} = \sigma_{SB} A \varepsilon (T_a^4 - T_b^4) \tag{5.1}$$

Where σ_{SB} is the Stefan-Boltzmann constant ($5.67 \cdot 10^{-8} \frac{W}{m^2 K^4}$), A is the surface area, ε is the emissivity of the surface, T_a and the T_b are the temperatures of the object and the ambient respectively.

An estimate of the heat transferred by radiation is set up in the following. The emissivity of epoxy is set to 0.91 [Thermoworks, 2015] while the surface temperature of the epoxy shell is assumed to be 75° C (348 K), and the ambient air temperature is assumed to be 21° C (294 K). The surface area of the epoxy shell is 0.0911 m^2. The heat emitted from the epoxy shell for the given case, is estimated by equation 5.2.

$$P_{rad} = 5.67 \cdot 10^{-8} \frac{W}{m^2 K^4} \cdot 0.0911 m^2 0.91((348K)^4 - (294K)^4) = 33.8W \tag{5.2}$$

Compared to the total power loss of 1000 W, the 33.8 W of radiation stands for 3.4 % for this case.

Outer Surface Convection

The convection from the outer surface of the epoxy shell to the surrounding air, is calculated using the same assumptions as for radiation. The heat transfer coefficient h_{air} for natural convection in air is chosen to 8 $\frac{W}{m^2K}$, [Saidi and Abardeh, 2010].

$$P_{conv.air} = h_{air} A \Delta T = 8 \frac{W}{m^2 K} \cdot 0.0911 m^2 \cdot (75^\circ C - 21^\circ C) = 39.4 W \tag{5.3}$$

Equation 5.3 shows that 39.4 W of heat is shunted from the transformer by outer surface convection, equals 3.9 % of the total heat generated in the transformer.

The remaining 92.7 % heat generated in the transformer has to be removed by the cooling water convection. Cooling water convection is therefore the dominating heat transfer mechanism, in the transformer in case the assumptions holds.

Cooling water convection

The main part of the generated heat, is shunted from the transformer by conduction and then convection through the water cooling system. Allowing an increase of 10° C of the cooling water, enables calculating the required cooling water mass flow, see equation 5.4.

$$\begin{aligned} P_{in} &= P_{out} \\ &\Downarrow \\ P_{loss} &= \dot{m} c_{H_2O} \Delta T + P_{rad} + P_{conv.air} \\ &\Downarrow \\ \dot{m} &= \frac{P_{loss} - P_{rad} - P_{conv.air}}{c_{H_2O} \Delta T} = \frac{1000W - 33.8W - 39.4W}{4186 \frac{J}{kg \cdot K} \cdot 10K} = 0.022 \frac{kg}{s} = 1.33 \frac{l}{min} \end{aligned} \tag{5.4}$$

The smallest cross sectional area (A) in the water cooling path appears in the in- and outlet tubes. To judge if a flow of 0.022 kg/s is achievable, the maximum flow velocity, equation 5.5, and Reynolds number, equation 5.6, is calculated at this location.

$$u = \frac{\dot{V}}{A} = \frac{0.022 \frac{kg}{s} \cdot 10^{-3} \frac{m^3}{kg}}{(0.002m)^2 \cdot \pi \cdot 2} = 0.88 \frac{m}{s} \tag{5.5}$$

Where $\dot{V}$ is the volume flow.

Reynolds number in in- and outlet, [Andersen and Hansen].

$$Re = \frac{u \cdot D_h}{\nu} = \frac{0.95\frac{m}{s} \cdot 0.004m}{0.5531 \cdot 10^{-6}\frac{m^2}{s}} = 6331 \tag{5.6}$$

Where D_h is the hydraulic diameter of the in- and outlet tubes and ν_{50C} is the kinematic viscosity of the cooling water at the assumed average temperature of 50° C, [Viscopedia, 2015]. A Renolds number above 2300 is said to give turbulent flow [Incropera et al., 2006], so 6331 is definitely turbulent.

The flow velocity and Reynolds number in the 1mm x 1mm core cooling channels, around the windings windows, are likewise calculated by equation 5.5 and equation 5.6 to $0.34\frac{m}{s}$ and 621, respectively. This shows that the inlet and outlet tubes are the bottleneck in the cooling system.

5.1.2 Temperature Distribution

The temperature distribution in some parts of the transformer is analytically estimated by using the heat diffusion equation 5.7 [Incropera et al., 2006].

$$\frac{\partial}{\partial x}\left(k\frac{\partial T}{\partial x}\right) + \frac{\partial}{\partial y}\left(k\frac{\partial T}{\partial y}\right) + \frac{\partial}{\partial z}\left(k\frac{\partial T}{\partial z}\right) + \dot{q} = \rho c_p \frac{\partial T}{\partial t} \tag{5.7}$$

Where T is the temperature, k are the thermal conductivity, $\dot{q}$ is the volumetric heat generation, ρ is the density, c_p is the specific heat at constant pressure and t is time.

Equation 5.7 is derived by studding a cubic infinitesimal control volume with the dimensions $dx \cdot dy \cdot dz$, and analyse the energy balance together with the conduction heat rates over the surfaces, using a first order Taylor series expansion and Fourier's law of thermal conduction $\left(q''_n = -k\frac{\partial T}{\partial n}\right)$.

In words equation 5.7 states that *"at any point in the medium the net rate of energy transfer by conduction into a unit volume plus the volumetric rate of thermal energy generation must equal the rate of change of thermal energy stored within the volume"* [Incropera et al., 2006].

The general heat transfer equation is simplified to equation 5.8, by assuming constant thermal conductivity k, steady-state conditions $\left(\rho c_p \frac{\partial T}{\partial t} = 0\right)$ and one directional heat flow $\left(\frac{\partial}{\partial y}\left(k\frac{\partial T}{\partial y}\right) + \frac{\partial}{\partial z}\left(k\frac{\partial T}{\partial z}\right) = 0\right)$.

$$\frac{d^2T}{dx^2} + \frac{\dot{q}}{k} = 0 \tag{5.8}$$

By integrating the one dimensional steady state heat transfer, equation 5.8, gives the first derivative of the temperature, see equation 5.9.

$$\frac{dT}{dx} = -\frac{\dot{q} \cdot x}{k} + C_1 \tag{5.9}$$

Integrating it a second time gives the analytic solution to the temperature distribution along the x axis, see 5.10.

$$T(x) = -\frac{\dot{q} \cdot x^2}{2k} + C_1 \cdot x + C_2 \tag{5.10}$$

The integration constants C_1 and C_2 are to be determined by the boundary conditions.

The transformer is situated in a Cartesian coordinate system, see figure 5.7, with the x axis normal to the winding windows and origo at the middle of the transformer.
Taking the design of the cooling system into account, it may be justified that the main part of the thermal energy is removed from the sides of the winding windows, perpendicular to the x axis (because these sides has a greater area than the sides parallel to the x-axis). This assumption justifies a one dimensional heat flow along the x axis. An analytic steady state study of the heat distribution along the x-axis in the transformer is conducted using equation 5.8. The problem is sketched in figure 5.1, showing a one dimensional cut of the thermal elements 1.1, 1.2 1.3 and 1.4, described in section 5.2.4.

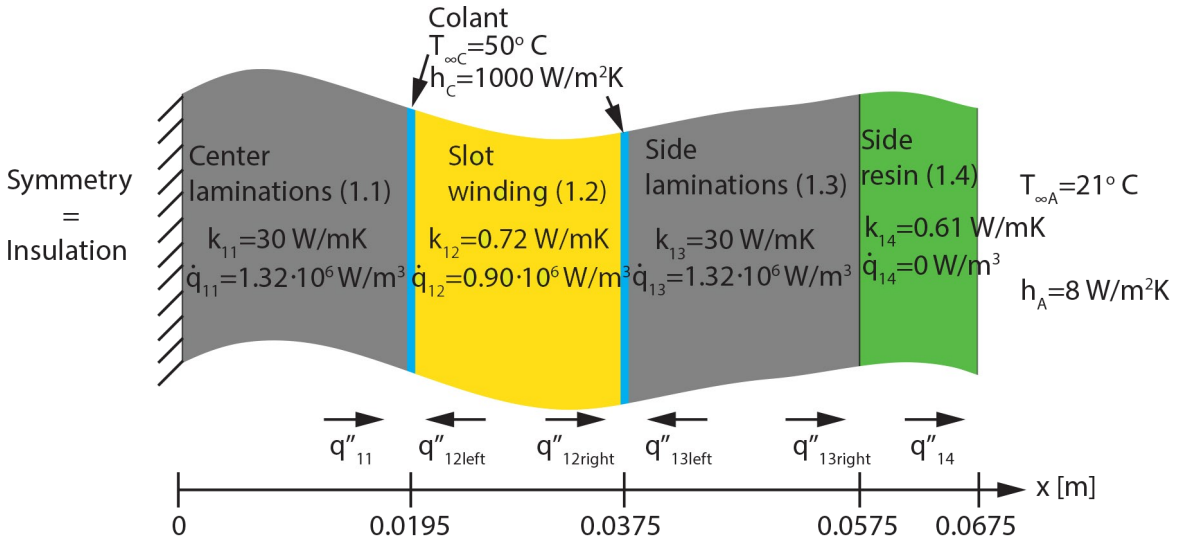

Figure 5.1. One dimensional model of the heat conduction problem along the x axis.

The volumetric heat generation rate in the laminations elements is set to $\dot{q} = 1.32 \cdot 10^6 \frac{W}{m^3}$ corresponding to a total iron loss of 750 W in the transformer, while the volumetric heat generation rate in the winding element is set to $\dot{q} = 0.90 \cdot 10^6 \frac{W}{m^3}$ corresponding to a total copper loss of 250 W in the transformer.
The thermal conductivities (k_{11}, k_{12}, k_{13}, k_{14}) of the core, winding and epoxy elements are determined from data sheets and discussed further in 5.2.4.

The temperature and the heat transfer coefficient of the ambient air is set to $T_{\infty A} = 21^\circ$ C and $h_A = 8 \frac{W}{m^2 K}$ [Mathiasen and Olesen, 2014], respectively.

The cooling water is assumed to have a constant temperature of $T_{\infty C} = 50^\circ$ C, which is seen as an

average between an inlet temperature of $T_{in} = 45°$ C and an outlet temperature of $T_{out} = 55°$ C. The heat transfer coefficient h_C for forced water convection is set to 1000 $\frac{W}{m^2K}$, based on [Alagesan and Sundaram] and [Al-Saiman and Thamer], see figure 5.2. It is seen that the heat transfer coefficient for forced water convection depends on Reynolds number and turbulence conditions. The actual heat transfer coefficient for water might be in the range from 500 $\frac{W}{m^2K}$ to 5000 $\frac{W}{m^2K}$, and is a main parameters that must be determined experimentally, see section 6.2.

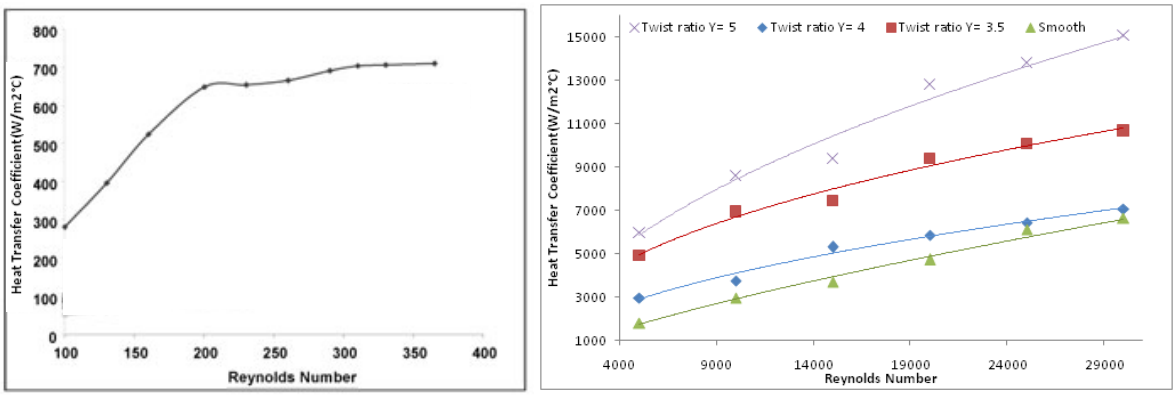

Figure 5.2. The heat transfer coefficient for forced water convection as function of Reynolds number. Figure a) shows for low Reynolds numbers [Alagesan and Sundaram], and figure b) shows for high Reynolds numbers at different turbulence enhancement levels [Al-Saiman and Thamer].

An analytic study for each of the four elements along the x axis is set up, starting with the centre laminations 1.1.

Element 1.1

Because of symmetry over the y-z plane, the left side (x=0) of element 1.1 is as adiabatic, which means that the temperature gradient is equal to zero. This provides the first boundary condition, see equation 5.11

$$\left.\frac{dT}{dx}\right|_{x=0} = 0 \tag{5.11}$$

The first integration constants C_1 is determined by substitution equation 5.11 into equation 5.9.

$$\begin{aligned} 0 &= -\frac{q_{i1} \cdot 0}{k} + C_1 \\ &\Updownarrow \\ C_1 &= 0 \end{aligned} \tag{5.12}$$

The second integration constant C_2 is determined from the boundary condition at the right side of element 1.1 at x=0.0195 m, where cooling water at a temperature of $T_{\infty C}$ and with a heat transfer coefficient of h_C is flowing. This gives a convection boundary condition, see equation 5.13.

$$q''_{11} = h_C(T_{0.0195} - T_{\infty C}) \tag{5.13}$$

The heat flux q''_{11} is equal to the total heat flux generated in element 1.1, given by the volumetric heat generation ($q\dot{}_{11}$) times the length (Δx_{11}). This means that the surface temperature of element 1.1, exposed to water can be determined as:

$$\begin{aligned} q\dot{}_{11} \cdot \Delta x_{11} &= h_C(T_{0.0195} - T_{\infty C}) \\ &\Updownarrow \\ T_{0.0195} &= T_{\infty C} + \frac{dotq_{11} \cdot \Delta x_{11}}{h_C} \end{aligned} \tag{5.14}$$

Substituting equation 5.14 into equation 5.10 gives an expression for C_2, equation see 5.15.

$$\begin{aligned} T_{\infty C} + \frac{q\dot{}_{11} \cdot \Delta x_{11}}{h_C} &= -\frac{q\dot{}_{11} \cdot x_{11}^2}{2k} + C_2 \\ &\Updownarrow \\ C_2 &= \frac{q\dot{}_{11} \cdot x_{11}^2}{2k} + \frac{q\dot{}_{11} \cdot \Delta x_{11}}{h_C} + T_{\infty C} \end{aligned} \tag{5.15}$$

C_2 is calculated using the value given in figure 5.1, see equation 5.16.

$$C_2 = \frac{1.32 \cdot 10^6 \cdot 0.0195^2}{2 \cdot 30} + \frac{1.32 \cdot 10^6 \cdot (0.0195 - 0)}{1000} + 50 = 84 \tag{5.16}$$

The simplified analytic solution to the temperature distribution along the x-axis in element 1.1 is thereby given in equation 5.17.

$$T(x) = -\frac{1.32 \cdot 10^6 \cdot x^2}{2 \cdot 30} + 84 \tag{5.17}$$

The maximum temperature is 84° C at x=0 m, while the minimum is 76° C at x=0.0195 m.

Element 1.2

The temperature distribution in the slot winding (element 1.2), is solved by nearly the same procedure. The only difference is that the first boundary condition is applied to the mid plane of element 1.2, as this is adiabatic because of symmetrical boundary conditions on the left and right side, which means that q''_{12left} equals $q''_{12right}$. The detailed analytic calculations for element 1.2, 1.3 and 1.4 can be found in appendix A.

The analytic expression for the temperature distribution in element 1.2 is given in equation 5.18

$$T(x) = -\frac{0.9 \cdot 10^6 \cdot x^2}{2 \cdot 0.72} + 35630 \cdot x - 391 \tag{5.18}$$

The maximum temperature in the element is 117° C at the mid plane (x=0.0285 m), while the minimum temperature is 62° C at the boundaries (x=0.0195=0.0375 m).

Element 1.3

The temperature distribution for element 1.3 can not be solved analytic, as the distribution between the heat flux q''_{13left} and $q''_{13right}$ is coupled to the unknown left and right surface temperatures of the element. This gives four unknown, and only three equation: The left and right boundary conditions, plus the energy balance equation ($q_{13} \cdot \Delta x_{13} = q''_{13left} + q''_{13right}$). An approximation of the temperature distribution is made by assuming that the right side of element 1.3 is adiabatic, as $q''_{13left} >> q''_{13right}$ because of the low thermal conductivity of epoxy, combined with the low heat transfer coefficient of air at the right side of the epoxy. Making this assumption makes element 1.3 a mirror image of element 1.1, meaning that the maximum temperature arise between elements 1.3. and 1.4 and will be 85° C. The actual maximum temperature will be lower than the calculated, because of the ignored heat transfer through the epoxy element 1.4.

Using the assumption of an adiabatic boundary condition, gives the expression seen in equation 5.19 for the temperature distribution in element 1.3.

$$T(x) = -\frac{1.32 \cdot 10^6 \cdot x^2}{2 \cdot 30} + 2530 \cdot x - 12.46 \tag{5.19}$$

Element 1.4

The general heat transfer equation reduces to $\frac{d^2T}{dx^2} = 0$, as there is no internal heat generation in element 1.4. This means that the temperature distribution becomes $T(x) = C_1 \cdot x + C_2$, i.e. a linear declining line towards the right side of element 1.4. Unfortunately it is impossible to determine the two integration constants, as the heat flux through element 1.4 is unknown. Using the same assumption as used in element 1.3 ($q''_{13right} = 0 = q''_{14}$), means that the temperature is constant through element 1.4.

Assembled Temperature Profile

The assembled analytic temperature profile along the x axis is seen in figure 5.3.

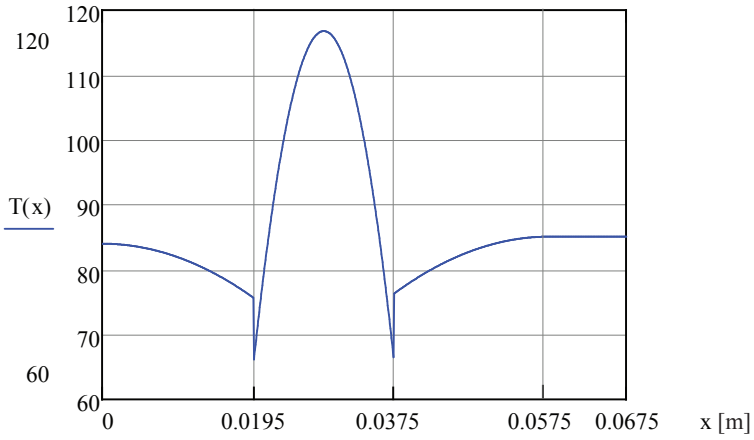

Figure 5.3. The assembled analytic temperature profile along the x axis.

The temperature profile appears to be discontinuous at x=0.0195 m and x=0.0375. This is because the cooling channels are assumed to be of negligible width.

The maximum temperature of 117° C is seen to arise in the winding, mainly because of the low conductivity of the resin that surrounds the winding. The temperature is below the maximum allowable temperature of 155° C, thereby indicating that the enhanced core cooling system has potential to cool the PMSM in the water chiller.

The next section describes the lumped parameter thermal model of the transformer.

5.2 GD Novel Lumped Parameter

A conventional lumped parameter model is a simple way to describe a thermal system. The system is divided into a number of elements from geometric and thermal properties. Each element is represented by a central node, and the notes are connected by thermal conduction resistances and capacitors. For steady state analysis, the model may be simplified by omitting the thermal capacitance.

The lumped parameter model is a concentrated loss model, as the distributed power loss from an element is applied to the central node in the element. This entail an uncertainty, and a compensation method has to be introduces. In [Mathiasen and Olesen, 2014] a study of several heat sources compensation methods is made, and compared to analytic and as well as FEM solutions. [Mathiasen and Olesen, 2014] concludes that the novel GD [Gerling and Dajaku] is the most appropriate and accurate compensation method for multiple dimensions systems, when symmetry is applied. The GD novel lumped parameter is chosen on this basis.

5.2.1 Electrical Analogue

The parameters in a thermal lumped parameter model has analogue electrical parameters [Incropera et al., 2006], hence the laws for electrical circuits may be used for thermal circuits, see table 5.1.

Electric	**Unit**	**Thermal**	**Unit**
Current (I)	[A]	Heat flow (P)	[W]
Voltage (U)	[V]	Temperature (T)	[K/$^{\circ}C$]
Resistance (R)	[Ω]	Resistance (R)	[K/W]
Conductivity (k)	$[A/(Vm)]$	Conductivity (k)	[W/(m K)]
Ohm's law	U=RI	Fourier's law	ΔT=RP
Kirchhoff's current law	$\sum I_{in} = \sum I_{out}$	Energy equilibrium	$\sum P_{in} = \sum P_{out}$

Table 5.1. Analogy between electrical and thermal circuit parameters, [Incropera et al., 2006].

Thermal capacitances are not included, as only steady state temperatures is of interest.

5.2.2 Thermal Resistances

Four different types of thermal resistances are used in a thermal lumped parameter model:

- Conduction resistance: The elements ability to transport heat internally.
- Convection resistance: The surroundings ability transport heat over an element surface by convection.
- Radiation resistance: The elements/surroundings ability to transport heat over a surface by radiation.
- Contact resistance: The elements ability to transport heat between each other.

A cuboid element in a cartesian coordinate system has three thermal resistances, one in each direction; x,y and z.

Conduction Resistance

The heat transfer by conduction is given by equation 5.20, [Incropera et al., 2006].

$$P_{cond} = \frac{\Delta T k A}{l} \tag{5.20}$$

Using Fourier's law in equation 5.20, gives the conduction resistance, see equation 5.21.

$$R_{cond} = \frac{l}{kA} \tag{5.21}$$

The conduction resistance of an element is calculated from its length (l) in the desired resistive direction, the perpendicular cross sectional areal (A) and the thermal conductivity (k) in the length

direction. The node representing the element is located in the geometric/resistive centre, see figure 5.4, why the conductive resistance is split in two halves, see equation 5.22.

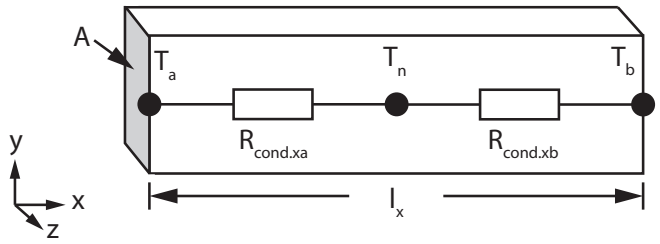

Figure 5.4. Classical lumped parameter one-dimensional thermal element.

$$R_{cond.xa} = R_{cond.xb} = \frac{l_x}{2kA} \tag{5.22}$$

Convection Resistance

The convection resistance depends on the thermal properties of the ambient medium. The transformer is surrounded by air and cooled by water inside. The convection resistance is derived from equation 5.3 using Fourier's law, and is given in equation 5.23.

$$R_{conv} = \frac{1}{h_{conv}A} \tag{5.23}$$

It is seen that the convection resistance depends on the surface area in contact with the ambient medium, and the heat transfer coefficient (h_{conv}).

Radiation

The radiation resistance is calculated using Fourier's law in equation 5.1.

$$R_{rad} = \frac{1}{h_{rad}A} \tag{5.24}$$

Where the heat transfer coefficient for radiation, h_{rad}, is given by equation 5.25.

$$h_{rad} = \frac{\sigma_{SB}\varepsilon(T_a^4 - T_b^4)}{T_a - T_b} \tag{5.25}$$

It is seen that the heat transfer coefficient for radiation, and thereby the radiation resistance, depends on the ambient and element surface temperatures. This means that the lumped parameter model, when radiation is included, has to be solved iteratively to estimate the element surface temperature.

Contact Resistance

Contact resistances are introduced to allow for small air gaps, that will arise when different elements in a structure are assembled. Equation 5.26 is used to calculate the contact resistance. The equivalent thickness t_{eq} of the gab between elements depends on surface roughness.

$$R_{cont} = \frac{t_{eq}}{k_{cont} A} \tag{5.26}$$

No contact resistances are used in the lumped parameter model of the transformer, as the transformer is moulded into epoxy, which is supposed to penetrate all gaps.

5.2.3 Heat Sources and Cooling

Applying the total power loss to the internal element note, will result in over predicting the internal temperature. A simple solution is to apply only half of the actual power loss. This works fine for a single element, but when a thermal system consisting of several elements are analysed, the omitted half part of the power loss is going to be missing in the neighbour elements, leading to underestimations of the temperature.

In the GD novel compensation method, the total power loss is applied in the central node. To avoid internal temperature overestimation, a compensation temperature T_{comp} is subtracted from the internal temperature, [Gerling and Dajaku]. The compensation temperature is given in equation 5.27.

$$T_{comp} = R_a \frac{P_{loss\,a}}{2} \tag{5.27}$$

Where R_a is the thermal resistance between the central note and the boundary of the element, and $P_{loss\,a}$ is the part of the heat loss going from the central note through R_a.

The diagram for a heat source element is seen in figure 5.5.

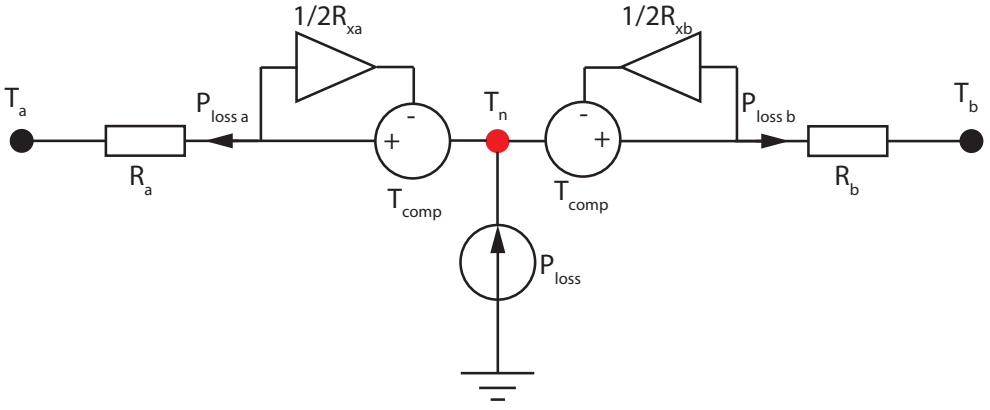

Figure 5.5. Novel GD heat source compensation.

The temperature of the central note can be calculated by equation 5.28.

$$T_n = T_a + R_a \cdot P_{lossa} - T_{comp} = T_a + R_a \frac{P_{lossa}}{2} \tag{5.28}$$

The water cooling and the ambient is introduced in the lumped parameter model as constant temperatures, see figure 5.6. The thermal cooling resistance R_{co} is calculated from equation 5.23.

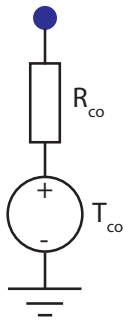

Figure 5.6. Lumped parameter cooling note.

5.2.4 Model

A simplified lumped parameter model of the transformer is constructed in this section.

Geometry Considerations

The transformer is assumed to be symmetric over the three planes stretched between the x-y, x-z and y-z axis. This assumption allows to model an eight part of the transformer. The origo and axis convention for the eight part lumped parameter model is shown in figure 5.7.

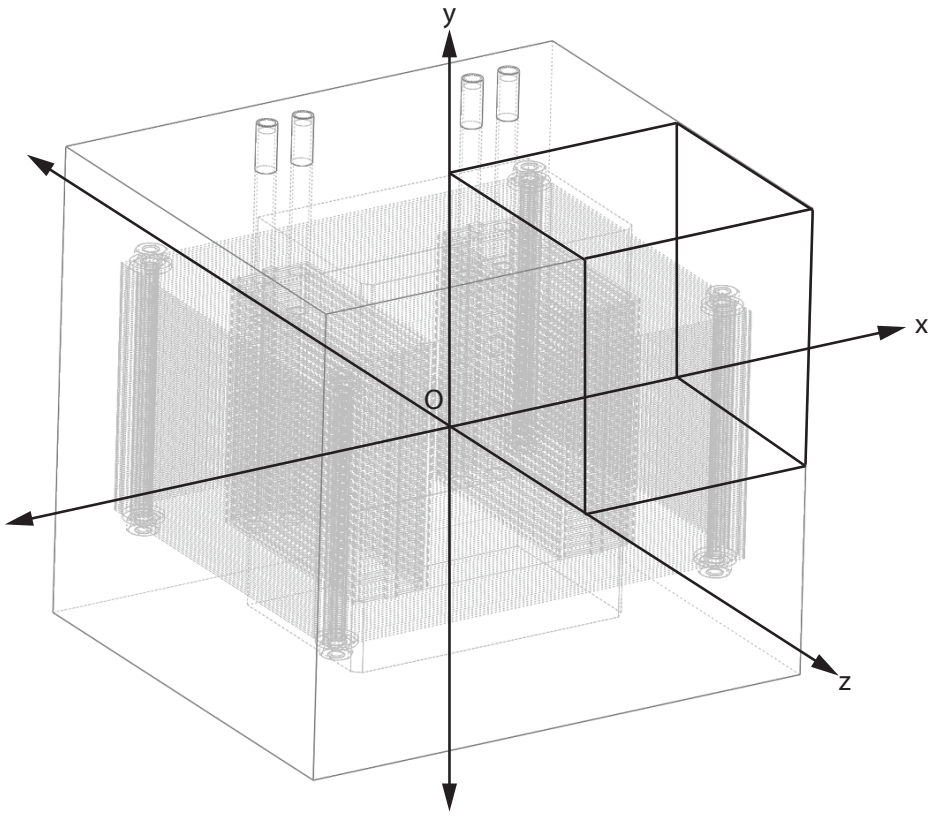

Figure 5.7. The black box shows the modelled eight part of the transformer. The origo (O) and the axis convention for the lumped parameter model relates to this figure.

Thermal Resistive Elements

The modelled eight part of the transformer is divided into three planes in the z-direction, and each plane is divided into a number of elements. The division is made on basis of geometric and thermal properties. Figure 5.8 shows the model elements, the red numbers states the number of the elements, where the first digit in the element number refers to the plane. The elements are coloured by material: Grey elements are core laminates, yellow elements are windings/epoxy and green elements are epoxy.

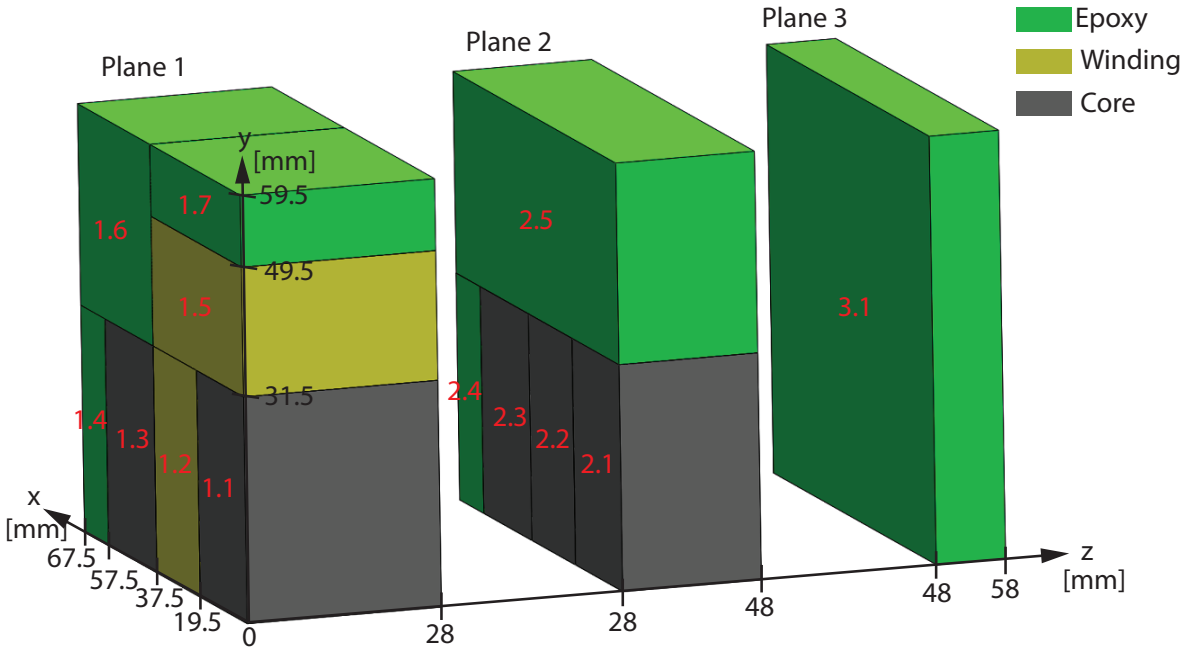

Figure 5.8. The elements of the lumped parameter model. Red numbers states the element numbers. Grey elements are core laminates, yellow elements are windings/epoxy and green elements are epoxy.

Plane 1 consists of seven elements, plane 2 consists of five elements and plane 3 consists of one element. In total 13 elements. The elements and their properties are listed in table 5.2.

Element no.	**Material**	**Dimension (x,y,z) [mm]**	**Conductivity (x,y,z) [$\frac{W}{mK}$]**	**Resistance (x,y,z) [$\frac{K}{W}$]**
1.1	Laminations	(19.5, 31.5, 28.0)	(30, 1.5, 30)	(0.74, 38.50, 1.52)
1.2	Copper/epoxy	(18.0, 31.5, 28.0)	(0.61, 401, 0.61)	(28.24, 1.00, 68.32)
1.3	Laminations	(20.0, 31.5, 28.0)	(30, 1.5, 30)	(0.76, 37.5, 1.48)
1.4	Epoxy	(10.0, 31.5, 28.0)	(0.61)	(18.59, 184.43, 145.72)
1.5	Copper/epoxy	(37.5, 18.0, 28.0)	(401, (0.61 · 2.5), 0.61)	(1.19, 9.49, 145.71)
1.6	Epoxy	(30.0, 28.0, 28.0)	(0.61)	(62.73, 54.64, 54.64)
1.7	Epoxy	(37.5, 10.0, 28.0)	(0.61)	(219.56, 15.61, 122.40)
2.1	Laminations	(19.5, 31.5, 20.0)	(30, 1.5, 30)	(1.03, 53.85, 1.09)
2.2	Laminations	(18.0, 31.5, 20.0)	(30, 1.5, 30)	(0.95, 58.33, 1.18)
2.3	Laminations	(20.0, 31.5, 20.0)	(30, 1.5, 30)	(1.06, 52.50, 1.06)
2.4	Epoxy	(10.0, 31.5, 20.0)	(0.61)	(26.02, 258.20, 104.09)
2.5	Epoxy	(67.5, 28.0, 20.0)	(0.61)	(197.60, 34.00, 17.35)
3.1	Epoxy	(67.5, 59.5, 10.0)	(0.61)	(185.98, 144.51, 4.08)
$R_{x,tape}$	Electrical tape	(2·0.083, 31.5, 28.0)	(0.141)	(1.33, -, -)
$R_{z,tape}$	Electrical tape	(18.0, 31.5, 2·0.083)	(0.141)	(-, -, 2.08)
$R_{x,fin}$	Laminations fins	(1.0, (0.5 · 31.5), 28.0)	(30)	(0.08, -, -)
$R_{z,fin}$	Laminations fins	(18.0, (0.5 · 31.5), 1.0)	(30)	(-, -, 0.12)

Table 5.2. Lumped parameter element properties.

In addition to the 13 elements, four thermal resistances are listed in table 5.2. $R_{x,tape}$ and $R_{z,tape}$ are thermal conduction resistances counting for the electrical tape used to isolate the windings from the core laminates and water cooling channels. The thickness of the tape is multiplied by two because a double layer of tape is used. $R_{x,fin}$ and $R_{z,fin}$ are thermal conduction resistances, counting for the heat conduction through the lamination fins that connects the slot winding element to the surrounding core elements. The y dimension of these elements are multiplied by 0.5, as the cooling channels takes half of the cross sectional area.

Epoxy elements are assumed to be thermally isotropic, why only one value for thermal conductivity is given in table 5.2.

The thermal conductivity of the laminations depends on the silicon content, and varies from $40\frac{W}{mK}$ to $20\frac{W}{mK}$ when the silicon percentage varies from 1 % to 5 % [Staton et al., 2003]. The silicon percentage in the lamination steel is unknown, why an average thermal conductivity of 30 $\frac{W}{mK}$ in the laminate plane (x,z) is chosen.
The core is an orthotropic material because of the insulation between the laminations, which reduces the thermal conductivity in the normal direction to the laminate plane to approximately $\frac{1}{20}$ [Staton et al., 2003], corresponding to 1.5 $\frac{W}{mK}$.

The winding elements are modelled as an orthotropic material as well, because the thermal conductivity is better along the conductors than perpendicular to the conductors. The winding elements consists of copper and epoxy, see figure 5.9a.

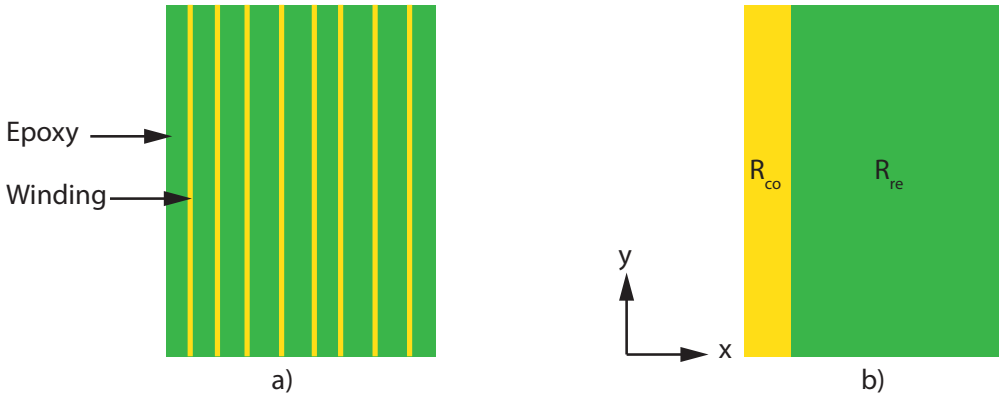

Figure 5.9. Figure a) shows a winding element consisting of winding (yellow) cast into resin (green). Figure b) shows a simplified model of the winding element consisting of two thermal resistances.

Figure 5.9b shows a simplified model of the winding element consisting of two thermal resistances, R_{co} and R_{re}. The resistances are serial connected in the x direction and parallel connected in the y direction.

As an example, the thermal resistance for winding element 1.2 is calculated in both the x- and y direction. Epoxy and copper has a thermal conductivity of 0.61 $\frac{W}{mK}$, and 401 $\frac{W}{mK}$ respectively. The copper fill factor is calculated to K_{co}=0.156 in equation 3.3.

The thermal resistance of copper in the x direction is calculated in equation 5.29.

$$R_{cond(xco)} = \frac{l_x \cdot K_{co}}{k_{co} \cdot A_{yz}} = \frac{0.018m \cdot 0.156}{401\frac{W}{mK} \cdot 0.000882m^2} = 0.0079\frac{K}{W} \tag{5.29}$$

The thermal resistance of resin in the x direction is calculated in equation 5.30.

$$R_{cond(xre)} = \frac{l_x \cdot (1-K_{co})}{k_{re} \cdot A_{yz}} = \frac{0.018m \cdot (1-0.156)}{0.61\frac{W}{mK} \cdot 0.000882m^2} = 28.24\frac{K}{W} \tag{5.30}$$

The total resistance in the x direction is calculated in equation 5.31

$$R_{cond(xtot)} = R_{cond(xco)} + R_{cond(xre)} = 0.0079\frac{K}{W} + 28.24\frac{K}{W} = 28.25\frac{K}{W} \tag{5.31}$$

It is seen that the thermal resistance of the resin is dominating in the direction perpendicular to the winding, why the thermal resistance of the copper can be neglected in this direction. Equation 5.30 is therefore used to calculate the thermal resistance for the winding elements, perpendicular to the winding.

The thermal resistance of copper in the y-direction is calculated in equation 5.32.

$$R_{cond(yco)} = \frac{l_y}{k_{co} \cdot A_{xz} \cdot K_{co}} = \frac{0.0315m}{401\frac{W}{mK} \cdot 0.000504m^2 \cdot 0.156} = 0.99\frac{K}{W} \tag{5.32}$$

The thermal resistance of resin in the y direction is calculated in equation 5.33.

$$R_{cond(yre)} = \frac{l_y}{k_{re} \cdot A_{xz} \cdot (1-K_{co})} = \frac{0.0315m}{0.61\frac{W}{mK} \cdot 0.000504m^2 \cdot (1-0.156)} = 121.40\frac{K}{W} \tag{5.33}$$

The total resistance in the y direction is calculated in equation 5.34

$$R_{cond(ytot)} = \frac{R_{cond(yco)} \cdot R_{cond(yre)}}{R_{cond(yco)} + R_{cond(yre)}} = \frac{0.99\frac{K}{W} \cdot 121.40\frac{K}{W}}{0.99\frac{K}{W} + 121.40\frac{K}{W}} = 0.991\frac{K}{W} \tag{5.34}$$

It is seen that the thermal resistance of the copper is dominating in the direction of the winding, why the thermal resistance of the resin can be neglected in this direction. Equation 5.32 is therefore used to calculate the thermal resistance for the winding elements, parallel to the winding.

The model contains two winding elements, 1.2 and 1.5. The orthotropy of element 1.5 is rotated 90° compared to element 1.2, because of the winding orientation. In reality element 1.2 and 1.5 are connected through the winding, which gives a good conductivity between the two elements. It is difficult to model this connection, without introducing a third element as the corner connecting the two elements. A solution to the problem is to multiply the conductivity in the y direction of element 1.5 by a factor greater than one, thereby enforcing the conductivity between element 1.2 and 1.5. Experiments shows that a factor of 2.5 is convenient. This "trick" entail some errors, e.g. the conductivity between element 1.1 and 1.5 will also be enforced. It is assumed that errors are minor, but it should be kept in mind when the results are judged.

Convection Resistances

In addition to the thermal conduction elements, the model contains a number of convection resistances to the ambient air and the cooling water. These are calculated from equations 5.23, and listed in table 5.3. The heat transfer coefficients for forced water convection and the ambient air, is set to 1000 $\frac{W}{m^2K}$ and 9.1 $\frac{W}{m^2K}$, respectively. The actual thermal resistances, used in the lumped parameter model, depends on the heat transfer coefficients for forced water convection. The heat transfer coefficient is found to depend on Reynolds number, and will therefore depend on the applied flow rate of cooling water, see section 6.2. The thermal resistances seen in table 5.3 is only shown to get an overview of their general magnitude.

Name	**Type**	**Resistance [$\frac{K}{W}$]**
$R_{x,cool}$	Water convection	1.13
$R_{z,cool}$	Water convection	1.76
$R_{x,amb14}$	Air convection	124.59
$R_{x,amb16}$	Air convection	140.17
$R_{y,amb16}$	Air convection	130.82
$R_{y,amb17}$	Air convection	104.66
$R_{x,amb24}$	Air convection	174.43
$R_{x,amb25}$	Air convection	196.23
$R_{y,amb25}$	Air convection	81.40
$R_{x,amb31}$	Air convection	184.69
$R_{y,amb31}$	Air convection	162.80
$R_{z,amb31}$	Air convection	27.36

Table 5.3. Water cooling and ambient air convection resistances.

The first index of a resistance indicates the effective direction (x, y or z), and the second index indicates what two elements or mediums the resistance is crossing, e.g. $R_{x,amb31}$ is in x-direction from the ambient air to element 3.1.

It is seen that the resistances to the cooling water is two decades lower than the resistances to the ambient air. This indicates how effective the water cooling is compared to the natural air cooling.

No outer surface radiation resistances are listed, as these depends on the surface temperature, why they

will change depending on the loss in the transformer. It is decided to neglect radiation in the lumped parameter model, as it stands for a small part of the total heat dissipation from the transformer. The error introduced by omitting radiation is investigated in section 7.1.

Thermal Network

The element nodes are placed in the centre of each element, except for the elements next to symmetry planes, where the notes are placed at the symmetry planes. This means that the notes in plane 1 are placed at z=0 mm, notes in plane 2 are placed at z=38 mm and the notes in plane 3 are placed at z=53 mm.

The three thermal networks in the x-y plane are seen in figures 5.10, 5.11 and 5.12. The red notes are heat sources, the blue notes are cooling and the black notes are passive.

Plane 1, z=0 mm.

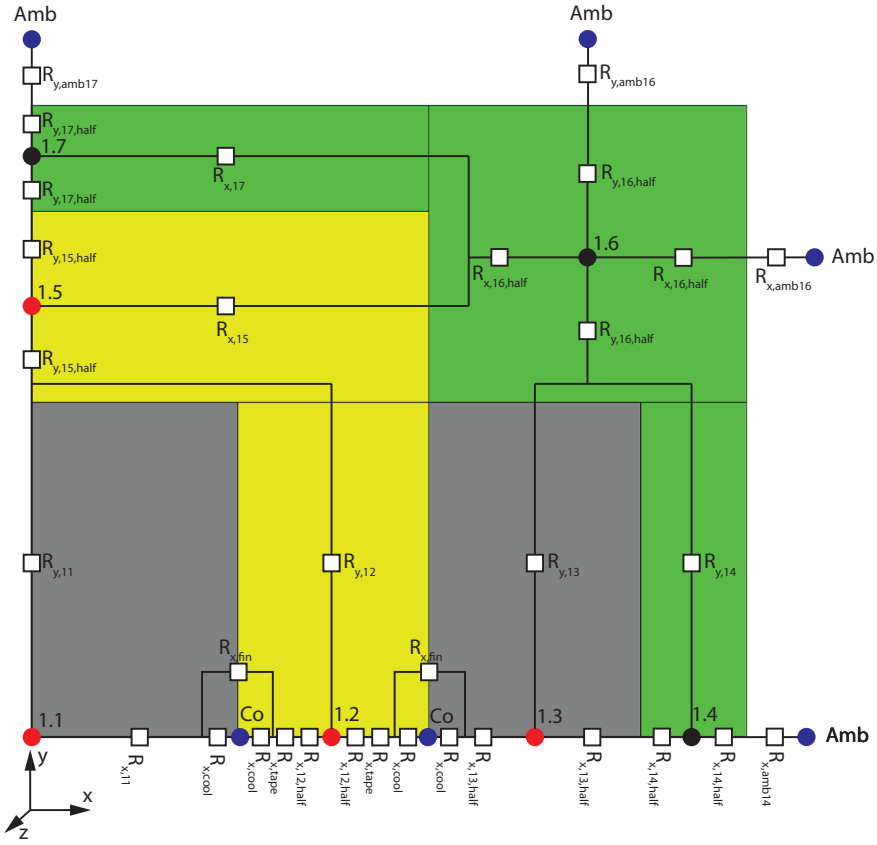

Figure 5.10. The thermal network in plane 1, z=0 mm.

The fin conduction resistances and the cooling water convection resistances, between the slot winding element and the surrounding core elements, are parallel connected, as the interface between these elements are a mix of conduction through the fins and convection to the cooling water.
Surface radiation could be included in the model by connecting radiation resistances in parallel with the ambient convection resistances.

Plane 2, z=38 mm.

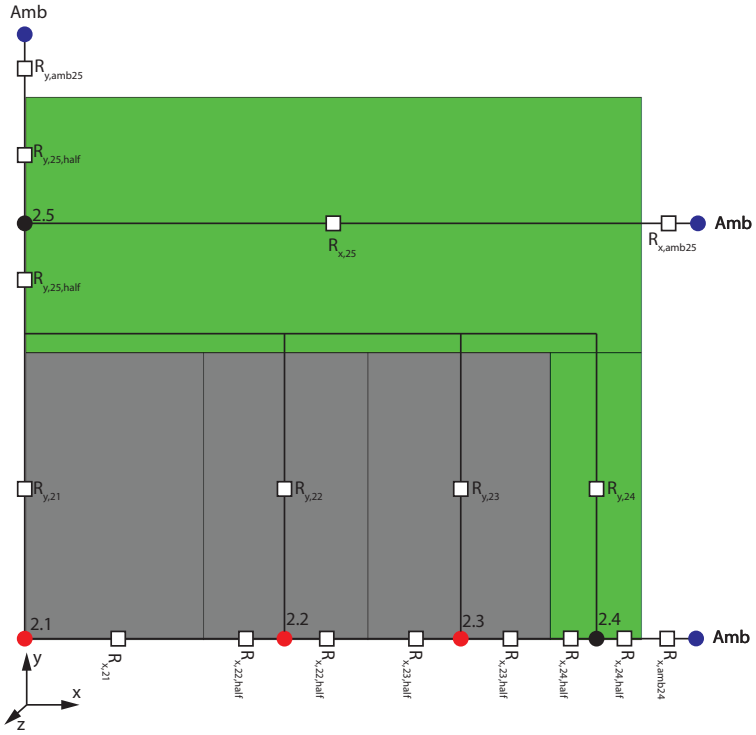

Figure 5.11. The thermal network in plane 2, z=38 mm.

Plane 3, z=53 mm.

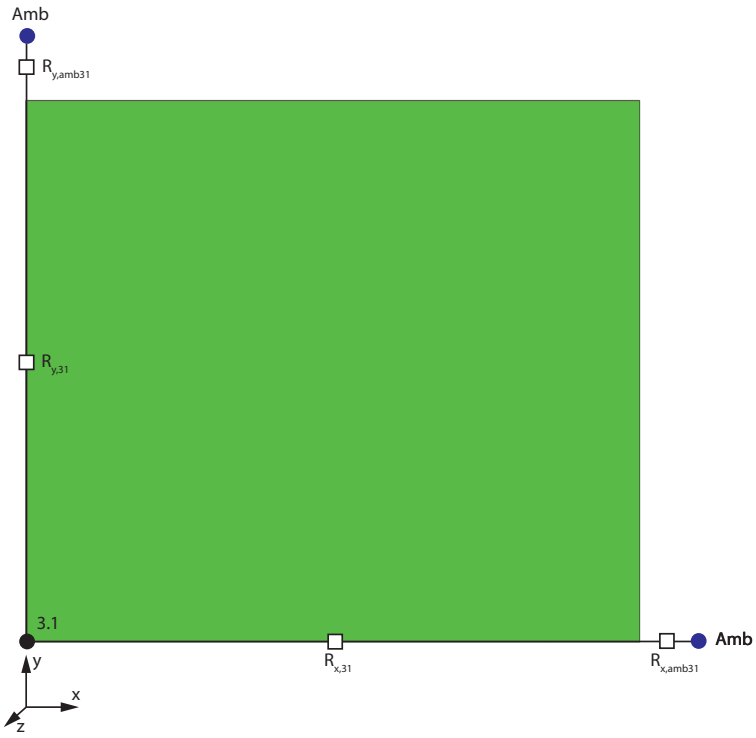

Figure 5.12. The thermal network in plane 3, z=53 mm.

The three thermal networks from plane 1, 2, and 3 are assembled in the z-direction, see figure 5.13. The bold lines represent the three xy-planes. Thermal resistances and connection in the xy-planes are omitted to increase the overview.

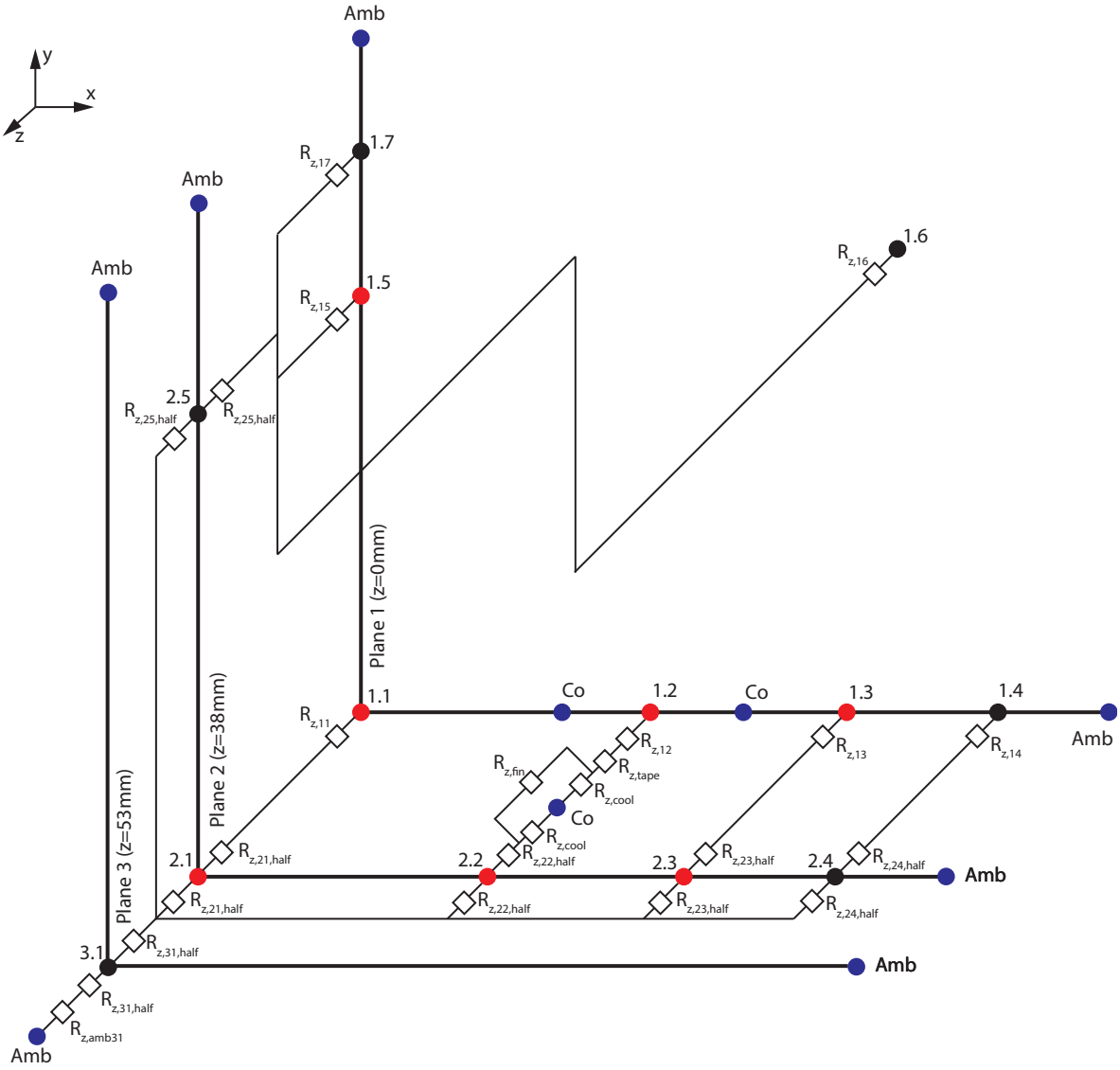

Figure 5.13. The thermal network in the z-direction.

The thermal network is build in Simulink/PLECS, and every heat source is implemented as shown in figure 5.5 and the cooling/ambient is implemented as shown in figure 5.6. The thermal model is found at the appendix CD (*Matlab/thermalmodel_V3.slx*). The thermal resistances used in the lumped model are calculated in a Matlab script, also found at the appendix CD (*Matlab/thermalconstants.m*). The model is solved using the ode45 variable step Dormand-Prince solver, which is the default solver in Simulink [Matlab, 2015]. The solver performs fast and stable, why no other solvers are attempted.

5.3 Thermal FEM Analysis

The thermal FEM (Finite Element Method) study is conducted in Solidworks simulation. It is convenient to use Solidworks as a geometric model of the transformer is constructed in this program, thereby gathering the preprocessing, solving and postprocessing in the same program. The FEM analysis entails the following steps:

- Create geometry.
- Define material properties.
- Define contact sets between material blocks.
- Apply heat sources.
- Apply boundary conditions (convection and radiation).
- Mesh.
- Solve problem.
- Plot results.

The thermal FEM analysis is set up similar to the lumped parameter model, using the same simplified cuboid material blocks, material conductivities and heat transfer coefficients for convection and radiation. The heat sources are implemented as volumetric distributed, which better represent the reality than the concentrated loss model used in the lumped parameter. Convection and radiation at the outer surface of the transformer, and from the water cooling is modelled as boundary conditions. The main advantage of the FEM analysis over the lumped parameter, is that the temperature is evaluated in all the finite elements, and not just in the centre of the material blocks. This allows to discover hot spots, that the lumped parameter did not reveal.

The mesh is made of 223246 tetrahedron elements with four Jacobian points each. The tetrahedron elements is the default element type in Solidworks, like in most other FEM programs, as they can be used for any geometry and are the only kind of elements that can be used with adaptive mesh refinement [Comsol, 2013]. The FEM model is found at the appendix CD ($Solidworks/Transformer\,Thermal\,model/thermalmodel$).

The meshed FEM model is seen in figure 5.14.

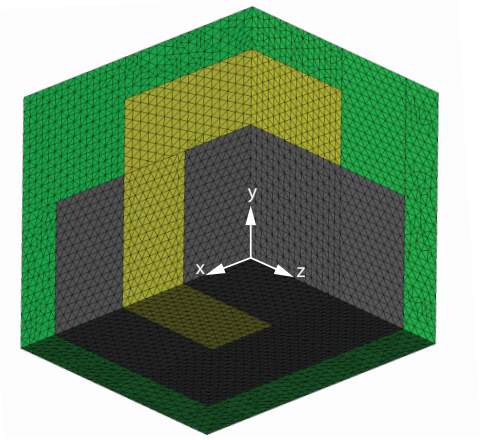

Figure 5.14. The meshed FEM model.

5.4 Fluid Flow/Thermal CFD analysis

The final model is a Computational Fluid Dynamics (CFD) model. The CFD model is intended to resemble the real transformer and cooling system in details.

The CFD analysis is conducted by solving a set of partial differential equations (PDE) describing the flow and heat transfer. The PDS's have their basis in physics laws e.g. conservation of mass and energy, equilibrium of momentum and continuity equations. Solidworks flow simulation uses the finite volume method (FVM) to solve the PDE's. FVM solves the PDE's in integral form, which is beneficial in fluid problems, as the boundary conditions often are given as derivatives e.g. flow [Versteeg and Malalasekera, 2012].

The fluid domain can be seen in figure 5.15.

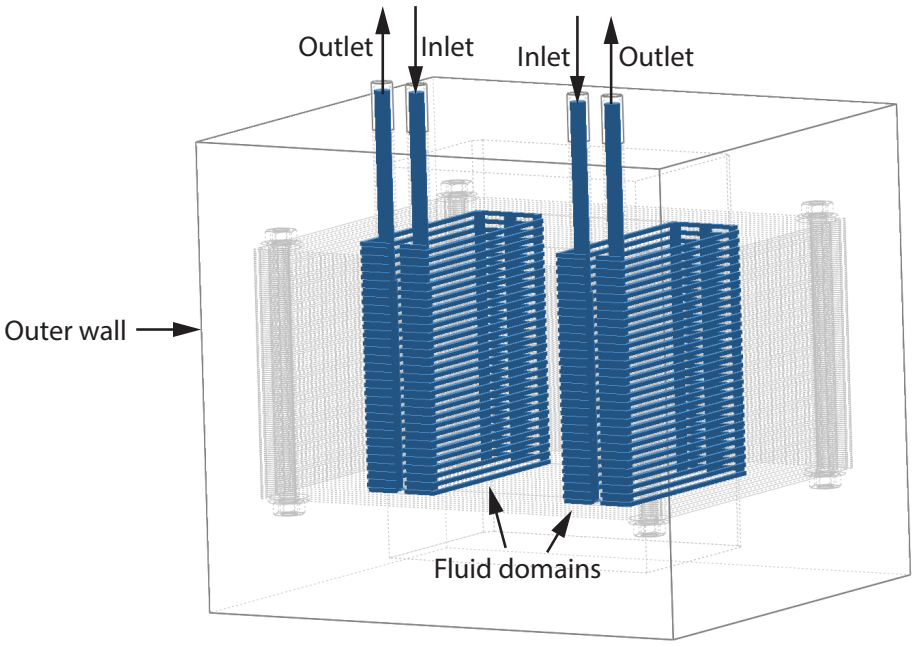

Figure 5.15. The fluid domain, inlets, outlets and outer wall of the CFD model.

The fluid as well as the solids is divided in small elements by a build in mesh generator. The mesh is generated by specifications of the minimum gabs in the fluid and solids, respectively. Further mesh refinement is conducted to capture all details in the cooling system. The mesh consist of 1638342 fluid cells, 1323563 solid cells and 1987420 partial cells. The partial cells are used to model the boundary walls between fluid and solid domains.

In the CFD model the flow and boundary layer are assumed laminar, as Reynolds number in the cooling channels do not exceed 2000 in any of the experiments.

The inlet condition is given by mass flow, and the outlet condition is given by an environmental pressure of 101325 Pa. The surrounding epoxy shell is modelled as a wall, allowing both convection and radiation heat transfer to the ambient air. Two volumetric distributed heat sources are included, the

core laminates and the winding. All solid materials are modelled, this entails core laminates, epoxy, steel core clamps, plastic manifolds and stainless steel needle tubes. The winding is modelled as ten separate squared turns, each with a cross sectional area corresponding to the 20 parallel wires in the actual turn. The medium length of each turn is 300 mm, as in the real winding. The ten turns are surrounded by resin, see figure 5.16.

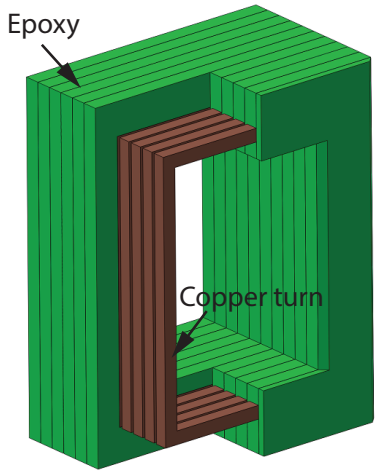

Figure 5.16. The winding element in the CFD model.

The CFD model is found at the appendix CD (*Solidworks/Transformer/transformer_finish.SLDASM*).

Thermal parameters for the developed models are experientially determined in the next chapter.

Thermal parameter determination 6

Initially, the heat transfer coefficients for the ambient air convection and for the forced cooling water convection was set to 8 $\frac{W}{m^2K}$ and 1000 $\frac{W}{m^2K}$ respectively. The emissivity ε of the epoxy was set to 0.91. These constants needs to be verified experimentally and adjusted to resemble the experiments.

6.1 Ambient Air heat Transfer Coefficient and Epoxy Emissivity

Two 200 Hz AC experiments with power losses of respectively 40.9 W and 83.5 W are conducted. The Enhanced Core Cooling is disabled during the experiments, which means that the power loss has to be removed by convection and radiation to the ambient. These experiments serves to determine the heat transfer coefficient of the ambient air and the emissivity ε of the epoxy.

Figure 6.1a and 6.1b shows the temperatures on the back xy, top xz and left yz surface, where the axis are crossing the surfaces planes, for the power losses of 40.9 W and 83.5 W, respectively. The 83.5 W experiment is stopped before steady state temperatures are reached, as the winding temperatures exceeded 155° C. A graphical extrapolation of the average surface temperature is made and showed as a stippled line.

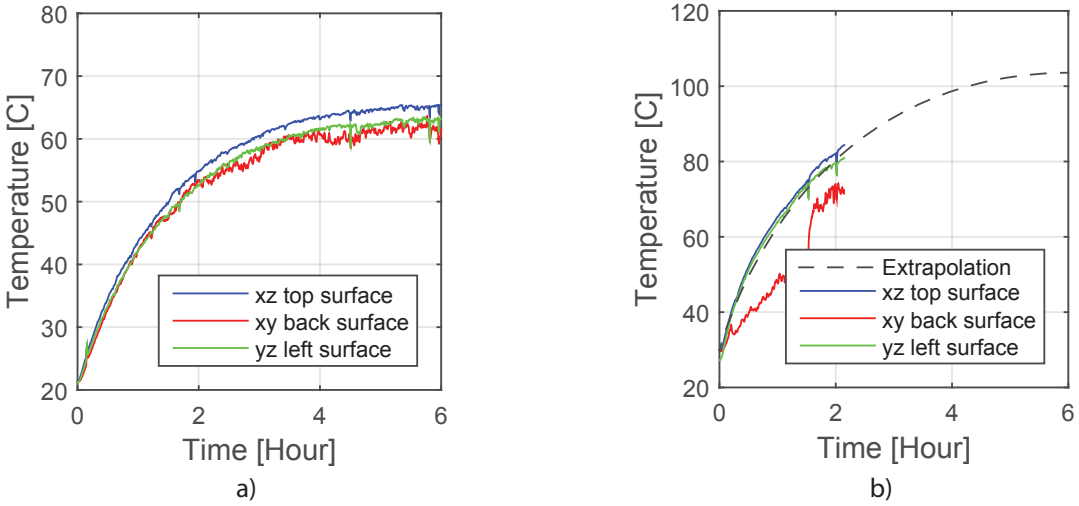

Figure 6.1. Back xy, top xz and left yz surface planes temperatures when the transformer is exposed to AC current, and the Enhanced Core Cooling system is disabled. Figure a) shows for a power loss of 40.9 W, and figure b.) shows for a power loss of 83.5 W, the stippled line is a graphical extrapolation of the experimental data.

The average steady state surface temperature at the 40.9 W and 83.5 W experiments are determined to 63° C (336 K) and 104° C (377 K), respectively. The ambient air temperature is 21° C (294 K) and the surface area of the transformer is 0.0911 m^2.
The energy balance equation seen in 6.1, is set up for the experiments.

$$P_{loss} = P_{conv.air} + P_{rad} \tag{6.1}$$

Substituting equation 5.3 and 5.1 into the energy equation gives equation 6.2.

$$P_{loss} = h_{air} A \Delta T + \sigma_{SB} A \varepsilon (T_a^4 - T_b^4) \tag{6.2}$$

Using the data from the two experiments gives two equation with two unknown,see equation 6.3.

$$\begin{aligned} 40.9W &= h_{air} 0.0911 m^2 (336K - 294K) + 5.67 \cdot 10^{-8} \frac{W}{m^2 K^4} \varepsilon \left((336K)^4 - (294K)^4 \right) \\ 83.5W &= h_{air} 0.0911 m^2 (377K - 294K) + 5.67 \cdot 10^{-8} \frac{W}{m^2 K^4} \varepsilon \left((377K)^4 - (294K)^4 \right) \end{aligned} \tag{6.3}$$

Solving the equations with respect to the ambient air heat transfer coefficient and the epoxy emissivity, results in $h_{air} = 9.1 \frac{W}{m^2 K}$ and $\varepsilon = 0.22$. An ambient air heat transfer coefficient of 9.1 $\frac{W}{m^2 K}$ is in the expected range, as the literature research in [Mathiasen and Olesen, 2014] concludes that 8 $\frac{W}{m^2 K}$ is reasonable. The epoxy emissivity of $\varepsilon = 0.22$ is lower than expected, as the emission constant of epoxy is 0.91, and 0.82 [Thermoworks, 2015] for plywood traces left on the transformer. The reason for the calculated low emission constant, might be caused by the assumptions of a small object placed in an infinite space is not satisfied. The transformer is placed on a table and surrounded by miscellaneous experimental equipment. Regardless the calculated emission constant is lower than expected, it is seen as accurate for the experimental set-up.

6.2 Forced Cooling Water Heat Transfer Coefficient

It is difficult to determine the heat transfer coefficient for forced cooling water convection, as it is dependent on the flow velocity, Reynolds number and turbulence conditions of the cooling water, see figure 5.2.

The heat transfer coefficient for forced water convection, in the enhanced core cooling system, is experimentally determined as a function of Reynold number, by analytic calculations and by fitting the heat transfer coefficient in the model, so that it resembles the experiments.

Five 558 W AC experiments and four 190 W DC experiments are conducted, with only the cooling water flow rate changed from experiment to experiment. These nine experiments are the basis to determine the heat transfer coefficient for forced water convection in the transformer.

The analytic calculations, the lumped parameter model and the thermal FEM studies consists of cuboid material blocks, and do not include the toothing (fins) surface from the cooling channals, see figure 3.2. The effective cooling area is actually unchanged because of the fins, compared to two parallel surfaces. This can be explained by figure 6.2 showing the 1x1 mm water cooling channels. It is seen that the pattern is repeated for every 2 mm, why it is sufficient to analyse this section. For every 2 mm, there is 3 mm of core laminate in contact with water (the red line), and 1 mm of winding (the white line).

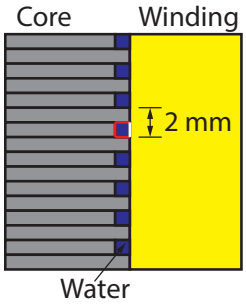

Figure 6.2. Cross section of the toothing cooling surface inside the transformer.

This results in a 4 mm cooling line for every 2 mm, compared to two parallel surfaces separated by cooling water which also have a cooling line of 4 mm for every 2 mm.

6.2.1 Core

The heat transfer coefficient for a convective boundary condition is given by equation 5.13. This means that the heat transfer coefficient can be determined by knowing the heat flux over the boundary, and the temperatures of the surface and cooling water, respectively. The central core element 1.1 is used to determine the heat transfer coefficient between the core and the cooling water, as the heat flux can be determined because of the adiabatic central plane and the assumption of one dimensional heat flow. The following calculations are for the AC experiment with a total power loss of 558 W, and a cooling water flow of 0.56 l/min. The 558 W loss correspond to a volumetric heat generation rate of $0.9766 \cdot 10^6 \frac{W}{m^3}$ in the core, when the copper loss is subtracted.

The cooling water temperature is assumed to vary linear as a function of the cooling paths travelled, starting at the inlet temperature when it enters the transformer, and leaving the transformer at the outlet temperature. The cooling water has travelled one fourth of the cooling path, when it is aligned with the middle of element 1.1. The cooling water temperature is therefore assumed to be give by equation 6.4.

$$T_{\infty C} = T_{in} + \frac{T_{out} - T_{in}}{4} = 25^\circ C + \frac{33^\circ C - 25^\circ C}{4} = 27^\circ C \tag{6.4}$$

The surface temperature of element 1.1, where the x axis crosses (x = 0.0195 m), has to be calculated as no thermocouple is fitted at this location. The temperature is calculated analytically from the

temperature measured by the centrally places thermocouple 1.1, using the same assumptions and approach as in section 5.1.1. The surface is given by equation 6.5.

$$T_{0.0195} = \frac{-\dot{q}x^2}{2K} + T_{11} = \frac{-0.9766\frac{W}{m^3} \cdot (0.0195m)^2}{2 \cdot 30\frac{W}{mK}} + 68^\circ C = 61.8^\circ C \tag{6.5}$$

The heat transfer coefficient can now be determined by equation 6.6

$$h_C = \frac{\dot{q}\Delta x}{T_{0.0195} - T_{\infty C}} = \frac{0.9766 \cdot 10^6 \cdot 0.0195m}{61.8^\circ C - 27^\circ C} = 547\frac{W}{m^2K} \tag{6.6}$$

The heat transfer coefficient of 547 $\frac{W}{m^2K}$ is tested in the lumped parameter model for the given experiment, and the modelled temperatures are compared to the measured temperatures. It is concluded that a model resembles the measured temperature closer by fitting the heat transfer coefficient to 340 $\frac{W}{m^2K}$. The fitted heat transfer coefficient is lower than the calculated, which can be explained by the assumption of one dimensional heat flow used in the analytic calculations. The actual heat flow over the analysed boundary will be minor due to three dimensional heat flow, which will result in a minor heat transfer coefficient.

The heat transfer coefficient between the core and water is determined for five different flow rates. The results are presented in table 6.1.

Flow rate [l/min]	**Reynolds number**	**Calculated** $h_C[\frac{W}{m^2K}]$	**Fitted** $h_C[\frac{W}{m^2K}]$
0.56	178	547	340
1.10	962	962	620
2.13	1656	1656	1200
3.20	2048	2048	1600
4.10	2265	2267	1900

Table 6.1. Calculated and fitted heat transfer coefficients between the core laminates and the cooling water.

6.2.2 Winding

The heat transfer coefficient between the winding and water is calculated in the same way as for the core, except that the DC experiments are used, why the losses are only present in the winding. A copper loss of 190 W, corresponding to $0.6829 \cdot 10^6 \frac{W}{m^3}$ is present in all the DC experiments. Element 1.2 is used for the calculations. The result are seen in table 6.2.

Flow rate [l/min]	**Reynolds number**	**Calculated** $h_C[\frac{W}{m^2K}]$	**Fitted** $h_C[\frac{W}{m^2K}]$
0.50	143	189	300
1.23	351	231	700
2.38	679	258	1100
4.00	1141	292	1700

Table 6.2. Calculated and fitted heat transfer coefficients between the core laminates and the cooling water.

The calculated heat transfer coefficients for the DC experiments are very low. The reason for the unrealistic low values may be caused by the simplifications made during the analytic calculations. These are:

- The heat flux is three dimensional, and not one dimensional as assumed.
- Element 1.2 is assumed to have a adiabatic mid plane, which is incorrect as the cooling water has different temperatures at each side. This will shift the adiabatic plane in the element, why the heat flux over the analysed boundary is changed.
- The thermal conductivity of the winding is simplified to an orthotropic material. Actual, the copper is concentrated at some locations in the winding element, which will make the thermal conductivity at a certain point unpredictable.
- The copper loss is not volumetric even distributed in the winding element, but concentrated in the copper winding itself. The thermocouple that measures the winding temperature is attached to the copper winding, and will therefore measure a higher temperature, than if the losses where volumetric even distributed in the winding element.

The last point is judged to have a great influence on the analytic calculations, as these build on the assumption of volumetric even distributed losses, and because the measured temperature is an input to calculate the integration constant. On basis of the rudeness of the assumptions used in the analytic DC calculations, it is judged that these calculations are incorrect and can not be used to determine the heat transfer coefficient for forced water convection.

The result from tabel 6.1 and 6.2 are plottet in figure 6.3. The blue and orange data points are from AC experiments, and are respectively calculated and fitted values. The grey and green data points are from DC experiments, and are respectively calculated and fitted. The trendlines are second order polynomials and are forced to be zero when Reynolds number is zero. No trendline is made for the calculated winding data, as these are seen as corrupt.

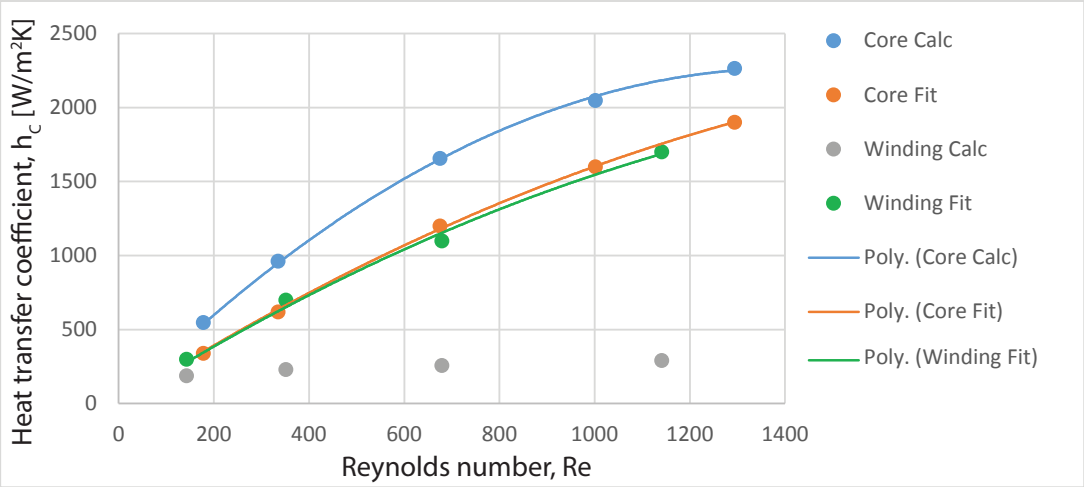

Figure 6.3. The heat transfer coefficient as function of Reynolds number. The blue and orange data points are from AC experiments, and are calculated and fitted respectively. The grey and green data points are from DC experiments, and are calculated and fitted respectively.

The determined heat transfer coefficients are seen to have an acceptable agreement with the ones found in literature [Alagesan and Sundaram] and [Al-Saiman and Thamer], see figure 5.2.

It is seen that the fitted heat transfer coefficients for forced water convection are close to identical for the AC and DC experiments. The fitted heat transfer coefficients are considered as more reliable than the calculated, as the calculated builds on a number of simplifications in the analytic calculations.

The equations for the trendlines describing the fitted heat transfer coefficients for the AC (core) and DC (winding) experiments are respectively: $h_C = -4.49 \cdot 10^{-4} \cdot Re^2 + 2.05 \cdot Re$ and $h_C = -4.78 \cdot 10^{-4} \cdot Re^2 + 2.02 \cdot Re$. The heat transfer coefficients for forced water convection is determined to be the average of the two trendlines, given by equation 6.7

$$h_C = -4.64 \cdot 10^{-4} \cdot Re^2 + 2.04 \cdot Re \tag{6.7}$$

Test and Verification 7

This chapter describes the test of the enhanced core cooling transformer. The measured temperatures during the tests are compared to the modelled temperatures in the lumped parameter model, the FEM model, and analytic calculated temperatures for the elements along the x axis.

The results from the CFD analysis is not used in the direct comparison, as the modelled temperatures are too low, e.g. the modelled temperatures for the high power experiment are approximately $30°C$ below the measured. This is properly caused by the effective heat transfer coefficients for forced water convection, which the CFD analysis apparently overestimates. An explanation of why the CFD analysis overestimates the heat transfer coefficient, is that the actual heat transfer coefficient in the transformer is lowered because of wax remains and corrosion. Instead of using the CFD analysis in a direct comparison, it is used to investigate the symmetry assumptions.

7.1 Results and Comparison of Models

The models are evaluated towards five experiments each at different power and cooling levels. The experiments are:

1. DC experiment - Power: 91 W, cooling water flow: 2.57 l/min.
2. No cooling AC experiment - Power: 40.9 W, cooling water flow: 0/min.
3. Low power AC experiment - Power: 391 W, cooling water flow: 1.32 l/min.
4. Medium power AC experiment - Power: 1203 W, cooling water flow: 2.55 l/min.
5. High power AC experiment - Power: 2347 W, cooling water flow: 1.73 l/min.

Radiation is left out in all of the models, as it is judged that the heat transfer from radiation is negligible. This hypothesis is tested in the low Power, no cooling AC experiment.

The power loss separated into copper loss and core loss as described in section 4.3.2. One eight part of the losses is applied to the model, as only one eight is modelled due to symmetry.
The copper loss is even volumetric distributed in the winding elements (1.2 and 1.5), and the core loss is even volumetric distributed in the core elements (1.1, 1.3, 2.1, 2.2 and 2.3), see figure 5.8.

7.1.1 DC Experiment

The measured and calculated data for the DC experiment are seen in table 7.1.

Measured		Calculated	
Parameter	**Value**	**Parameter**	**Value**
P	91 W	$\dot{q}_{ir}$	$0\ \frac{W}{m^3}$
U	0.567 V	$\dot{q}_{co}$	$0.0118 \cdot 10^6\ \frac{W}{m^3}$
I	160 A	h_A	$9.1 \frac{W}{m^2 K}$
$\dot{m}_C$	$2.57 \frac{l}{min}$	Re	700
T_{amb}	$21°C$	h_C	$1176 \frac{W}{m^2 K}$
T_{in}	$22°C$		
T_{out}	$22.5°C$		

Table 7.1. Experimental data for the DC experiment.

The measured and modelled temperatures for DC experiment are seen in table 7.2.

Location	**Measured** [$°C$]	**Lumped** [$°C$]	**FEM** [$°C$]	**Analytic** [$°C$]
1.1	25	25	23	22
1.2	52	53	39	46
1.3	26	25	23	22
1.4	26	26	23	22
1.5	59	60	51	
1.7	47	55	51	
2.1	25	24	23	
2.2	26	24	23	
2.3	26	24	23	
2.4	26	24	23	

Table 7.2. Temperature data for the DC experiment. The location number correspond to the node numbers used in the lumped parameter model.

The reason for the too low temperatures in the winding elements 1.2 and 1.5 in the FEM analysis, is due to the missing modelling of the electrical tape that confines the slot winding (element 1.2). The omitted tape increase the thermal conductivity between the slot winding and the surrounding core elements and cooling. The electrical tape is omitted in the FEM model as it would lead to very small elements. The electrical tape could have been modelled as a contact resistance between the slot winding and core elements, and a lower equivalent heat transfer coefficient for the water cooling in the slot winding. This is not investigated further as the FEM analysis has a satisfying accuracy at the AC experiments with cooling, as these experiments resembles the intended PMSM application.

The measured temperature in the resin element 1.7, which is located on top of the end winding, is in general measured lower than modelled. This is because thermocouple 1.7 is located close to the top surface of the element, and not in the middle as modelled.

Figure 7.1 shows the measured and modelled temperatures along the x axis.

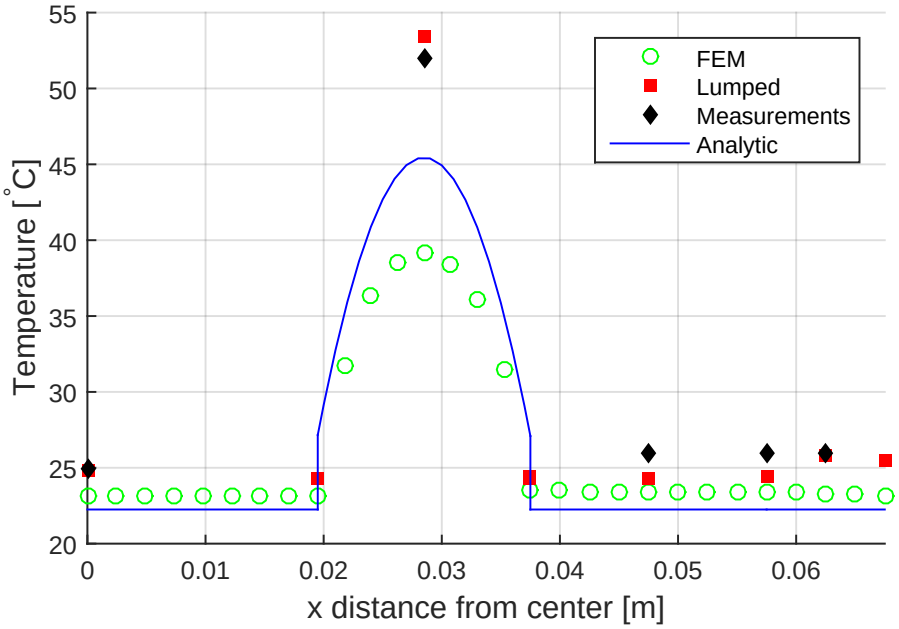

Figure 7.1. The measured and modelled temperatures along the x axis for the DC experiment.

7.1.2 No Cooling AC Experiment

The measured and calculated data for the no cooling AC experiment are seen in table 7.3.

Measured		**Calculated**	
Parameter	**Value**	**Parameter**	**Value**
P	40.9 W	$\dot{q}_{ir}$	$0.0719 \cdot 10^6 \frac{W}{m^3}$
f	200 Hz	$\dot{q}_{co}$	$0.00012 \cdot 10^6 \frac{W}{m^3}$
U_{RMS}	21 V	h_A	$9.1 \frac{W}{m^2 K}$
I_{RMS}	3.01 A	Re	0
$\dot{m}_C$	$0 \frac{l}{min}$	h_C	$0 \frac{W}{m^2 K}$
T_{amb}	$21°C$		
T_{in}	-		
T_{out}	-		

Table 7.3. Experimental data for the no cooling AC experiment.

The measured and modelled temperatures for the no cooling AC experiment are seen in table 7.4.

Location	Measured [$^{\circ}C$]	Lumped [$^{\circ}C$]	FEM [$^{\circ}C$]
1.1	82	87	95
1.2	79	85	91
1.3	80	87	94
1.4	74	82	89
1.5	78	83	88
1.7	62	78	80
2.1	81	86	95
2.2	81	86	95
2.3	79	86	94
2.4	73	83	88

Table 7.4. Temperature data for the no cooling AC experiment. The location number correspond to the node numbers used in the lumped parameter model.

The analytic calculations are left out in the no cooling AC experiment, as the convection boundary conditions do not apply when the water cooling is disabled. This makes the analytic problem more complex, as each element can not be treated separately, because the heat has to be removed by conduction from the centre towards the outer surface.

The modelled temperatures are in general higher than the measured, this is properly because radiation is left out in the models. When the water cooling is disabled, all the heat has to be dissipated from the outer surface of the transformer. This, and the fact that only 40.9 W is lost in the transformer, means that even a minor radiation power will have a relative big temperature influence in this case. The thesis is tested by including radiation, with a emissivity constants of 0.22, in the FEM analysis. The results are seen table 7.5

Location	FEM Radiation [$^{\circ}C$]
1.1	88
1.2	84
1.3	86
1.4	81
1.5	80
1.7	72
2.1	87
2.2	87
2.3	86
2.4	80

Table 7.5. FEM temperature results, when radiation is included, for the no cooling AC experiment. The location number correspond to the node numbers used in the lumped parameter model.

Comparing the results from the FEM analysis with and without radiation, it is seen that the temperatures in the model including radiation is 7° C to 8° C, lower than the model without radiation. This greatly improves the FEM model for this case, which makes sense as analytic calculations show

that the transformer emits 8.3 W via radiation when the average surface temperature is 75° C. It is obviously that 8.3 W of radiation makes a difference, when the total power loss is 40.9 W, and at the same time it justifies that radiation can be left out in the other cases where the power loss is much higher.

Even radiation has a major influence in this case, it is not included in the other cases with water cooling and higher losses, as tests shows that it results in a temperature changes of less that 0.5° C. On this basis it is judged that radiation is too computational demanding compared to the gain, as the calculation time for the simple FEM analysis goes from 2 minutes to 24 minutes when radiation is included.

Figure 7.2 shows the measured and modelled temperatures along the x axis.

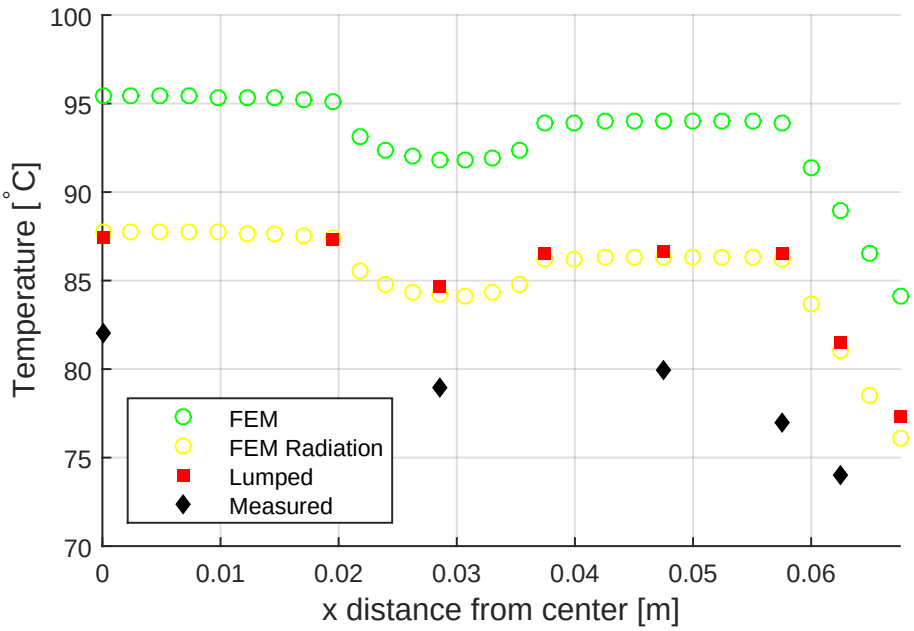

Figure 7.2. The measured and modelled temperatures along the x axis for the no cooling AC experiment.

It is seen that the modelled temperatures still are too high after radiation is included, which indicate that the emissivity constant is properly higher than 0.22.

7.1.3 Low Power AC Experiment

The measured and calculated data for the low power AC experiment are seen in table 7.6.

Measured		Calculated	
Parameter	**Value**	**Parameter**	**Value**
P	391 W	$\dot{q}_{ir}$	$0.6820 \cdot 10^6 \ \frac{W}{m^3}$
f	400 Hz	$\dot{q}_{co}$	$0.0118 \cdot 10^6 \ \frac{W}{m^3}$
U_{RMS}	72.28 V	h_A	$9.1 \frac{W}{m^2 K}$
I_{RMS}	31.73 A	Re	403
$\dot{m}_C$	$1.32 \frac{l}{min}$	h_C	$736 \frac{W}{m^2 K}$
T_{amb}	$21°C$		
T_{in}	$25.5°C$		
T_{out}	$28.5°C$		

Table 7.6. Experimental data for the low power AC experiment.

The measured and modelled temperatures for the low power AC experiment are seen in table 7.7.

Location	**Measured** [$°C$]	**Lumped** [$°C$]	**FEM** [$°C$]	**Analytic** [$°C$]
1.1	42	45	44	49
1.2	40	41	40	28
1.3	47	45	45	49
1.4	46	43	45	50
1.5	42	42	40	
1.7	38	41	39	
2.1	47	49	50	
2.2	46	47	48	
2.3	49	49	50	
2.4	47	48	48	

Table 7.7. Temperature data for the low power AC experiment. The location number correspond to the node numbers used in the lumped parameter model.

It is seen that the measured and modelled temperatures has a good correlation. This was expected as the heat transfer coefficient was determined for experiments in the same power loss range, and similar cooling water flow rates.

The analytic calculated temperature for element 1.2 is remarkably low compared to the measured and modelled temperatures. This is because each element is treated separately in the analytic analysis, why the heat conducted from the core elements to the winding is not present. This, and because resin element 1.4 is assumed adiabatic, also explains why the analytic calculated core temperatures are too high.

Figure 7.3 shows the measured and modelled temperatures along the x axis.

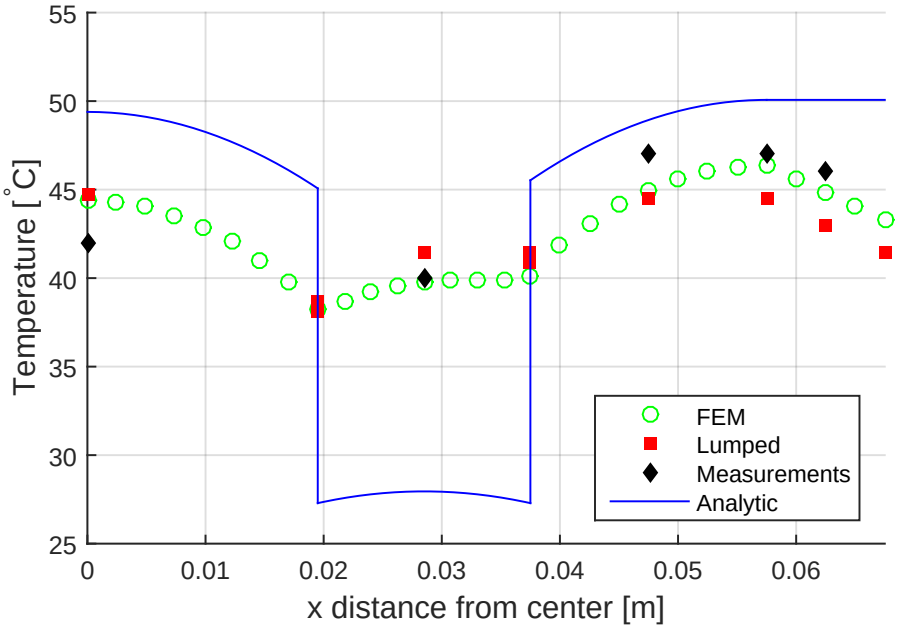

Figure 7.3. The measured and modelled temperatures along the x axis for the low power experiment.

7.1.4 Medium Power AC Experiment

The measured and calculated data for the medium power AC experiment are seen in table 7.8.

Measured		**Calculated**	
Parameter	**Value**	**Parameter**	**Value**
P	1203 W	$\dot{q}_{ir}$	$2.1151 \cdot 10^6 \frac{W}{m^3}$
f	900 Hz	$\dot{q}_{co}$	$0.0020 \cdot 10^6 \frac{W}{m^3}$
U_{RMS}	139.2 V	h_A	$9.1 \frac{W}{m^2 K}$
I_{RMS}	12.76 A	Re	1074
$\dot{m}_C$	$2.55 \frac{l}{min}$	h_C	$1603 \frac{W}{m^2 K}$
T_{amb}	$21°C$		
T_{in}	$39°C$		
T_{out}	$44°C$		

Table 7.8. Experimental data for the medium power AC experiment.

The measured and modelled temperatures for the medium power AC experiment are seen in table 7.9.

Location	Measured [°C]	Lumped [°C]	FEM [°C]	Analytic [°C]
1.1	72	75	74	81
1.2	57	62	59	42
1.3	76	73	74	78
1.4	75	69	75	82
1.5	61	64	60	
1.7	53	61	57	
2.1	82	88	89	
2.2	78	80	82	
2.3	81	87	89	
2.4	77	84	84	

Table 7.9. Temperature data for the medium power AC experiment. The location number correspond to the node numbers used in the lumped parameter model.

The modelled temperatures are in general higher than the measured, this indicates that the heat transfer coefficient are set too low in the models, as this is the main heat transfer path from the transformer. The cooling water flow rate is within the investigated range for heat transfer coefficients, but the power loss is more than the double. It is not expected that the heat transfer coefficient depends on the power loss in the transformer, and the high power AC experiments do not show this trend, so it is more likely that the generally higher modelled temperatures in this case, is caused by the common uncertainties discussed in section 7.2.

Figure 7.4 shows the measured and modelled temperatures along the x axis.

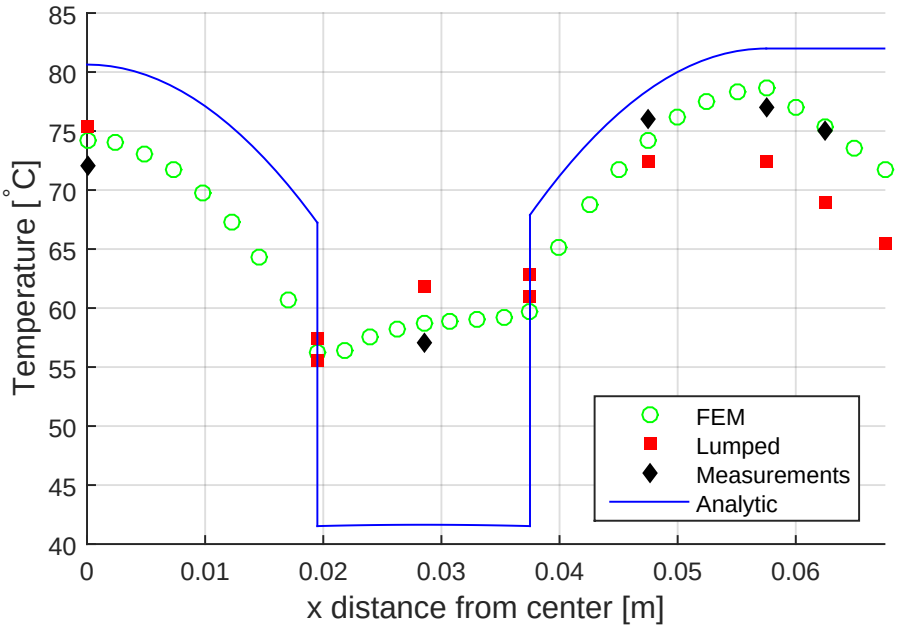

Figure 7.4. The measured and modelled temperatures along the x axis for the medium power experiment.

7.1.5 High Power AC Experiment

The measured and calculated data for the high power AC experiment are seen in table 7.10.

Measured		Calculated	
Parameter	**Value**	**Parameter**	**Value**
P	2347 W	$\dot{q}_{ir}$	$4.0349 \cdot 10^6 \frac{W}{m^3}$
f	900 Hz	$\dot{q}_{co}$	$0.1909 \cdot 10^6 \frac{W}{m^3}$
U_{RMS}	196.6 V	h_A	$9.1 \frac{W}{m^2 K}$
I_{RMS}	111.5 A	Re	867
$\dot{m_C}$	$1.73 \frac{l}{min}$	h_C	$1384 \frac{W}{m^2 K}$
T_{amb}	$21°C$		
T_{in}	$46°C$		
T_{out}	$61°C$		

Table 7.10. Experimental data for the high power AC experiment.

The measured and modelled temperatures for the high power AC experiment are seen in table 7.11.

Location	**Measured** [$°C$]	**Lumped** [$°C$]	**FEM** [$°C$]	**Analytic** [$°C$]
1.1	126	123	121	136
1.2	122	115	101	67
1.3	132	121	124	132
1.4	114	115	126	139
1.5	130	123	111	
1.7	98	116	106	
2.1	151	150	146	
2.2	136	134	138	
2.3	147	148	151	
2.4	128	141	143	

Table 7.11. Temperature data for the high power AC experiment. The location number correspond to the node numbers used in the lumped parameter model.

It is seen that the winding (element 1.2 and 1.5) temperatures in the FEM analysis is respectively 15° C and 19° C lower than measured. This is caused by the missing modelling of the electrical tape as discussed in the DC experiment, but properly also because of the uncertainty in the actual copper loss, as the lumped parameter model also under predict the winding temperatures. The uncertainty in losses is discussed in 7.2.

Figure 7.5 shows the measured and modelled temperatures along the x axis.

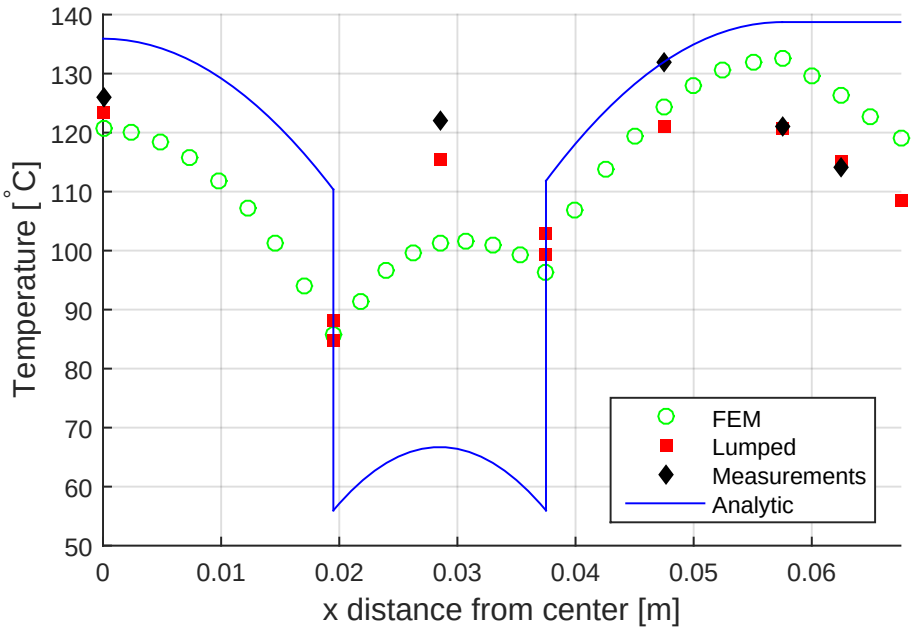

Figure 7.5. The measured and modelled temperatures along the x axis for the high power experiment.

7.2 Discussion and Uncertainties

All of the models has a number of common uncertainties, these include:

- The power loss (defect power meter, low resolution on oscilloscope).
- The distribution of the losses (core vs copper), and uneven volumetric distributed.
- Cooling water flow measurement uncertainty.
- The cooling water temperature.
- Temperature measurement uncertainty - location, noise and steady state definition.
- Blocked cooling channels because of wax remaining.
- Corrosion of core laminates.
- The simplified geometry of the model elements.
- Only an eight part of the transformer is modelled due to symmetry assumptions.
- The thermal conductivities of materials.
- The contact conductivities between the materials, i.e. air pockets.
- The heat transfer coefficients for convection and radiation.

7.2.1 Measured Power Loss

At the DC experiments the power loss is determined by the current displayed on the power supply, times the measured voltage drop over the winding. Both measurements may have a minor uncertainty, but are seen as quite accurate. The DC power loss is only present in the copper in the winding, and it is assumed to be even distributed in the copper. In the models the copper loss is assumed to be even distributed in the entire winding element, which consist of 15.6 % copper and 84.4% resin. This assumption is based on an even distribution of the copper wires in the resin, but as seen in figure

3.8, the 20 parallel wires in the winding are twisted together, which make the copper, and thereby the loss, concentrate in some areas of the winding element. The thermocouples measuring the winding temperatures are mounted directly on the copper winding, why the measured winding temperature is likely to be measured higher than modelled.

The loss and loss distribution at the AC experiments are more uncertain than at the DC experiments. This is mainly caused by two reasons: The measurements of the total input power to the transformer is uncertain, and the exact distribution of the losses in the transformer elements are uncertain.

The total input power to the transformer is measured by the build in power analyser in the AC power supply. Unfortunately the power analyser is giving some inconsistent measurements (increasing the current over a certain point makes the measured power drop), why the accuracy of the power analyser is questionable. The input current and voltage is measured by an oscilloscope, and the calculated power is compared to the power analyser. At the low power experiments, the power calculated on basis of the oscilloscope measurements is generally 15% above the power measured by the power analyser. It is difficult to explain why the oscilloscope measures a higher power than the power analyser, by other than the power analyser must be defective.

It would make more sense if it was the other way around, as some power will be lost in the utility wires between the power analyser and the transformer.

The power measured by the oscilloscope deviates up to 6% from measurement to measurement, when measuring on the same set-up at the high power experiments (>2000 W). The reason for the uncertainties in the oscilloscope measurements might be caused by the 8-bit resolution, which almost gives an uncertainty of 1 Volt and 0.5 Ampere at the high power experiments. This uncertainty result in a rough power calculation, as the voltage and current is phase shifted. It is concluded that the power analyser measurements are untrustworthy, why the input power is determined on basis of the oscilloscope. The 6% measurement uncertainty makes the inputs to the models uncertain, and thereby the modelled temperatures uncertain.

7.2.2 Power Loss Distribution

The loss distribution in the transformer elements are uncertain. During the models, it is assumed that the copper loss is given by the rms current squared times the temperature corrected winding resistance. This method should be accurate at low frequencies, but at high frequencies the copper loss might be increased by skin and proximity effects. The iron loss is calculated as the total power input minus the copper loss, and then distributed to the different core elements by volume, thereby assuming that the iron loss is volumetric even distributed. Iron loss highly depends on the flux density of the core, so assuming volumetric even distributed of iron loss, entails an assumption of even flux density in the entire core. The core laminates are designed to have an even flux density, by having an almost even cross sectional area along the magnetic path. Due to the squared shape of the laminates and the winding windows, the cross sectional area is greater in the corners, meaning that the core elements 2.1 and 2.3 in general will have a minor flux density than core elements 1.1, 1.3 and 2.2. The iron loss will therefore be volumetric major in the core elements 1.1, 1.3 and 2.2. It can not be seen on the temperature measurements that these elements heads more than element 2.1 and 2.3. This can

easily be explained by the core cooling system, as this directly cools element 1.1, 1.3 and 2.2, but only indirectly cools element 2.1 and 2.3.

7.2.3 Flow Measurement

The cooling water flow is measured by a ultrasonic flowmeter (Burkert DN15), where the flow is calculated from the relative velocity of sound through the water. The flowmeter has a measurement range from 0.06 l/min to 20 l/min. During the experiments it is used to measure flows in the range from 0.5 l/min to 5 l/min. From the accuracy diagram, figure 7.6, it is seen that the flowmeter has an accuracy around ± 2 to $\pm 3\%$.

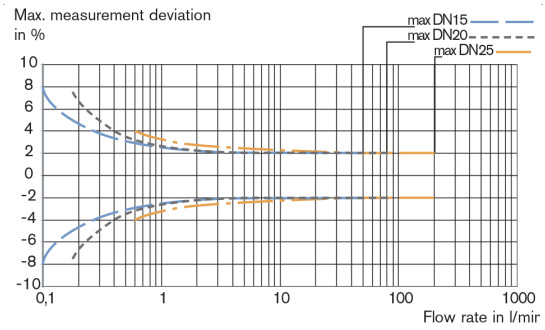

Figure 7.6. The accuracy diagram for the DN15 flowmeter used to measure the cooling water flow. From data sheet found on appendix CD.

The accuracy is acceptable. What is more problematic, is that the flow is slowly dropping at low flow rates. This is seen in figure 7.7a, where the flow initially is limited to 0.55 l/min by a valve. After five minutes the flow is dropped to 0.45 l/min, why the flow valve manually is opened a little more. This pattern is seen to repeat five times before the experiment is stopped. It is unclear what course the flow to drop. A hypothesis is that dirt and wax remains in the cooling water, slowly builds up in the small orifice of the flow limiting valve. Another explanation may be that the pump does not sustain constant pressure as the efficiency of the motor drops as it heats up. The problem is only present at flow rates below 1 l/min. Figure 7.7b shows the flow measurement when the flow is adjusted to 3.2 l/min. It is seen that the flow is kept constant.

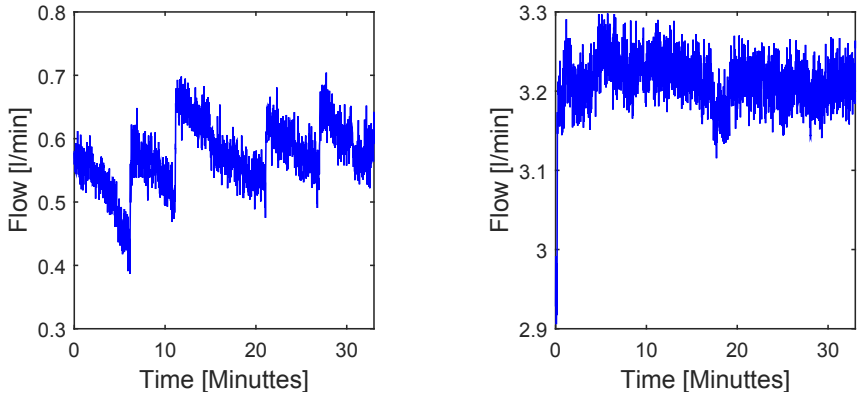

Figure 7.7. The measured flow for two 558 W AC experiments. a.) shows the manually regulated flow around 0.56 l/min. b.) shows a constant flow around 3.2 l/min.

The accuracy of the flow measurement, the manually regulated flow at low flows and flow read of accuracy, is judges to give an uncertainty in flow of up to $\pm 10\%$ at low flow and about $\pm 4\%$ a higher flows. The uncertainty in the flow measurement gives an uncertainty regarding determine the heat transfer coefficient for water convection, as the heat transfer coefficient is a function of Reynolds number and thereby the flow. A too low or too high flow, will therefore result in generally too high or too low modelled temperatures in all elements. This might be an explanation of the too high modelled temperatures in the medium power AC experiment.

7.2.4 Cooling Water Temperature

The cooling water temperature is measured when it leaves and enters the cooling rig. The core cooling system is connected to the cooling rig via two 2 m long silicone hoses. As the cooling water is warmer than the ambient, some heat will be dissipated from the hoses, which means that the actual temperature of the inlet cooling water is colder than measured, and the actual temperature of the outlet cooling water is hotter than measured.

In the lumped parameter and the FEM models, the cooling water temperature are divided into three. At the boundary between element 1.1 and 1.2 it is assumed to be at the inlet temperature. At the boundary between element 1.2 and 1.3 it is assumed to be at the outlet temperature, and at the boundary between element 1.2 and 2.2 it is assumed to be an average temperature of the inlet and outlet.
If the actual inlet temperature is lower than modelled, the models will over predict the temperature in element 1.1. And if the actual outlet temperature is higher than modelled, the models will under predict the temperature in element 1.3. This tendency is seen in both the low and medium power AC experiments. The effect, of the uncertainty in the cooling water temperature, will not be as strong on element 2.2, as the average temperature between inlet and outlet is used.

7.2.5 Temperature Measurement Uncertainty

Noise and general measurement uncertainties are seen to be negligible for the temperature measurements, compared to the temperature uncertainties introduced by loss concentration and the precision in location.

The thermocouples are assumed to be located precisely in the middle of each element. The thermocouples installed inside the core is placed with tolerances of less than half a millimetre, as they are placed in cut outs in the centre laminate. The thermocouples are glued into the cut outs to secure the thermocouples, and to enforce the conductivity to the core. However, the glue has a lower conductivity than the laminates, why it will insulate the thermocouples. This is not expected to give any measurable difference as the tolerances of the cut outs are quite tight, and the amount of glue is very limited.

The location of the winding thermocouples are more imprecise, as they are glued to the copper winding. However, the location of the winding thermocouples are not seen as the major problem, relative to the loss contraction in the copper of the winding element disused earlier in this section.

The location of the resin element thermocouples is the most critical as the resin shell is only 10 mm

thick, why a misplacement of ± 1 mm makes a relative big difference. It is know that the thermocouple in resin element 1.7 is placed too close to the surface, as the top layer of resin is only 5 mm thick above the winding, instead of 10 mm as modelled, due to lack of resin. This explains why thermocouple 1.7 generally measures a too low temperature.

7.2.6 Blocked Cooling Channels

In section 3.5 it was revealed that one third of the wax still remains in the cooling system. During the high power experiments it was observed that wax remains was flushed out of the transformer, but it is unclear how much is left. If some of the cooling channels are blocked, or partly blocked, it will result in a redirecting of the cooling water flow. The result is that some spots are hotter and other colder that expected.

Wax in the cooling system will decrease the effectiveness of the cooling system, but it is not judged to be a problem during the experiments, as the heat transfer coefficient for water is determined at the present circumstances.

7.2.7 Symmetry

Only an eight part of the transformer is modelled due to assumption of symmetry over the xy, xz and yz planes. The CFD model is the only model that do not use any symmetry assumptions, why it is used to investigate if the symmetry assumptions holds. Temperature cut plots from the CFD analysis at the xy, xz and yz planes for the high power AC experiment are seen in figure 7.8.

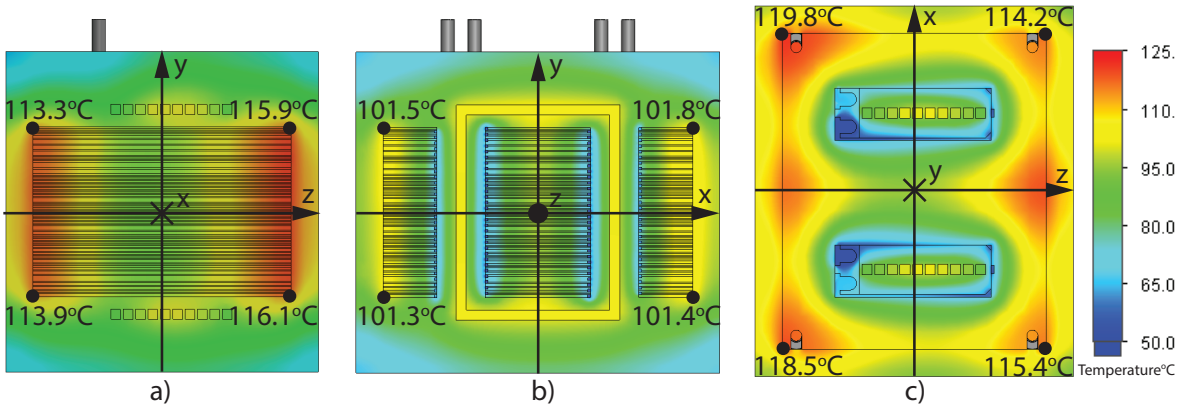

Figure 7.8. Temperature cut plots from the CFD analysis at the xy, xz and yz planes for the high power AC experiment. The explicit temperatures shown at the middle edges of the core is used for symmetry evaluation.

The inlet/outlet manifolds and the raising water temperature through the cooling system are violating the symmetry assumption over the xy plane. This is seen from figure 7.8a, which shows that the temperature is lower at left side next to the inlet, than to the right side where the cooling water has heated up. The same tendency is in seen in figure 7.8c, where the temperature is about 5° C higher to the left next to the outlet, than to the right side. The non symmetric effect depends on how much the

cooling water heats up, i.e. the cooling water flow rate and the power losses, why the effect is most pronounced at high power experiments. Therefore, the non symmetric effect over the xy plane has to be kept in mine, when the models are used around the power/temperature limit of the transformer.

The temperatures is seen to be close to mirrors over the xz and zy planes as expected, why the assumption of symmetry over these planes holds.

7.2.8 The Thermal Conductivities of Materials

The thermal conductivities for the epoxy and the copper used in the transformer are taken from their respective date sheets, and are expected to be quite accurate. The thermal conductivity for the core laminates are based on the numbers used [Mathiasen and Olesen, 2014], which is 30 $\frac{W}{mK}$ in the laminate plane and one twentieth in the normal direction, corresponding to 1.5 $\frac{W}{mK}$. The in plane thermal conductivity highly depends on the silicon content in the steel, and varies from 38-20 $\frac{W}{mK}$ when the silicon content is varied from 1-4% [Staton et al., 2003]. The value of 30 $\frac{W}{mK}$ is choose as reasonable for a 2.5% silicon steel, but the actual silicon content in the SURA M400-50A steel does not appear from the data sheet. The thermal conductivity in the normal direction is 20-40 times smaller than in the plane of the laminate, depending on lamination thickness, lamination surface finish, stacking factor, clamping pressure and interlamination insulation material [Mathiasen and Olesen, 2014]. In lack of better data, the mean values for thermal conductivities in the normal direction and in the plane are used for the core laminates. However, these values are relative uncertain and should ideally be determined experimentally. In the end it should be noted, that the temperatures predicted by the models, do not show any pattern that can be explained incorrect thermal conductivities in the core laminates. It is therefore conclude that the applied thermal conductivities are of acceptable accuracy.

7.2.9 The Heat Transfer Coefficients for Convection and Radiation

The radiation emissivity of epoxy and the heat transfer coefficients for the ambient air and the cooling water convection are all determined by experiments, described in chapter 6. The experimental determined values are affected of almost all of the uncertainties regarding the test set up. However, the most critical value, the heat transfer coefficient for forced water convection, is determined on basis of several experiments and a trendline is fitted to the data. This approach will eliminate general measurement and read off uncertainties, but systematic errors in the models will have an influence on the determined parameters, e.g. wrong thermal conductivities of the core laminates. The consistency of the model indicates that it do not contain any major errors, which can not be explained by the mentioned uncertainties. On this basis the heat transfer coefficients are seen as reliable.

Projection to PMSM 8

This chapter discuses how the Enhanced Core Cooling System can be implemented in a the PMSM, used to drive the axial compressor in the water vapour chiller.

8.1 Johnson Controls Solution

Johnson Controls has suggested a solution of how the Enhanced Core Cooling system can be integrated in a PMSM, see appendix B. The idea entails to supply the Enhanced Core Cooling system through slits in the core laminates, thereby connecting the cooling water supplied from the central axle to the stator teeth, see figure 8.1a. The cooling water feeding slits stops approximately half way between the axle and the winding windows, thereby ensuring that the magnetic path in the laminates are not completely violated. The laminates is turned upside down in a predetermined pattern, so that the cooling water feeding slits of type 1 is overlapping the slits of type 2 successive in layers, and thereby secure the cooling water supply to the winding windows.

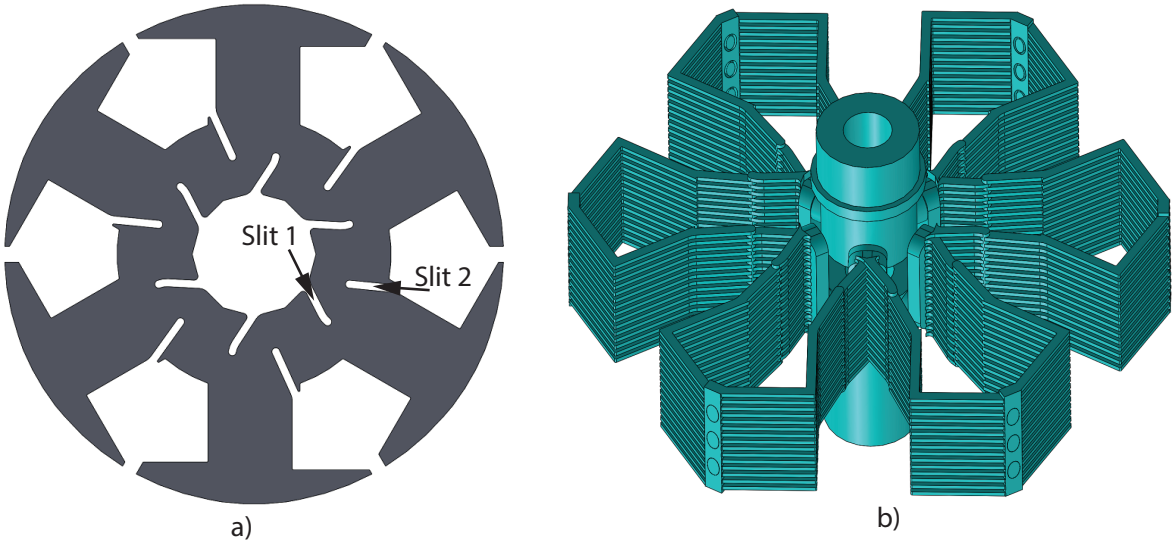

Figure 8.1. a) The design of the stator laminate for the PMSM. b) The fluid domain of the Enhanced Core Cooling system for the PMSM suggested by Johnson Controls.

The cooling water is flowing from the axle, through the laminations slits, around the windings and back to the axle through the laminations slits. The fluid domain of this path is seen in figure 8.1b. The surface area of the fluid domain in the PMSM is 0.078 m^2, which is 77 % larger that the total surface area of the fluid domain in the transformer. The cooling water surface area is assumed to be

proportional to the efficiency of the cooling system, why it is assumed that the cooling system in the PMSM can remove 77 % more heat than in the transformer.

The measured maximum temperature in the high power experiment is 147° C, which is close to the specified upper limit of 155° C. It should be noted that the cooling water flow rate is set quite low at the high power experiment (only 1.73 $\frac{l}{min}$), why the heat transfer coefficient is 1384 $\frac{W}{m^2K}$. A cooling water heat transfer coefficient of 2000 $\frac{W}{m^2K}$ can easily be obtained by increasing the cooling water flow (see table 6.1), which will increase the efficiency of the cooling system by 44 %. Combining the possible efficiency increase from the enlarged cooling water surface and the heat transfer coefficient, gives an estimate of how much heat the cooling system in the PMSM can sink, see equation 8.1.

$$P_{PMSM} = P_{\text{high power AC}} \cdot 1.77 \cdot 1.44 = 2347W \cdot 1.77 \cdot 1.45 = 6012W \tag{8.1}$$

Where $P_{\text{high power AC}}$ is the measured power loss in the high power experiment. It is seen that the cooling system integrated in the PMSM has a potential ability to remove more than 6 KW heat, which is six times more than required.

What is unknown at the solution suggested by Johnson Controls, is the effect of the cooling water feeding slits in the core laminations, as these approximately halves the cross sections of the magnetic paths. Offhand it might be stated that these bottlenecks will reach magnetic saturation way before rest of the core, and thereby heavily decrease the utilization of the core material. An analysis of the three dimensional magnetic effects is required to clarify the effect of the slits in the core.

An other aspect that has to be investigated at the Johnson Controls solution, is the effect of the 1.5 mm thick Mylar shrink wrap, that is intended to be warped around the perimeter of the stator laminations. The shrink wrap is applied to seal the stator for leaking water in between the laminations. Experiments at the transformer showed that water was leaking between the two ideally separate fluid domains, thus a sealing around the stator of the PMSM is required. The shrink wrap will give a larger "effective" air gap between the stator and rotor, which is undesirable as it will require more permanent magnet material to sustain the air gab flux density.

8.2 Alternative Solution

An alternative solution to implement the Enhanced Core Cooling system in a PMSM, is to supply the cooling system from end plates, like in [Mathiasen and Olesen, 2014], and to glue the core laminations together. In this way the slits in the laminations are avoided, and the shrink wrap in the air gap can be omitted.

In the end plate solution the cooling water is feed from the axle, through a union nut to the end surface of the stator teeth, see figure 8.2. The cooling water is distributed into axial channels by a special rippled end plate on the stator. The axial channels are going from a stator tooth end to the other end, following the direction of the conductors through the winding windows. The water is flowing back to the axle through a similar end plate and union nut at the opposite end of the stator. The union

nuts are threaded, so that they can clamp the core laminates together and thereby reducing the risk of leakage between the laminations. Further it may be suggested that the union nuts entails an O-ring solution, thereby preventing leakage along the axle. This solution gives a minor surface area of the fluid volume, but the end windings are ensured better cooling and the magnetic path is not interrupted.

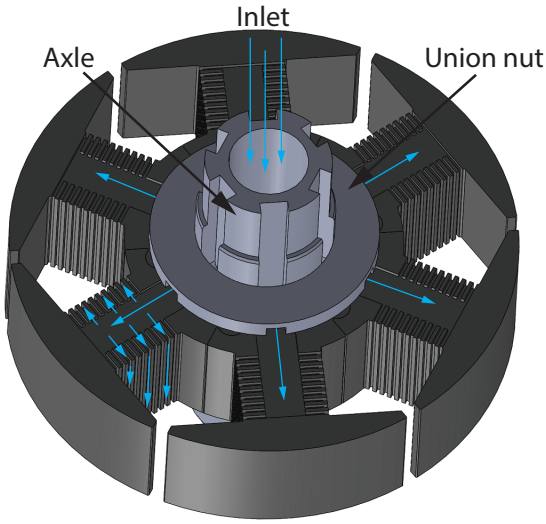

Figure 8.2. The end plate supplied solution of integrating the Enhanced Core Cooling system in a PMSM.

The shrink wrap applied at the perimeter of the stator in Johnson Controls solution is avoided, by applying a liquid gasket sealant in between the laminations when the core is assembled.
An alternative is to sprayed a thin layer of finish over the assembled core, thereby reject the water in the cooling system from penetrating in between the laminations.

The PMSM is meant to be produced in the same way as the transformer, this including wax injection, electrical taping, winding, resin moulding and melting out the wax. It is important that the resin mould is tight fitting at the perimeter of the stator, thereby ensuring the tolerances of the air gab is not disrupted by resin.

Conclusion 9

This chapter concludes the Enhanced Core Cooling concept for a transformer and recommends future work.

9.1 Design and Manufacturing of Prototype Transformer

A transformer containing the Enhanced Core Cooling system is successful designed and manufactured. The core consist of 124 special produced laminations, which makes basis for the cooling channels by using a special stacking sequence. The winding windows are encircled by 31 cooling channels, with a squared cross sectional of 1x1 mm. To avoid the waterproofing resin to penetrate the cooling channels, the cooling system is filled with wax before the resin casting. It proves to be problematic to inject wax into the entire cooling system, as the wax hardens too quickly and hence blocks the flow to the most remote channels. Several attempts of preheating the transformer, to slowing the hardening process are accomplished, but it did not eliminate the problem. The unfilled cooling channels is manually filled with wax.

The transformer is wound to 10 turns, so that a maximum voltage of 200 V at a frequency of 1000 Hz can bring the core to saturation. 14 thermocouples of type J is installed in the transformer, measuring the temperatures in the core, winding and resin.

The resin casting is successful as the cooling system did not leak at any time. The wax, filling the cooling system, is melted off during the final curing of the resin. Measurements shows that approximately one third of the wax is remaining in the cooling system. It is recommended that wax in future projects is water-soluble.

9.2 Thermal Modelling and Verification

The heat distribution in the transformer is modelled by four different models: an analytic, a lumped parameter, a FEM and a CFD analysis.

Radiation is omitted as it drastically reduces calculation time. It is found to be acceptable when the cooling system is active, as it removes the major part of the heat generated in the transformer.

Due to symmetry assumptions, only one eight part of the transformer modelled in the lumped parameter model and the FEM analysis. The eight part of the transformer is divided into 13 elements by geometric and thermal properties.

The analytic model is one dimensional and is bounded to the x axis, starting at the centre of the transformer, going normal through the slot winding and ending at the resin shell enclosing the transformer. Each element on the x axis is threaded separately, by assuming pure convection boundary conditions at each side of the elements. The assumptions regarding one dimensional heat flow and the pure convection boundary conditions makes the analytic model quite rough. In spite of this, the analytic model shows the right tendencies and is of acceptable accuracy in the core materiel. The temperature in the slot winding is calculated too low for AC experiments, as the core heats up the slot winding by conduction.

The novel GD approach is used in the lumped parameter model to implements the heat sources in the core and winding elements. The thermal resistances for each of the 13 elements are determined in three dimensions. The lumped parameter model is build in three xy planes, and subsequently connected in the z direction. The elements are represented by their thermal resistances. The internal convection to the cooling system and the external convection to the ambient are introduced as thermal resistances depending on the heat transfer coefficients.

The lumped parameter model is generally consistent with the measurements, and may be used as a simple and effective design tool in the further development of the Enhanced Core cooling system in electrical machines.

The heat transfer coefficient to the ambient is determined to 9.1 $\frac{W}{m^2K}$. The heat transfer coefficient for the forced water convection in the cooling system is found to highly dependent on Reynolds number in the cooling channels. Equation 9.1 is determined to reflect the heat transfer coefficient for forced water convection. This means that heat transfer coefficients in the range of 2000 $\frac{W}{m^2K}$ is achievable on the prototype setup.

$$h_C = -4.64 \cdot 10^{-4} \cdot Re^2 + 2.04 \cdot Re \tag{9.1}$$

The FEM analysis builds on the same basis as the lumped parameter model, i.e. same geometry, thermal conductivities and heat transfer coefficients. The models deviates in the way the sources are implemented, as the lumped parameter uses a concentrated loss model and the FEM analysis use distributed losses. This results in minor differences in the modelled temperature between the two models. The FEM model is a good support to the lumped parameter model, as it predicts the temperatures at more locations, why it may reveal undiscovered hot spots.

The CFD analysis generally under predicts the temperature, why it is not used in the direct comparison with the other models and the measurements. Instead, the CFD analysis is used to investigate the symmetry of the temperature distribution in the transformer. The symmetry over the xz and yz planes are found to be very good, while the symmetry over the xy plane is affected by the raising temperature of the cooling water as it passes through the cooling system. At the high power experiment, which is worst case as the cooling water is heated most, the temperature deviated up to $5^{\circ}C$ on each side of the xy plane. Considering that this is for the worst case, the symmetry assumptions are found acceptable.

9.3 Future work

The Enhanced Core Cooling system is proven to be very effective for cooling a transformer. The following task is to implement the Enhanced Core Cooling system in a PMSM. The thesis [Mathiasen and Olesen, 2014] concerns implementing a cooling system tighten by resin in a PMSM. The thesis revealed a number challenges regarding waterproofing and bearing losses.

It is challenging to make a PMSM waterproof as there is some very tight tolerances for the air gab between the stator and the rotor. Experiences from experiments on the transformer, showed that cooling water was leaking between the two cooling water domains, e.g. cooling water did flow in between the laminates. This means that the core containing the Enhanced Core Cooling system has to be completely confined, either by applying shrink wrap at the perimeter of the stator or by moulding a thin layer of resin around the stator. If this solution is choose, it has to be investigated how resin/shrink wrap in the air gab affects the efficiency of the PMSM.
Alternatives is to glue the laminations together by sealant during the core stacking, or to apply finish to the core after assembly.

An other challenging section to waterproofing is the interface between the resin and the centre axle, as the total allowable hight of the PMSM is limited. This means that the resin will have a short contact surface to the axle, why an O-ring solution might be to prefer.

The solution Johnson Controls suggest for implementing the Enhanced Core Cooling system in a PMSM entails cutting supply slits from the axle towards the stator teeth. This will impair the magnetic path in the PMSM, as the magnetic cross sectional area is reduced. The effects of the reduced magnetic cross sectional area has to be investigated if this solutions is choosen.

Test on the transformer shows that the Enhanced Core Cooling system has a large overcapacity compared to the expected losses of 1000 W in the PMSM. It is therefore worth considering replacing the cooling water by oil. Oil is a less effective coolant, as both the heat capacity and heat transfer coefficient typically are about half of the values for water. Oil will prevent corrosion of the silicon steel laminates and it has an excellent electrical insulation [Feinberg, 1979]. Replacing the cooling water by oil is considered to increase the lifetime and reliability of the PMSM.

Bibliography

Al-Saiman and Thamer. Q. Al-Saiman and O. Thamer. *Promotion of heat transfer using twisted tape to generate additional turbulent*.

Alagesan and Sundaram. V. Alagesan and S. Sundaram. *Two-phase experimental heat transfer studies on a water-diesel system in a shell and tube heat exchanger*.

Andersen and Omand, **2015**. L. S. Andersen and P. Omand. *Project proposal*, 2015.

Andersen and Hansen. T. O. Andersen and M. R. Hansen. *Fluid Power Systems*.

Cogent, **2009**. Cogent. *ETypical data for SURA M400-50A*. URL: http://cogent-power.com/cms-data/downloads/m400-50a.pdf, 2009. Accessed: 12/08-2015.

Comsol, **2013**. Comsol. *Meshing Your Geometry: When to Use the Various Element Types*. URL: http://www.comsol.com/blogs/meshing-your-geometry-various-element-types/, 2013. Accessed: 28/08-2015.

Feinberg, **1979**. R. Feinberg. *Modern Power Transformer Practice*. ISBN: 0-333-24537-1, Book. The Macmillan Press LTD, 1979.

Gerling and Dajaku. D. Gerling and G. Dajaku. *Thermal calculation of systems with distributed heat generation*.

Incropera, Dewitt, Bergman, and Lavine, **2006**. F. P. Incropera, D. P. Dewitt, T. L. Bergman, and A. S. Lavine. *Heat and Mass Transfer, 6. edition*. ISBN: 978-0-471-45728-2, Book. John Wiley & Sons, 2006.

Johnson, **2003**. Bill Johnson. *Removing Water From A Wet Heat Pump System*. URL: http://www.achrnews.com/articles/91517-btu-buddy-6-removing-water-from-a-wet-heat-pump-system, 2003. Accessed: 18/08-2015.

Galvan, Escarela-Perez, León, Campero-Littlewood, and Aviles Cruz. J. C. livares Galvan, R. Escarela-Perez, F. de León, E. Campero-Littlewood, and C. Aviles Cruz. *Separation of core losses in distribution transformers using experimental methods*.

Mathiasen and Olesen, **2014**. Dan M. Mathiasen and Nicolaj T. Olesen. *Manufacturing, Modelling and Control of a High Speed Permanent Magnet Synchronous Machine including a Thermal Analysis*, 2014.

Matlab, **2015**. Matlab. *Choose a Solver*. URL: http://se.mathworks.com/help/simulink/ug/choosing-a-solver.html, 2015. Accessed: 28/08-2015.

Matsch and Morgan, **1987**. L. W. Matsch and J. D. Morgan. *Electromagnetic and Electromechanical Machines, 3. edition*. ISBN: 0-471-61305-3, Book. John Wiley and sons, 1987.

Mohan, Undeland, and Robbins, **2003**. N. Mohan, T.M. Undeland, and W.P. Robbins. *Power electronics: converters, applications, and design*. vb. 1, Power Electronics: Converters, Applications, and Design. John Wiley & Sons, 2003. ISBN 9780471226932. URL: http://books.google.dk/books?id=ToYoAQAAMAAJ.

Saidi and Abardeh, **2010**. M. Saidi and R. H. Abardeh. *Air Pressure Dependence of Natural-Convection Heat Transfer*. URL: http://www.iaeng.org/publication/WCE2010/WCE2010_pp1444-1447.pdf, 2010. Accessed: 30/04-2015.

Sen, **2013**. P. C. Sen. *Principles of Electrical Machines and Power Electronics, 3. edition*. ISBN: 978-1-118-07887-7, Book. John Wiley and sons, 2013.

Staton, Boglietti, and Cavagnino, **2003**. D. Staton, A. Boglietti, and A. Cavagnino. *Solving the More Difficult Aspects of Electric Motor Thermal Analysis*. URL: http://www.motor-design.com/cmsAdmin/uploads/motor-cad_iemdc_2003.pdf, 2003. Accessed: 25/08-2015.

Thermoworks, **2015**. Thermoworks. *Emissivity Table*. URL: http://www.thermoworks.com/emissivity_table.html, 2015. Accessed: 22/06-2015.

Versteeg and Malalasekera, **2012**. H. K. Versteeg and W. Malalasekera. *An Introduction to Computational Fluid Dynamics, 2. edition*. ISBN: 978-81-317-2048-6, Book. Pearson Education Inc., 2012.

Viscopedia, **2015**. Viscopedia. *Water*. URL: http://www.viscopedia.com/viscosity-tables/substances/water/, 2015. Accessed: 23/04-2015.

Appendix A

Analytic calculated temperature distributions for the high power, medium power, low power and DC experiments, and for the 1000 W scenario in section 5.1.2.

High Power AC experiment

Constants

$q_{ir} := 4.034910^{6}$ $q_{co} := 0.1909010^{6}$ $h_A := 9.1$ $h_{Cir} := 138$ $h_{Cco} := h_{Cir}$

$k_{11} := 30$ $k_{12} := 0.7$ $k_{13} := 30$ $k_{14} := 0.6$ $T_{infC} := 53.$ $T_{infA} := 21$

$x_0 := 0$ $x_1 := 0.019$ $x_{12} := 0.028$ $x_2 := 0.037$ $x_3 := 0.057$ $x_4 := 0.067$

Analytic element 1.1

Left boundary condition (x=0)

$$\frac{d}{dx}T(x) := 0$$

$$\frac{d}{dx}T(x) := \frac{-q_{ir}\cdot x}{k_{11}} + C_{11}$$

$$0 := \frac{-q_{ir}\cdot x}{k_{11}} + C_{11}$$

$$C_{11} := 0$$

Right boundary condition (x=0.0195)

$$q_{ir}\cdot(x_1 - x_0) := h_{Cir}(T_1 - T_{infC})$$

$$T_1 := T_{infC} + \frac{q_{ir}\cdot(x_1 - x_0)}{h_{Cir}}$$

$$T(x_1) := \frac{-q_{ir}\cdot x_1^{2}}{2\cdot k_{11}} + C_{11}\cdot x_1 + C_{21}$$

$$T_{infC} + \frac{q_{ir}\cdot(x_1 - x_0)}{h_{Cir}} := \frac{-q_{ir}\cdot x_1^{2}}{2\cdot k_{11}} + C_{11}\cdot x_1 + C_{21}$$

$$C_{21} := T_{infC} + \frac{q_{ir}\cdot(x_1 - x_0)}{h_{Cir}} + \frac{q_{ir}\cdot x_1^{2}}{2\cdot k_{11}} - C_{11}\cdot x_1 = 135.921$$

Temperature distribution for 0<x<0.0195

$$T_{11}(x) := \frac{-q_{ir}\cdot x^{2}}{2\cdot k_{11}} + C_{11}\cdot x + C_{21}$$

Analytic element 1.2

Center boundary condition (x=0.0285)

$$\frac{d}{dx}T(x) := 0$$

$$\frac{d}{dx}T(x) := \frac{-q_{co}\cdot x_{12}}{k_{12}} + C_{12}$$

$$C_{12} := \frac{q_{co}\cdot x_{12}}{k_{12}} = 7.556\times 10^{3}$$

Right boundary condition (x=0.0375)

$$C_{22} := T_{infC} + \frac{q_{co}\cdot(x_2 - x_1)}{h_{Cco}} + \frac{q_{co}\cdot x_2^{2}}{2\cdot k_{12}} - C_{12}\cdot x_2 = -40.959$$

Temperature distribution for 0.0195x<0.0375

$$T_{12}(x) := \frac{-q_{co}\cdot x^{2}}{2\cdot k_{12}} + C_{12}\cdot x + C_{22}$$

$$T_{12}(0.0285) = 66.721$$

Analytic element 1.3

RIGHT boundary condition (x=0.0575)

$$\frac{d}{dx}T(x) := 0$$

$$\frac{d}{dx}T(x) := \frac{-q_{ir}\cdot x_3}{k_{13}} + C_{13}$$

$$C_{13} := \frac{q_{ir}\cdot x_3}{k_{13}} = 7.734\times 10^3$$

Left boundary condition (x=0.0375)

$$q_{ir}\cdot(x_3 - x_2) := h_{Cir}(T_2 - T_{infC})$$

$$T_2 := T_{infC} + \frac{q_{ir}\cdot(x_3 - x_2)}{h_{Cir}}$$

$$T(x_2) := \frac{-q_{ir}\cdot x_2^2}{2\cdot k_{13}} + C_{13}\cdot x_2 + C_{23}$$

$$T_{infC} + \frac{q_{ir}\cdot(x_3 - x_2)}{h_{Cir}} := \frac{-q_{ir}\cdot x_2^2}{2\cdot k_{13}} + C_{13}\cdot x_2 + C_{23}$$

$$C_{23} := T_{infC} + \frac{q_{ir}\cdot(x_3 - x_2)}{h_{Cir}} + \frac{q_{ir}\cdot x_2^2}{2\cdot k_{13}} - C_{13}\cdot x_2 = -83.633$$

Temperature distribution for 0.0375<x<0.0575

$$T_{13}(x) := \frac{-q_{ir}\cdot x^2}{2\cdot k_{13}} + C_{13}\cdot x + C_{23}$$

$$T_{13}(0.0475) = 131.982$$

Analytic element 1.4

Temperature distribution for 0.0575<x<0.0675

$T_{14}(x) := T_{13}(0.0575)$

$T_{14}(0.0575) = 138.707$

Analytic temperature distribution for element 1.1, 1.2, 1.3, 1.4

$$T(x) := \begin{cases} T_{11}(x) & \text{if } 0 \le x < 0.0195 \\ T_{12}(x) & \text{if } 0.0195 \le x < 0.0375 \\ T_{13}(x) & \text{if } 0.0375 \le x < 0.0575 \\ T_{14}(x) & \text{if } 0.0575 \le x < 0.0675 \end{cases}$$

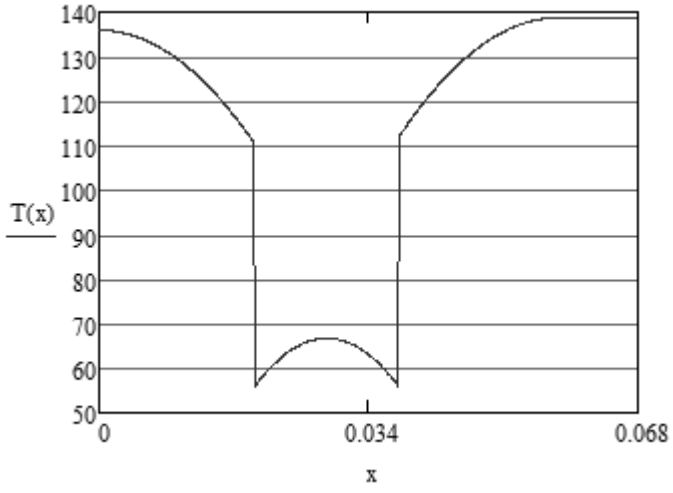

Medium Power AC experiment

Constants

$q_{ir} := 2.1151 \cdot 10^{6}$ $q_{co} := 0.002031 \cdot 10^{6}$ $h_A := 9.1$ $h_{Cir} := 160$ $h_{Cco} := h_{Cir}$

$k_{11} := 30$ $k_{12} := 0.72$ $k_{13} := 30$ $k_{14} := 0.61$ $T_{infC} := 41.5$ $T_{infA} := 21$

Analytic element 1.1

Left boundary condition (x=0)

$$\frac{d}{dx}T(x) := 0$$

$$\frac{d}{dx}T(x) := \frac{-q_{ir} \cdot x}{k_{11}} + C_{11}$$

$$0 := \frac{-q_{ir} \cdot x}{k_{11}} + C_{11}$$

$C_{11} := 0$

Right boundary condition (x=0.0195)

$$q_{ir} \cdot (x_1 - x_0) := h_{Cir}(T_1 - T_{infC})$$

$$T_1 := T_{infC} + \frac{q_{ir} \cdot (x_1 - x_0)}{h_{Cir}}$$

$$T(x_1) := \frac{-q_{ir} \cdot x_1^{2}}{2 \cdot k_{11}} + C_{11} \cdot x_1 + C_{21}$$

$$T_{infC} + \frac{q_{ir} \cdot (x_1 - x_0)}{h_{Cir}} := \frac{-q_{ir} \cdot x_1^{2}}{2 \cdot k_{11}} + C_{11} \cdot x_1 + C_{21}$$

$$C_{21} := T_{infC} + \frac{q_{ir} \cdot (x_1 - x_0)}{h_{Cir}} + \frac{q_{ir} \cdot x_1^{2}}{2 \cdot k_{11}} - C_{11} \cdot x_1 = 80.634$$

Temperature distribution for 0<x<0.0195

$$T_{11}(x) := \frac{-q_{ir} \cdot x^{2}}{2 \cdot k_{11}} + C_{11} \cdot x + C_{21}$$

Analytic element 1.2

Center boundary condition (x=0.0285)

$$\frac{d}{dx}T(x) := 0$$

$$\frac{d}{dx}T(x) := \frac{-q_{co}\cdot x_{12}}{k_{12}} + C_{12}$$

$$C_{12} := \frac{q_{co}\cdot x_{12}}{k_{12}} = 80.354$$

Right boundary condition (x=0.0375)

$$C_{22} := T_{infC} + \frac{q_{co}\cdot\left(x_2 - x_1\right)}{h_{Cco}} + \frac{q_{co}\cdot x_2^{2}}{2\cdot k_{12}} - C_{12}\cdot x_2 = 40.492$$

Temperature distribution for 0.0195x<0.0375

$$T_{12}(x) := \frac{-q_{co}\cdot x^{2}}{2\cdot k_{12}} + C_{12}\cdot x + C_{22}$$

$$T_{12}(0.0285) = 41.637$$

Analytic element 1.3

RIGHT boundary condition (x=0.0575)

$$\frac{d}{dx}T(x) := 0$$

$$\frac{d}{dx}T(x) := \frac{-q_{ir}\cdot x_3}{k_{13}} + C_{13}$$

$$C_{13} := \frac{q_{ir}\cdot x_3}{k_{13}} = 4.054\times 10^3$$

Left boundary condition (x=0.0375)

$$q_{ir}\cdot(x_3 - x_2) := h_{Cir}(T_2 - T_{infC})$$

$$T_2 := T_{infC} + \frac{q_{ir}\cdot(x_3 - x_2)}{h_{Cir}}$$

$$T(x_2) := \frac{-q_{ir}\cdot x_2^2}{2\cdot k_{13}} + C_{13}\cdot x_2 + C_{23}$$

$$T_{infC} + \frac{q_{ir}\cdot(x_3 - x_2)}{h_{Cir}} := \frac{-q_{ir}\cdot x_2^2}{2\cdot k_{13}} + C_{13}\cdot x_2 + C_{23}$$

$$C_{23} := T_{infC} + \frac{q_{ir}\cdot(x_3 - x_2)}{h_{Cir}} + \frac{q_{ir}\cdot x_2^2}{2\cdot k_{13}} - C_{13}\cdot x_2 = -34.561$$

Temperature distribution for 0.0375<x<0.0575

$$T_{13}(x) := \frac{-q_{ir}\cdot x^2}{2\cdot k_{13}} + C_{13}\cdot x + C_{23}$$

$$T_{13}(0.0475) = 78.465$$

Analytic element 1.4

Temperature distribution for 0.0575<x<0.0675

$T_{14}(x) := T_{13}(0.0575)$

$T_{14}(0.0575) = 81.99$

Analytic temperature distribution for element 1.1, 1.2, 1.3, 1.4

$$T(x) := \begin{cases} T_{11}(x) & \text{if } 0 \le x < 0.0195 \\ T_{12}(x) & \text{if } 0.0195 \le x < 0.0375 \\ T_{13}(x) & \text{if } 0.0375 \le x < 0.0575 \\ T_{14}(x) & \text{if } 0.0575 \le x < 0.0675 \end{cases}$$

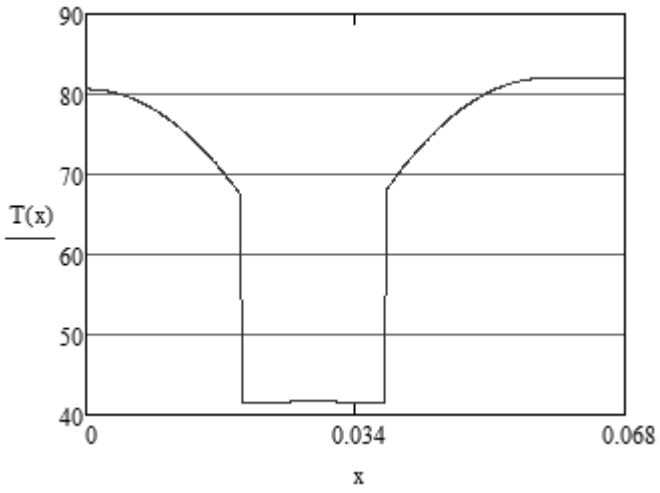

Low Power AC experiment

Constants

$q_{ir} := 0.682010^{6}$ $q_{co} := 0.011810^{6}$ $h_A := 9.1$ $h_{Cir} := 736$ $h_{Cco} := h_{Cir}$

$k_{11} := 30$ $k_{12} := 0.72$ $k_{13} := 30$ $k_{14} := 0.61$ $T_{infC} := 27$ $T_{infA} := 21$

Analytic element 1.1

Left boundary condition (x=0)

$$\frac{d}{dx}T(x) := 0$$

$$\frac{d}{dx}T(x) := \frac{-q_{ir}\cdot x}{k_{11}} + C_{11}$$

$$0 := \frac{-q_{ir}\cdot x}{k_{11}} + C_{11}$$

$C_{11} := 0$

Right boundary condition (x=0.0195)

$$q_{ir}\cdot(x_1 - x_0) := h_{Cir}(T_1 - T_{infC})$$

$$T_1 := T_{infC} + \frac{q_{ir}\cdot(x_1 - x_0)}{h_{Cir}}$$

$$T(x_1) := \frac{-q_{ir}\cdot x_1^{2}}{2\cdot k_{11}} + C_{11}\cdot x_1 + C_{21}$$

$$T_{infC} + \frac{q_{ir}\cdot(x_1 - x_0)}{h_{Cir}} := \frac{-q_{ir}\cdot x_1^{2}}{2\cdot k_{11}} + C_{11}\cdot x_1 + C_{21}$$

$$C_{21} := T_{infC} + \frac{q_{ir}\cdot(x_1 - x_0)}{h_{Cir}} + \frac{q_{ir}\cdot x_1^{2}}{2\cdot k_{11}} - C_{11}\cdot x_1 = 49.391$$

Temperature distribution for 0<x<0.0195

$$T_{11}(x) := \frac{-q_{ir}\cdot x^{2}}{2\cdot k_{11}} + C_{11}\cdot x + C_{21}$$

Analytic element 1.2

Center boundary condition (x=0.0285)

$$\frac{d}{dx}T(x) := 0$$

$$\frac{d}{dx}T(x) := \frac{-q_{co}\cdot x_{12}}{k_{12}} + C_{12}$$

$$C_{12} := \frac{q_{co}\cdot x_{12}}{k_{12}} = 467.083$$

Right boundary condition (x=0.0375)

$$C_{22} := T_{infC} + \frac{q_{co}\cdot\left(x_2 - x_1\right)}{h_{Cco}} + \frac{q_{co}\cdot x_2^{2}}{2\cdot k_{12}} - C_{12}\cdot x_2 = 21.296$$

Temperature distribution for 0.0195x<0.0375

$$T_{12}(x) := \frac{-q_{co}\cdot x^{2}}{2\cdot k_{12}} + C_{12}\cdot x + C_{22}$$

$$T_{12}(0.0285) = 27.952$$

Analytic element 1.3

RIGHT boundary condition (x=0.0575)

$$\frac{d}{dx}T(x) := 0$$

$$\frac{d}{dx}T(x) := \frac{-q_{ir}\cdot x_3}{k_{13}} + C_{13}$$

$$C_{13} := \frac{q_{ir}\cdot x_3}{k_{13}} = 1.307\times 10^{3}$$

Left boundary condition (x=0.0375)

$$q_{ir}\cdot\left(x_3 - x_2\right) := h_{Cir}\left(T_2 - T_{infC}\right)$$

$$T_2 := T_{infC} + \frac{q_{ir}\cdot\left(x_3 - x_2\right)}{h_{Cir}}$$

$$T\left(x_2\right) := \frac{-q_{ir}\cdot x_2^{2}}{2\cdot k_{13}} + C_{13}\cdot x_2 + C_{23}$$

$$T_{infC} + \frac{q_{ir}\cdot\left(x_3 - x_2\right)}{h_{Cir}} := \frac{-q_{ir}\cdot x_2^{2}}{2\cdot k_{13}} + C_{13}\cdot x_2 + C_{23}$$

$$C_{23} := T_{infC} + \frac{q_{ir}\cdot\left(x_3 - x_2\right)}{h_{Cir}} + \frac{q_{ir}\cdot x_2^{2}}{2\cdot k_{13}} - C_{13}\cdot x_2 = 12.498$$

Temperature distribution for 0.0375<x<0.0575

$$T_{13}(x) := \frac{-q_{ir}\cdot x^{2}}{2\cdot k_{13}} + C_{13}\cdot x + C_{23}$$

$$T_{13}(0.0475) = 48.943$$

Analytic element 1.4

Temperature distribution for 0.0575<x<0.0675

$T_{14}(x) := T_{13}(0.0575)$

$T_{14}(0.0575) = 50.079$

Analytic temperature distribution for element 1.1, 1.2, 1.3, 1.4

$$T(x) := \begin{cases} T_{11}(x) & \text{if } 0 \le x < 0.0195 \\ T_{12}(x) & \text{if } 0.0195 \le x < 0.0375 \\ T_{13}(x) & \text{if } 0.0375 \le x < 0.0575 \\ T_{14}(x) & \text{if } 0.0575 \le x < 0.0675 \end{cases}$$

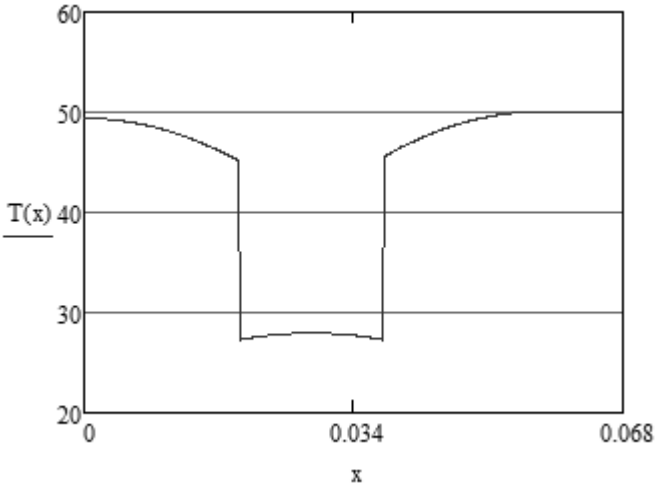

DC experiment

Constants

$q_{ir} := 0$ $q_{co} := 0.3257410^{6}$ $h_A := 9.1$ $h_{Cir} := 1176$ $h_{Cco} := h_{Cir}$

$k_{11} := 30$ $k_{12} := 0.72$ $k_{13} := 30$ $k_{14} := 0.61$ $T_{infC} := 22.25$ $T_{infA} := 21$

Analytic element 1.1

Left boundary condition (x=0)

$$\frac{d}{dx}T(x) := 0$$

$$\frac{d}{dx}T(x) := \frac{-q_{ir}\cdot x}{k_{11}} + C_{11}$$

$$0 := \frac{-q_{ir}\cdot x}{k_{11}} + C_{11}$$

$C_{11} := 0$

Right boundary condition (x=0.0195)

$$q_{ir}\cdot(x_1 - x_0) := h_{Cir}(T_1 - T_{infC})$$

$$T_1 := T_{infC} + \frac{q_{ir}\cdot(x_1 - x_0)}{h_{Cir}}$$

$$T(x_1) := \frac{-q_{ir}\cdot x_1^{2}}{2\cdot k_{11}} + C_{11}\cdot x_1 + C_{21}$$

$$T_{infC} + \frac{q_{ir}\cdot(x_1 - x_0)}{h_{Cir}} := \frac{-q_{ir}\cdot x_1^{2}}{2\cdot k_{11}} + C_{11}\cdot x_1 + C_{21}$$

$$C_{21} := T_{infC} + \frac{q_{ir}\cdot(x_1 - x_0)}{h_{Cir}} + \frac{q_{ir}\cdot x_1^{2}}{2\cdot k_{11}} - C_{11}\cdot x_1 = 22.25$$

Temperature distribution for 0<x<0.0195

$$T_{11}(x) := \frac{-q_{ir}\cdot x^{2}}{2\cdot k_{11}} + C_{11}\cdot x + C_{21}$$

Analytic element 1.2

Center boundary condition (x=0.0285)

$$\frac{d}{dx}T(x) := 0$$

$$\frac{d}{dx}T(x) := \frac{-q_{co}\cdot x_{12}}{k_{12}} + C_{12}$$

$$C_{12} := \frac{q_{co}\cdot x_{12}}{k_{12}} = 1.289\times 10^{4}$$

Right boundary condition (x=0.0375)

$$C_{22} := T_{infC} + \frac{q_{co}\cdot\left(x_2 - x_1\right)}{h_{Cco}} + \frac{q_{co}\cdot x_2^{2}}{2\cdot k_{12}} - C_{12}\cdot x_2 = -138.179$$

Temperature distribution for 0.0195x<0.0375

$$T_{12}(x) := \frac{-q_{co}\cdot x^{2}}{2\cdot k_{12}} + C_{12}\cdot x + C_{22}$$

$$T_{12}(0.0285) = 45.559$$

Analytic element 1.3

RIGHT boundary condition (x=0.0575)

$$\frac{d}{dx}T(x) := 0$$

$$\frac{d}{dx}T(x) := \frac{-q_{ir}\cdot x_3}{k_{13}} + C_{13}$$

$$C_{13} := \frac{q_{ir}\cdot x_3}{k_{13}} = 0$$

Left boundary condition (x=0.0375)

$$q_{ir}\cdot\left(x_3 - x_2\right) := h_{Cir}\left(T_2 - T_{infC}\right)$$

$$T_2 := T_{infC} + \frac{q_{ir}\cdot\left(x_3 - x_2\right)}{h_{Cir}}$$

$$T\left(x_2\right) := \frac{-q_{ir}\cdot x_2^2}{2\cdot k_{13}} + C_{13}\cdot x_2 + C_{23}$$

$$T_{infC} + \frac{q_{ir}\cdot\left(x_3 - x_2\right)}{h_{Cir}} := \frac{-q_{ir}\cdot x_2^2}{2\cdot k_{13}} + C_{13}\cdot x_2 + C_{23}$$

$$C_{23} := T_{infC} + \frac{q_{ir}\cdot\left(x_3 - x_2\right)}{h_{Cir}} + \frac{q_{ir}\cdot x_2^2}{2\cdot k_{13}} - C_{13}\cdot x_2 = 22.25$$

Temperature distribution for 0.0375<x<0.0575

$$T_{13}(x) := \frac{-q_{ir}\cdot x^2}{2\cdot k_{13}} + C_{13}\cdot x + C_{23}$$

$$T_{13}(0.0475) = 22.25$$

Analytic element 1.4

Temperature distribution for 0.0575<x<0.0675

$$T_{14}(x) := T_{13}(0.0575)$$

$$T_{14}(0.0575) = 22.25$$

Analytic temperature distribution for element 1.1, 1.2, 1.3, 1.4

$$T(x) := \begin{cases} T_{11}(x) & \text{if } 0 \le x < 0.0195 \\ T_{12}(x) & \text{if } 0.0195 \le x < 0.0375 \\ T_{13}(x) & \text{if } 0.0375 \le x < 0.0575 \\ T_{14}(x) & \text{if } 0.0575 \le x < 0.0675 \end{cases}$$

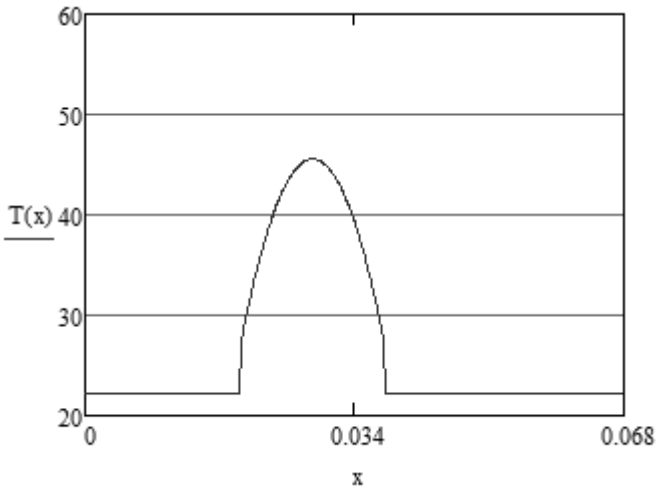

750 W iron loss and 250 W copper loss

Constants

$q_{ir} := 1.32 \cdot 10^{6}$ $q_{co} := 0.9 \cdot 10^{6}$ $h_A := 8$ $h_{Cir} := 100$ $h_{Cco} := h_{Cir}$

$k_{11} := 30$ $k_{12} := 0.7$ $k_{13} := 30$ $k_{14} := 0.6$ $T_{infC} := 50$ $T_{infA} := 21$

$x_0 := 0$ $x_1 := 0.019$ $x_{12} := 0.028$ $x_2 := 0.037$ $x_3 := 0.057$ $x_4 := 0.067$

Analytic element 1.1

Left boundary condition (x=0)

$$\frac{d}{dx}T(x) := 0$$

$$\frac{d}{dx}T(x) := \frac{-q_{ir} \cdot x}{k_{11}} + C_{11}$$

$$0 := \frac{-q_{ir} \cdot x}{k_{11}} + C_{11}$$

$C_{11} := 0$

Right boundary condition (x=0.0195)

$$q_{ir} \cdot (x_1 - x_0) := h_{Cir}(T_1 - T_{infC})$$

$$T_1 := T_{infC} + \frac{q_{ir} \cdot (x_1 - x_0)}{h_{Cir}}$$

$$T(x_1) := \frac{-q_{ir} \cdot x_1^{2}}{2 \cdot k_{11}} + C_{11} \cdot x_1 + C_{21}$$

$$T_{infC} + \frac{q_{ir} \cdot (x_1 - x_0)}{h_{Cir}} := \frac{-q_{ir} \cdot x_1^{2}}{2 \cdot k_{11}} + C_{11} \cdot x_1 + C_{21}$$

$$C_{21} := T_{infC} + \frac{q_{ir} \cdot (x_1 - x_0)}{h_{Cir}} + \frac{q_{ir} \cdot x_1^{2}}{2 \cdot k_{11}} - C_{11} \cdot x_1 = 84.105$$

Temperature distribution for 0<x<0.0195

$$T_{11}(x) := \frac{-q_{ir} \cdot x^{2}}{2 \cdot k_{11}} + C_{11} \cdot x + C_{21}$$

$T_{11}(0.0195) = 75.74$

Analytic element 1.2

Center boundary condition (x=0.0285)

$$\frac{d}{dx}T(x) := 0$$

$$\frac{d}{dx}T(x) := \frac{-q_{co}\cdot x_{12}}{k_{12}} + C_{12}$$

$$C_{12} := \frac{q_{co}\cdot x_{12}}{k_{12}} = 3.563\times 10^{4}$$

Right boundary condition (x=0.0375)

$$C_{22} := T_{infC} + \frac{q_{co}\cdot(x_2 - x_1)}{h_{Cco}} + \frac{q_{co}\cdot x_2^{2}}{2\cdot k_{12}} - C_{12}\cdot x_2 = -390.831$$

Temperature distribution for 0.0195x<0.0375

$$T_{12}(x) := \frac{-q_{co}\cdot x^{2}}{2\cdot k_{12}} + C_{12}\cdot x + C_{22}$$

$T_{12}(0.0285) = 116.825$

$T_{12}(0.0195) = 66.2$

Analytic element 1.3

RIGHT boundary condition (x=0.0575)

$$\frac{d}{dx}T(x) := 0$$

$$\frac{d}{dx}T(x) := \frac{-q_{ir}\cdot x_3}{k_{13}} + C_{13}$$

$$C_{13} := \frac{q_{ir}\cdot x_3}{k_{13}} = 2.53\times 10^3$$

Left boundary condition (x=0.0375)

$$q_{ir}\cdot(x_3 - x_2) := h_{Cir}(T_2 - T_{infC})$$

$$T_2 := T_{infC} + \frac{q_{ir}\cdot(x_3 - x_2)}{h_{Cir}}$$

$$T(x_2) := \frac{-q_{ir}\cdot x_2^2}{2\cdot k_{13}} + C_{13}\cdot x_2 + C_{23}$$

$$T_{infC} + \frac{q_{ir}\cdot(x_3 - x_2)}{h_{Cir}} := \frac{-q_{ir}\cdot x_2^2}{2\cdot k_{13}} + C_{13}\cdot x_2 + C_{23}$$

$$C_{23} := T_{infC} + \frac{q_{ir}\cdot(x_3 - x_2)}{h_{Cir}} + \frac{q_{ir}\cdot x_2^2}{2\cdot k_{13}} - C_{13}\cdot x_2 = 12.463$$

Temperature distribution for 0.0375<x<0.0575

$$T_{13}(x) := \frac{-q_{ir}\cdot x^2}{2\cdot k_{13}} + C_{13}\cdot x + C_{23}$$

$$T_{13}(0.0575) = 85.2$$

$$T_{13}(0.0475) = 83$$

Analytic element 1.4

Temperature distribution for 0.0575<x<0.0675

$$T_{14}(x) := T_{13}(0.0575)$$

$$T_{14}(0.0575) = 85.2$$

Analytic temperature distribution for element 1.1, 1.2, 1.3, 1.4

$$T(x) := \begin{cases} T_{11}(x) & \text{if } 0 \le x < 0.0195 \\ T_{12}(x) & \text{if } 0.0195 \le x < 0.0375 \\ T_{13}(x) & \text{if } 0.0375 \le x < 0.0575 \\ T_{14}(x) & \text{if } 0.0575 \le x < 0.0675 \end{cases}$$

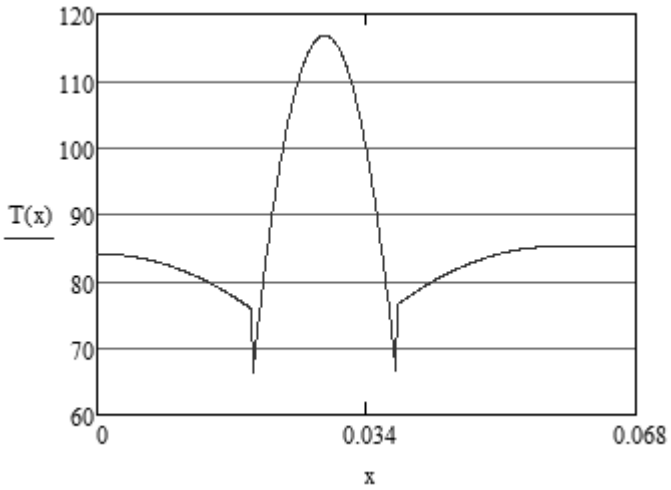

Appendix B

Johnson controls solution to incorporate the Enhanced Core Cooling system in a PMSM.

High Speed Permanent Magnet Syncronous Machine with Enhanced Core Cooling for Water Vapour Compression Application

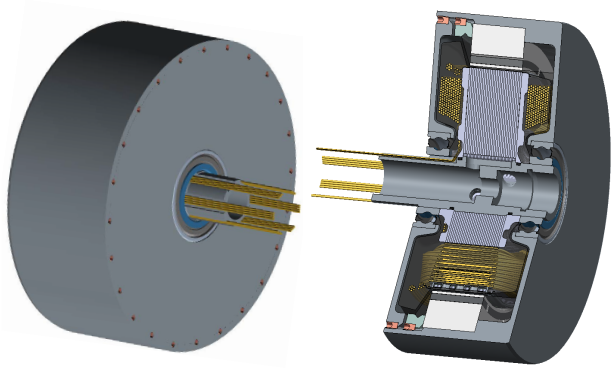

Improvements compared to previous conceptual prototype:

- Enhanced cooling
  - Cooling directly on iron core
  - Scalable
  - Approx 0.05 m^2 HEX-surface –say 1kW dissipation only require 20 K temperature difference iron->water
- One size smaller ball bearings (6006) enlarges winding head space, lower friction losses and increase bearing max speed allowance.
- O-ring based sealing to shaft.
- Mylar shrinkwrap seals laminates in airgap.
- Resin based potential leak passages length significantly enlarged, decreasing risk of local seep
- Winding wire length reduced – decreases copper loss.
- Overall 7 mm (10 %) decreased axial length

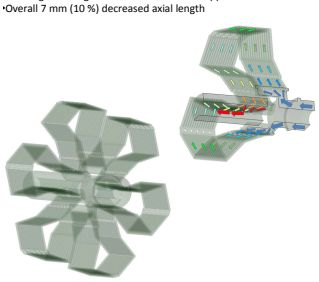

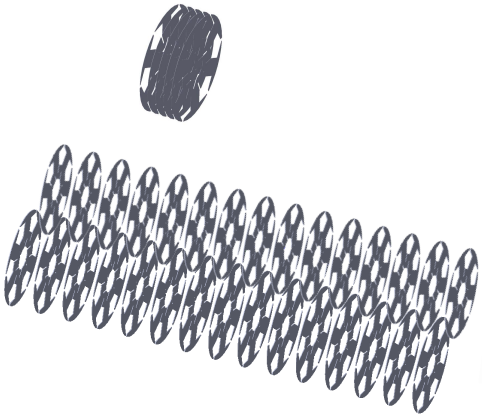

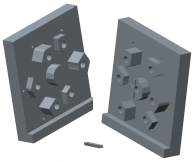

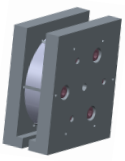

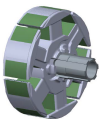

2 stacks of say 5 0.2 mm laminates assembled with same planar orientation and then put face-to-face say 15 times constitutes the stator iron core of 30 mm

Assemble iron core by wrapping coil columns and teeth with Mylar HS tape. Take care teeth OD only to be added two layers of 50µm , respecting needed airgap to be added tubing shrinkwrap, too.

Squeeze lamination stack in wax moulding tool, and close teeth gaps with spacers. Heat to shrink Mylar tape and after cooling inject wax at high pressure and at opening of tool, remove wax gating and fins.

Fill shaft water cavities with wax

Assemble lamination stack, shaft and endplates sealed with O-rings

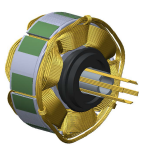

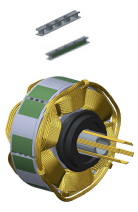

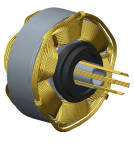

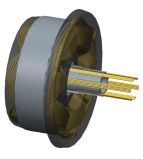

Wind the stator, solder the star point (Tools tightening end cap tools not shown)

Insert wax filled bridging strips between windings and teeth

Insert wax filled bridging strips between windings and teeth

Resin cast the stator and after curing melt/flush out the wax